PFC/RR-84-22
(DE85005873)
Distribution Categories UC-90g and UC-93

Plasma Fusion Center

Massachusetts Institute of Technology

Cambridge, MA 02139

MHD Magnet Technology Development Program Summary October 1982 - April 1984

Prepared for

U.S. Department of Energy

Pittsburgh Energy Technology Center

Pittsburgh, PA

Published

September 1984

Foreword

This report is issued by the MHD Magnet Technology Group of the Plasma Fusion Center (PFC), Massachusetts Institute of Technology (MIT).

The work reported herein has been carried out in performance of Task 3 of Department of Energy (DOE) Contract EX-76-A-01-2295.

The following staff members of the MHD Magnet Technology Group have contributed to this program:

H.D. Becker
A.M. Dawson
A.M. Hatch
W.G. Langton
W.R. Mann
P.G. Marston
J.M. Tarrh

Table of Contents

Table of Contents (cont)

List of Figures

List of Tables

List of Figures (cont.)

0.0 Abstract

The program of MHD magnet technology development conducted for the U.S. Department of Energy by the Massachusetts Institute of Technology in the period from October 1982 through April 1984 is summarized. This program, a continuation of the program underway during the preceding five years and separately reported, included the development of computer codes for design scaling and cost estimating, the use of these codes in evaluating the impact of design current density on magnet cost and reliability, the study of magnet winding design improvements for lower cost and increased reliability, and the review and documentation of past work on MHD magnet cost estimation and cost reduction.

Also included were an investigation of a major magnet structural failure, follow-up recommendation of actions to minimize failure risk in the future, review of channel-magnet interfacing with contractors involved in advanced power train studies and the development of several preliminary magnet designs and cost estimates in support of Pittsburgh Energy Technology Center MHD plant studies. The overall effort during the past 1-1/2 years tended to focus on smaller, early commercial size magnet systems rather than the large baseload systems that were given major attention earlier in the program.

1.0 Introduction

A program to develop superconducting magnets for commercial magnetohydrodynamic (MHD) power generation plants, initiated in 1976, is being carried out by the Massachusetts Institute of Technology, Plasma Fusion Center (PFC) under the sponsorship of the U.S. Department of Energy (DOE) and the Pittsburgh Energy Technology Center (PETC). The overall objective of the program is to prepare the technological and industrial base for minimum time, cost and risk implementation of superconducting magnets for MHD.

Work accomplished in the period from 1976 through 1982 was summarized in "MHD Magnet Technology Development Program Summary" published by MIT in November 1983 (Reference 1). The purpose of this report is to summarize the work accomplished in the period from October 1982 through April 1984. Because funding during this report period was at a drastically reduced level, it was possible to implement only a few of the recommended tasks listed in Section 3 of Reference 1. Specifically, effort was applied to upgrade cost estimation procedures, to determine the impact of design current density on magnet cost and to evaluate alternative conductors and winding designs. These tasks were selected because cost and reliability of windings are critical to the ultimate development of a satisfactory commercial-scale magnet.

Additional effort was expended in developing preliminary designs and cost estimates for magnets associated with alternative MHD flow trains under consideration by PETC, as well as in evaluating past MHD magnet experience and documenting magnet data.

Although limited in scope because of funding restrictions, the work accomplished in the report period has been valuable in establishing a firmer base for the future magnet technology development that will be necessary to reach the overall objectives of MHD.

2.0 Summary of Results

- Design current density has a significant impact on magnet cost and reliability, according to results of computer-aided studies at MIT (Appendix A, Reference 2) . The impact is greater in magnets in the size range for early commercial (small) MHD plants than in magnets sized for large baseload plants. The use of higher current density reduces cost significantly, but tends to affect reliability criteria adversely. Quantitative data have been generated to serve as a guide in making cost/risk trade-offs for future MHD

magnet designs.

- Winding designs can be modified successfully to permit higher current density operation (and hence lower overall magnet cost) with minimum adverse effect on reliability criteria, based on MIT studies which were underway at the end of the report period. The studies which focused on smaller, early commercial-size magnets, considered improvements involving the use of higher strength substructure with more compact bath-cooled conductors and also the use of internally-cooled cable conductors with minimal or no substructure.
- The failure of the force containment structure of the High Performance Demonstration Experiment (HPDE) MHD magnet during testing at Arvin/Calspan in Tullahoma can be attributed to an overload condition which had not been identified in stress analysis accomplished during the magnet design phase. This was the finding of the MIT investigation (Appendix B, Reference 3) done in 1983. A result of the failure and subsequent investigation was to call to the attention of the magnet community the need for action aimed at reducing the chances of failures in future large magnet systems. A specific action taken was the Magnet Failure Workshop (Appendix C) held in Grenoble, September 1983, in conjunction with the 8th International Conference on Magnet Technology.
- The following preliminary MHD magnet designs with accompanying cost estimates and recommendations were developed during the report period, in support of the PETC MHD program:
  - 4.5 T superconducting magnet design and cost estimate for MERDI (29 MWe)
  - 4.0 T water cooled magnet design and cost estimate (alternative ETF magnet)
  - 4.5 T water-cooled magnet design and cost estimate (retrofit, 50 MWe)
  - 4.5 T superconducting magnet design and cost estimate (retrofit, 35 MWe)
- MHD channel/magnet interfacing was reviewed with the GE and AVCO Advanced Power Train Study (APT) team in January 1984 and interfacing information packages were sent to APT contractors, GE and Westinghouse, and to PETC. A support program definition for technical assistance to APT contractors (GE, AVCO and Westinghouse) was supplied to PETC (Appendix D).

3.0 Recommendations

- Continue the development of conductor and winding designs incorporating improvements to provide for higher design current density with minimum adverse effect on reliability.
- Maintain and upgrade computer codes for MHD magnet design scaling and cost estimating. Continue use of codes in support of cost/risk trade-off studies of alternative magnet designs.
- Continue work on establishing structural design standards for MHD magnets and on other investigations (see Appendix B) to reduce chances of failure in large magnet systems.
- Work with APT contractors on channel/magnet interfacing considerations, including means to facilitate channel changeout and means for supporting the flow train and maintaining its alignment with respect to the magnet.
- Continue evaluation and documentation of past work in cost estimating, cost analysis and cost reduction of MHD magnets, with the end-product to be a report covering cost-related work done in the period from 1976 to the present.

Note: The above recommendations are related specifically to the tasks described in this report and worked on in the period October 1982 through April 1984. In addition to these recommendations, the recommendations listed in Tables 3.2-I and 3.2-II of Reference 1 remain valid and should be considered in connection with overall MHD magnet technology development.

4.0 Summary of Work Accomplished

Summaries of work accomplished in each of the tasks on which effort was expended in the period October 1982 to April 1984 are given in the sections which follow. Where appropriate, references containing more detailed information are cited and/or detailed data compilations are included as appendices to this report.

4.1 Development of Computer Codes for Design Scaling and Cost Estimating

Development of computer codes for design scaling and cost estimating of MHD magnets was started in 1982 as an initial step in a program to analyze the effect of design current density* variation on the overall cost and reliability of linear MHD magnet systems. Particular attention was given to the smaller systems presently envisioned for early commercialization.

To determine the effects of varying current density, it was planned to calculate major characteristics and estimated costs for a series of magnets, all of the same design and field strength, but with varying design current density (and also with varying bore size and active length in order that size, as affecting power generation, be taken into account). The variation of cost and of reliability criteria could then be plotted versus design current density to give a graphic representation of the magnitude of the effect. Scaling techniques and computer codes were developed to perform the calculations required.

The conceptual design of the magnet developed by MIT for the MHD Engineering Test Facility (ETF) 200 MWe Power Plant[4,5] was selected as a baseline for the design scaling and cost scaling operations. While this was not necessarily an optimum design, it was selected as being a representative design on which adequate technical data and estimated cost data were available. The winding in this magnet was of the rectangular saddle coil configuration, a shape also used in the CDIF/SM[6] and CSM[1] designs.

Two codes were developed, the first to calculate design characteristics and the second to calculate costs. The codes were put to use starting early in 1983 in the study of the impact of design current density on magnet cost and reliability (see Section 4.2). After the study was completed, the design scaling code was upgraded to calculate emergency discharge (dump) voltage and conductor heat flux. It was then used in a study of magnet winding design improvements (see Section 4.3). Further information on the codes is contained in Appendix A and Reference 2.

4.1.1 Design Scaling Code

The design scaling code (mhd scaler 1) was developed for use in obtaining preliminary design data and making parametric studies on magnets in the size range from test facility size (CDIF) to large baseload size. Field strength variation from 4 T to 7 T was taken as the range to be considered. (The codes will handle sizes and fields outside the stated ranges, but errors may become larger).

The code was not intended as a precise design tool, but rather as a simple means of determining approximate design characteristics to use in making comparative studies. It was intended that a portion of the output from the design scaling code (component weights, etc.) would be used as part of the input to the cost estimating code described in Section 4.1.2. The design scaling code assumes that the magnet incorporates a rectangular configuration of the type shown in Fig. 4.1.1.1 and a conductor and substructure arrangement as shown in Fig. 4.1.1.2.

The winding dimensions which determine the design characteristics of the magnet and which are used

* as used here, "design current density" is the average current density in the overall winding cross section when the magnet is operating at design field strength

in the computer code are shown in the winding elevation and plan views, Fig. 4.1.1.3, and in winding cross section in the plane of the peak on-axis field, Fig. 4.1.1.4.

The inputs to the design scaling code fall into five categories, as indicated in Tables 4.1.1-I and 4.1.1-II. An explanation of the nature of each category is contained in these tables. When using a given baseline design and studying the effects of variations due to changes in one design parameter, most of the inputs will remain constant. For example, it is necessary to vary only one input, namely "winding build," to make a series of calculations for magnets of different current densities, provided size, field strength and configuration remain the same.

It should be noted that the size-determining primary inputs are not actual warm bore dimensions, but are winding inside dimensions and characteristic lengths. When a new magnet size is to be analyzed using the scaling code, the appropriate winding dimensions must be arrived at by preliminary design work or by engineering estimate, starting with the desired warm bore dimensions.

It should also be noted that design current density is not introduced into the calculations as a direct input (current per unit area), but instead is specified indirectly through the input "winding build" (linear dimension). The code calculates the current density necessary to produce the specified peak on-axis field and supplies the appropriate current density value as an output. Although this approach may necessitate iteration and/or cross-plotting where data for a particular current density are desired, the approach makes for simplicity in calculating and was adopted for that reason.

The computation section uses simple mathematical relationships to calculate winding cross-sectional area, mean turn length and other dimensions. The ampere turns required to produce the specified field are calculated using a formula based on Maxwell's equations for magnetic fields produced by currents in infinitely long parallel wires. It is assumed that currents are concentrated in the centers of each winding quadrant. An empirical correction factor is used to account for the difference between infinite parallel wires and the finite saddle coil geometry. Approximate magnetic forces and pressures in the plane of peak on-axis field are also calculated using formulae based on Maxwell's equations with empirical factors. Stored energy is scaled from the baseline design using a formula including ampere turns and characteristic lengths.

The portion of winding cross-sectional area allocated to substructure is determined based on calculated magnetic pressures and input design stress in substructure. Areas allocated to superconductor, stabilizer, insulation and helium passages are then calculated using input design current density in superconductor and input space factors. Finally, volumes are calculated using appropriate areas and mean turn lengths (calculation of weights is accomplished in the cost calculating code described in Section 4.1.2).

Safety criterion "dump voltage" is calculated using the input "heating factor" which is related to a preselected maximum allowable conductor temperature during quench. Stability criterion "heat flux" is calculated using inputs "copper resistivity" and "cooled perimeter."

The output of the design scaling code includes dimensions and design characteristics of the winding, volumes of winding components, scaling factors with reference to the baseline design, safety and stability criteria, and approximate overall dimensions of the magnet. The output data which are used as inputs to the cost calculating code described in Section 4.1.2 are listed in Table 4.1.1-II.

Table 4.1.1-I

Design Scaling Code Inputs Listed by Categories, with Explanations, Sheet 1

Category	Input	Symbol	Explanation
1. Magnet size and field strength parameters	Distance, winding side bundle to X-Z centerplane in plane of peak on-axis field	m	These inputs change only when magnet size and/or field strength change.
	Distance, end winding bundle to X-Y centerplane, inlet end	f_1	
	Distance, end winding bundle to X-Y centerplane, exit end	f_2	
	Mean length, winding side bundle	ℓ_s	
	Distance, plane of peak on-axis field to inlet end of side winding bundle	ℓ_m	
	Peak on-axis field	B_{prime}	
2. Magnet configuration (shape) parameters	Angle, magnet centerline to winding side bundle centerpoint, quadrant cross section, plane of B_{prime}	phi	These inputs change only when magnet configuration (winding shape, etc.) changes
	Distance, side bundle to X-Y centerplane, quadrant cross section, plane of B_{prime}	e	
	End turn-up angle	theta	
	Crossover corner radius, inside	r	
	Winding bundle divergence from X-Y plane	alpha	
	Winding bundle divergence from X-Z plane	beta	
3. Conductor and winding detail design parameters	Winding build	b	Winding build is changed to produce change in design current density
	Design current in conductor	I_c	
	Space factor, conductor metal	lam-m	Design current is generally increased

Table 4.1.1-1, cont.

Design Scaling Code Inputs Listed by Categories, with Explanations, Sheet 2

Category	Input	Symbol	Explanation
3. cont.	Shape factor, conductor	K14	with increasing magnet
	Design current density in superconductor	jsc	size (engineer's judgment) Design current density
	Conductor insulation thickness	t_i	in superconductor and copper resistivity (both
	Conductor insulation solidity factor	K19	related to maximum field in winding) should be
	Design stress, substructure	sig-sub	changed when peak
	Substructure solidity factor	K3	on-axis field is changed.
	Heating factor	G	Other inputs may remain
	Copper resistivity	rho	constant over moderate
	Cooled perimeter factor	K18	range of sizes and field strengths
4. Empirical factors	Correction factor, field-current relationship	K1prime	These inputs may remain constant for a given
	Overall length factor (add on)	K4	baseline design, over a moderate range of
	Overall diameter factor (add on)	K5	sizes, field strengths and design current
	Force factor, Y direction	K6	densities
	Force factor, Z direction	K7	
	Maximum pressure factor, Y direction	K8	
	Maximum pressure factor, Z direction	K9	
5. Baseline design data (for scaling and checking)	Cross sectional area of substructure, quadrant	a_{subb}	These inputs are constant for a given
	Ampere turns	I_b	baseline design.
	Mean distance between end bundles	ℓ_{cb}	Stored energy, ampere turns and mean distance
	Overall distance over end bundles	ℓ_{ob}	between end bundles are used by code in
	Winding volume	V_{wb}	scaling calculations.
	Substructure volume	V_{subb}	The other inputs
	Conductor metal volume	V_{mb}	are for checking only.
	Radial distance to corner, exterior	u2b	
	Stored energy	E_b	

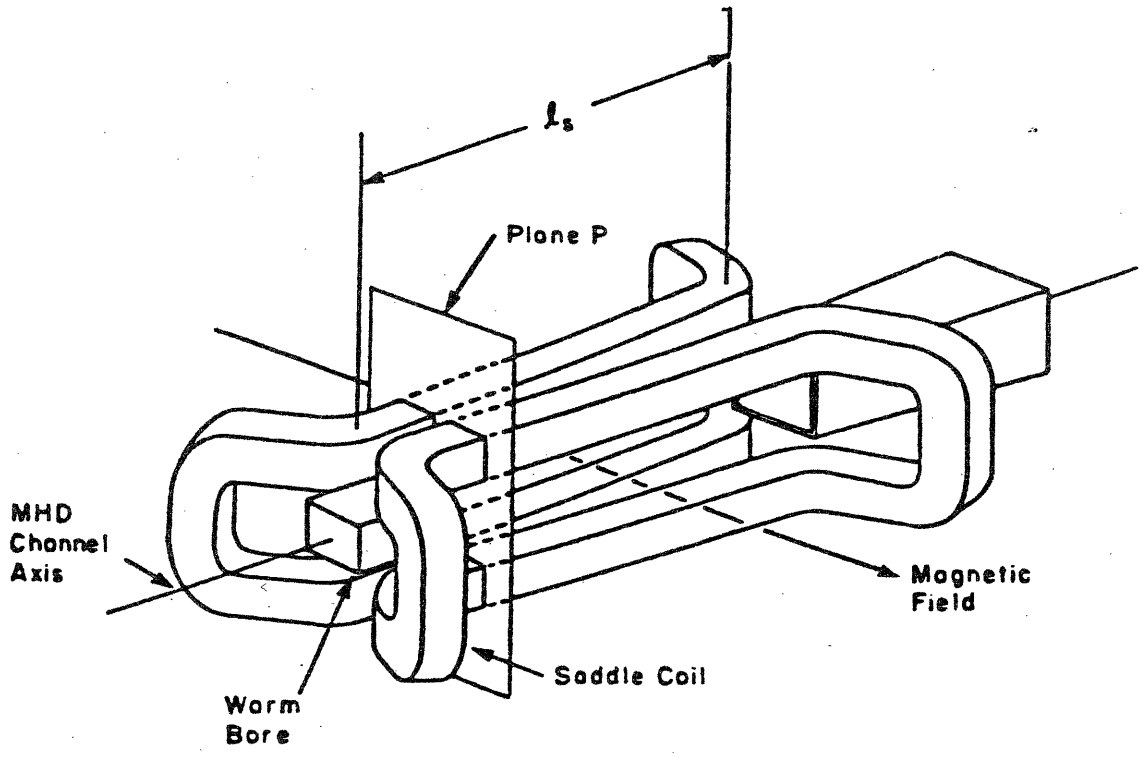

Fig. 4.1.1.1 Rectangular saddle coil winding configuration

Fig. 4.1.1.2 Conductor and substructure concept

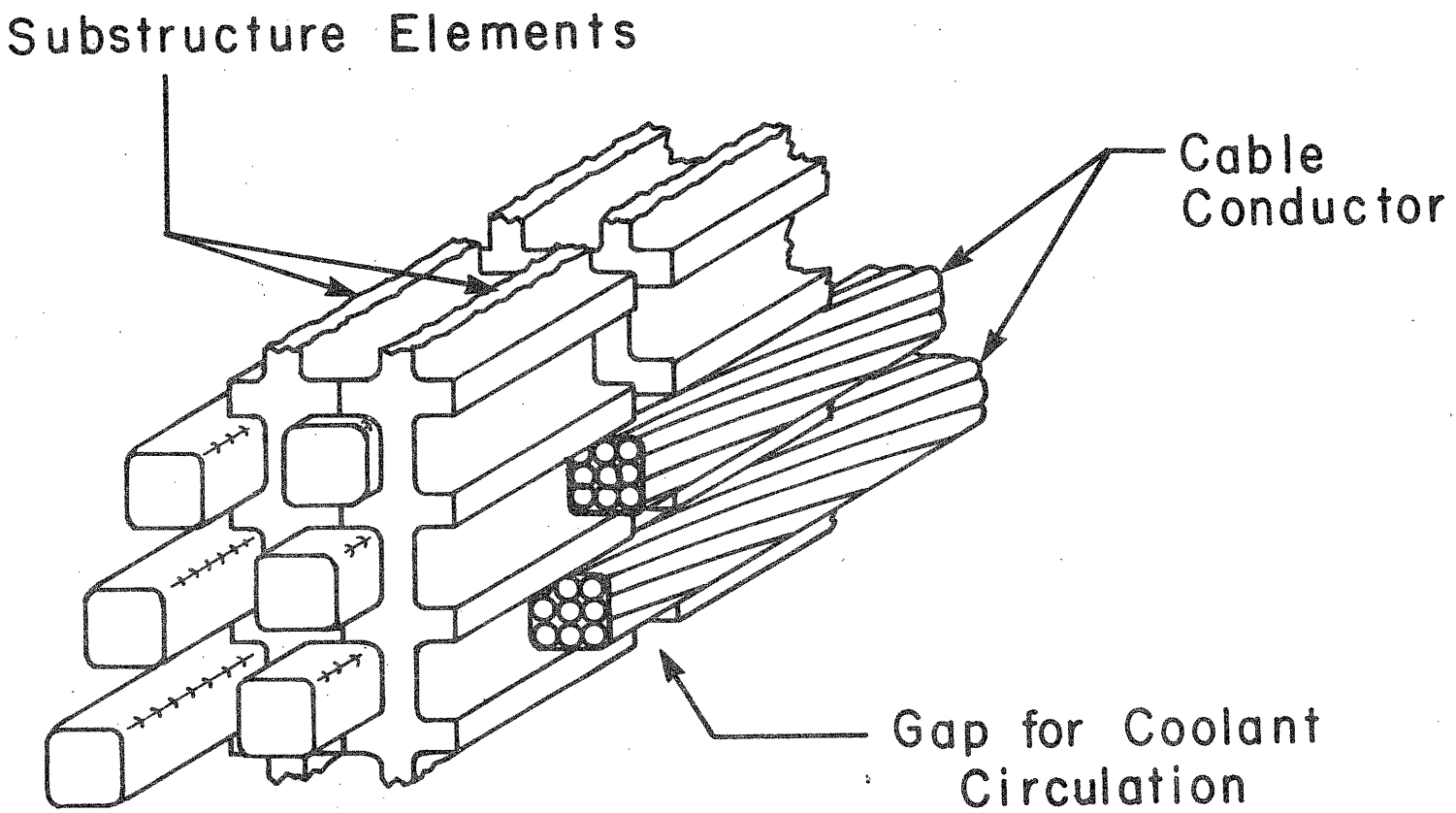

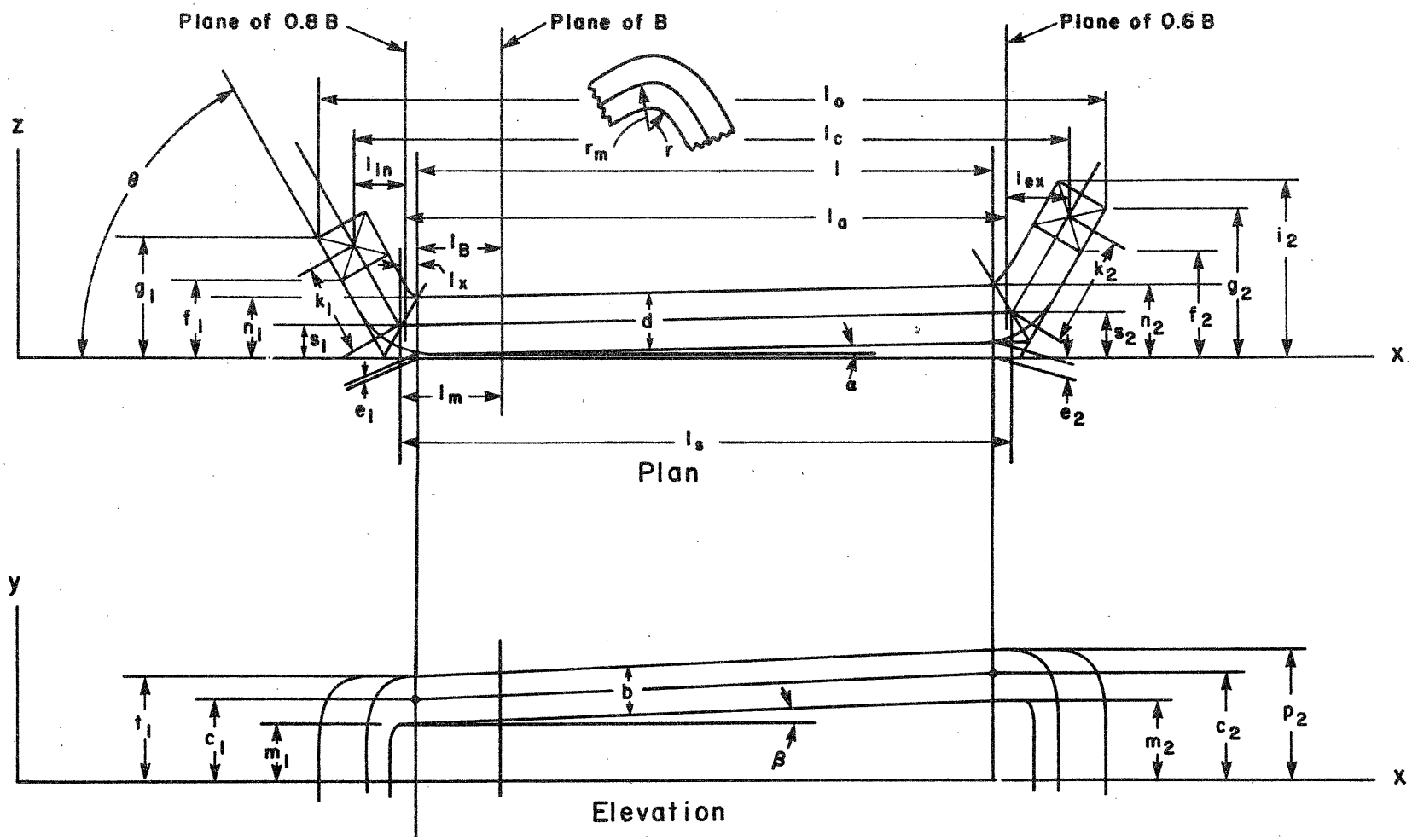

Fig. 4.1.1.3 Elevation and plan views, typical MHD magnet winding

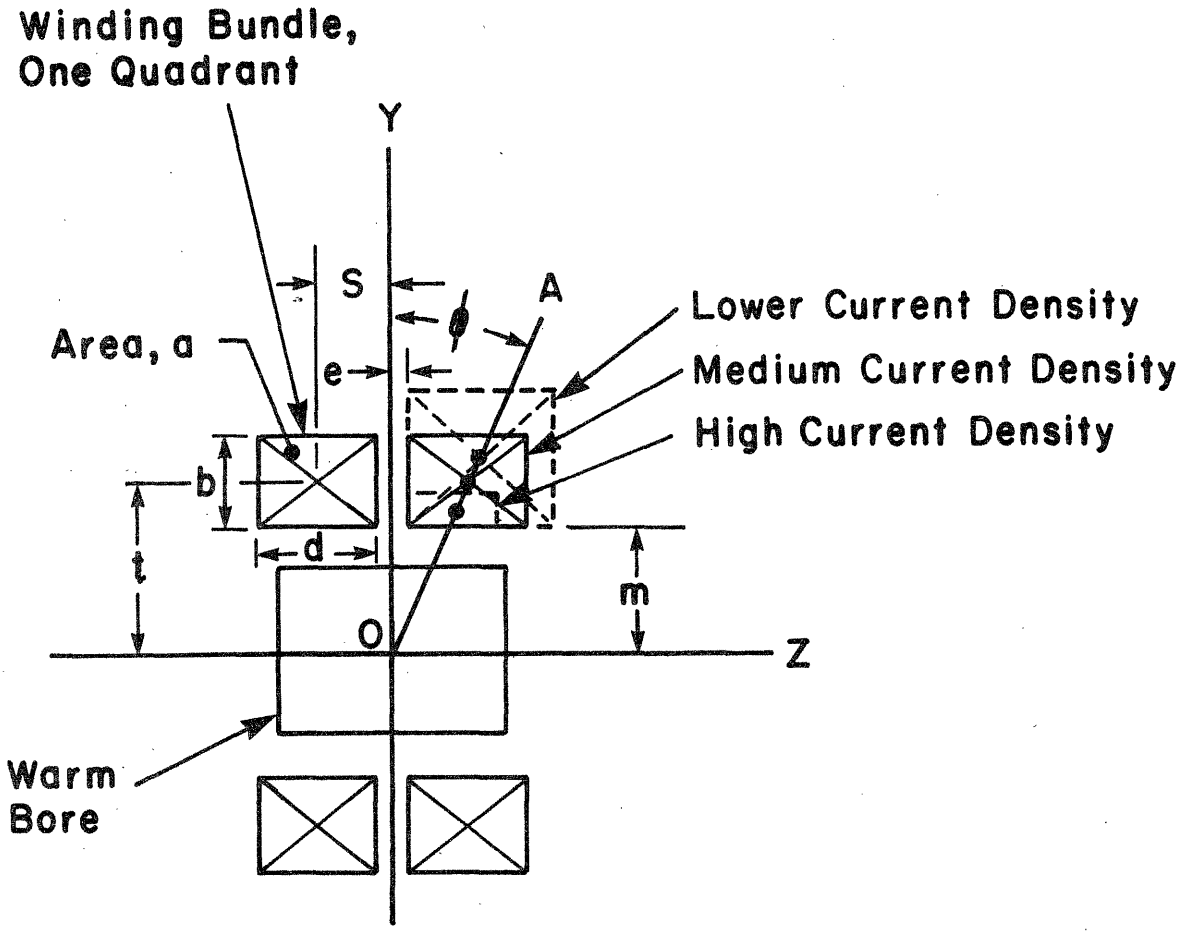

Fig. 4.1.1.4 Winding cross section in plane of peak on-axis field, typical MHD magnet winding

4.1.2 Cost Calculating Code

The cost calculating code (mhd scaler proc 2) was developed to calculate MHD magnet component weights and costs, and overall system costs using input data (component volumes, scaling factors) obtained with the aid of the Design Scaling Code described in Section 4.1.1 (see Table 4.1.1-III) together with material densities, cost algorithms and empirical factors derived from past experience in magnet construction and cost estimating, and baseline magnet data.

The calculation section of the code calculates weights of winding components by multiplying volumes from the design code by the appropriate input densities. It calculates weights of other components by scaling from the baseline data, using scaling factors from the design code. It calculates costs of components and manufacturing operations by applying cost algorithms (costs per unit weight) to the appropriate weights. It calculates other costs (accessories, design and analysis, project management, etc.) by applying an (input) empirical factor to the square root of the total accumulated cost up to that point. It calculates contingency allowance by applying a (input) contingency factor to the total magnet system cost including other costs.

The output data include component weights, component and magnet system costs, magnet and magnet system cost per unit of weight ($/kg) and magnet system cost per unit of stored energy ($/kJ).

4.1.3 Future Modifications

The codes in their present form have been very useful in cost studies and design improvement investigations (including cost/risk tradeoff studies). The experience led to the conclusion that continued use would be worthwhile and modifications should be incorporated to increase the versatility of the codes.

Work was started on modification of the design scaling code to accomplish the following:

Accept warm bore dimensions as input.

Calculate magnet design characteristics directly (without "baseline" design input).

Calculate component and system weights (this was done previously as part of the cost calculating code).

Handle circular saddle coil configuration as alternative to rectangular saddle coil configuration.

Work was started on modifying the cost calculating code to incorporate both an alternative conductor cost algorithm ($/kA-m) and a more complete breakdown of costs.

It is recommended that this effort be continued and that both codes be upgraded to increase their usefulness in future design and cost studies.

Table 4.1.1-II

Inputs to Cost Calculation Code Which are Outputs of Design Scaling Code

Input	Symbol
Total length, conductor	ℓ_{ct}
Ratio, copper to superconductor	R_c
Volume, superconductor	V_{sc}
Volume, copper	V_{cu}
Volume, substructure	V_{sub}
Scaling factor, surface of cold mass (envelope)	F_s
Scaling factor, winding volume	F_w
Scaling factor, energy	F_E
Scaling factor, volume of cold mass (envelope)	F_v

4.2 Study of Impact of Design Current Density* on Cost and Reliability of MHD Magnets

It has been generally recognized that the cost of an MHD magnet tends to become lower as design current density is increased, although the magnitude of the effect was not identified. It has been understood also that when high design current densities are selected in the interest of cost reduction, magnet protection becomes more difficult and the overall design may become less conservative from the safety and reliability standpoints.

Therefore, selecting design current density for commercial size MHD magnets clearly requires careful cost/risk assessment. It was evident that to accomplish this, quantitative data on the effect of design current density on magnet system cost was needed, together with information on the effects on reliability criteria such as conductor heat flux, emergency discharge voltage and winding temperature rise under quench conditions.

A computer-aided study (Appendix A, Reference 2) was made at MIT in 1983 to determine analytically the effect of design current density on magnet system cost and on safety and reliability criteria. The study made use of computer codes described in Section 4.1. Major emphasis was placed on magnet systems of the size required for linear MHD generators in the channel power output range of 100 to 1100 MWe. Copper-stabilized NbTi windings with average current densities from 0.75×10^7 A/m^2 to 2.5×10^7 A/m^2 were considered.

A relatively simple analytical approach was used in the study, which sought to identify general trends only. The results, tempered by engineering judgment to reflect the influence of factors not taken into account in the analysis, indicate that a saving of roughly 20% may be realized on magnet systems at the large end of the size range, by increasing current density from 1×10^7 A/m^2 to 2×10^7 A/m^2. The equivalent savings for magnet systems at the small end of the size range would be 25% or more.

Fig. 4.2.1 contains curves of magnet weight vs. design current density and Fig. 4.2.2 contains curves of magnet system cost vs. design current density. Figs. 4.2.3, 4.2.4 and 4.2.5 contain curves of heat flux, initial discharge voltage and final conductor temperature (after quench), respectively, as functions of design current density.

The basis for the above curves was a series of magnet reference designs of different bore sizes, representing magnets for power plants in the 100 to 1100 MWe range, and all embodying the same design concepts. For each magnet size, at least three current densities between 0.75×10^7 A/m^2 and 2.5×10^7 A/m^2 were considered. With the aid of computer programs and using scaling techniques, the characteristics and estimated costs of magnets of each bore size and current density were calculated.

For the limited number of computer-generated designs covered in this study, characteristics at the extremes of the parametric range, although indicative, do not necessarily represent good design practice. Values of heat flux, discharge voltage and conductor temperature shown on the curves were determined by scaling from reference magnet designs created with median conditions in mind, and therefore not optimized for the extreme conditions. (For example, high heat fluxes could be reduced by changing the detail design of the conductor; high discharge voltages could be lowered by increasing design current and/or by using parallel power supplies). In considering future magnet designs, the data in this study should be regarded as indicative of trends only.

---

* refers to the average current density in the overall winding cross section when the magnet is operating at its design field strength

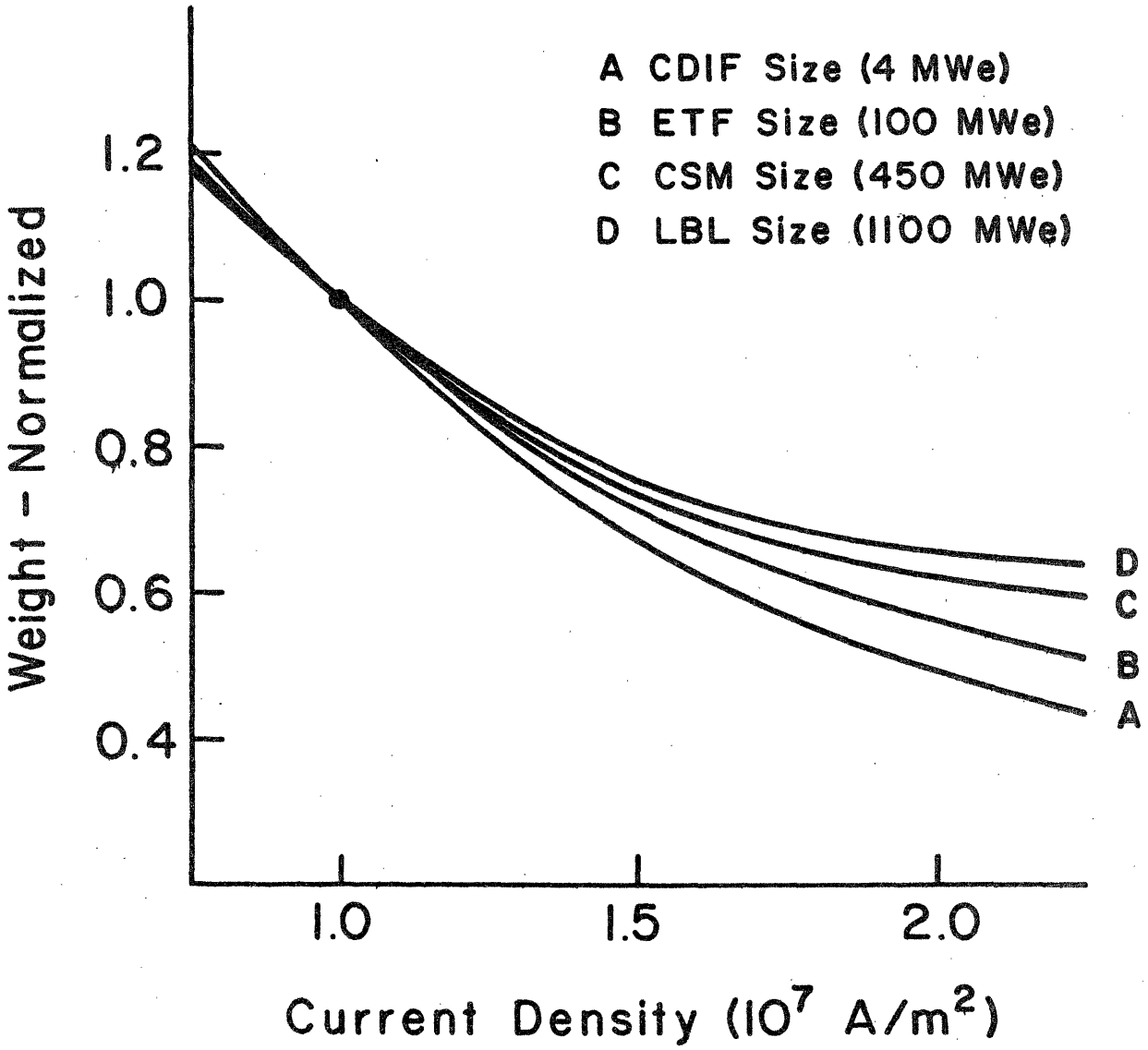

Fig. 4.2.1 Curves of normalized magnet weight vs. design current density

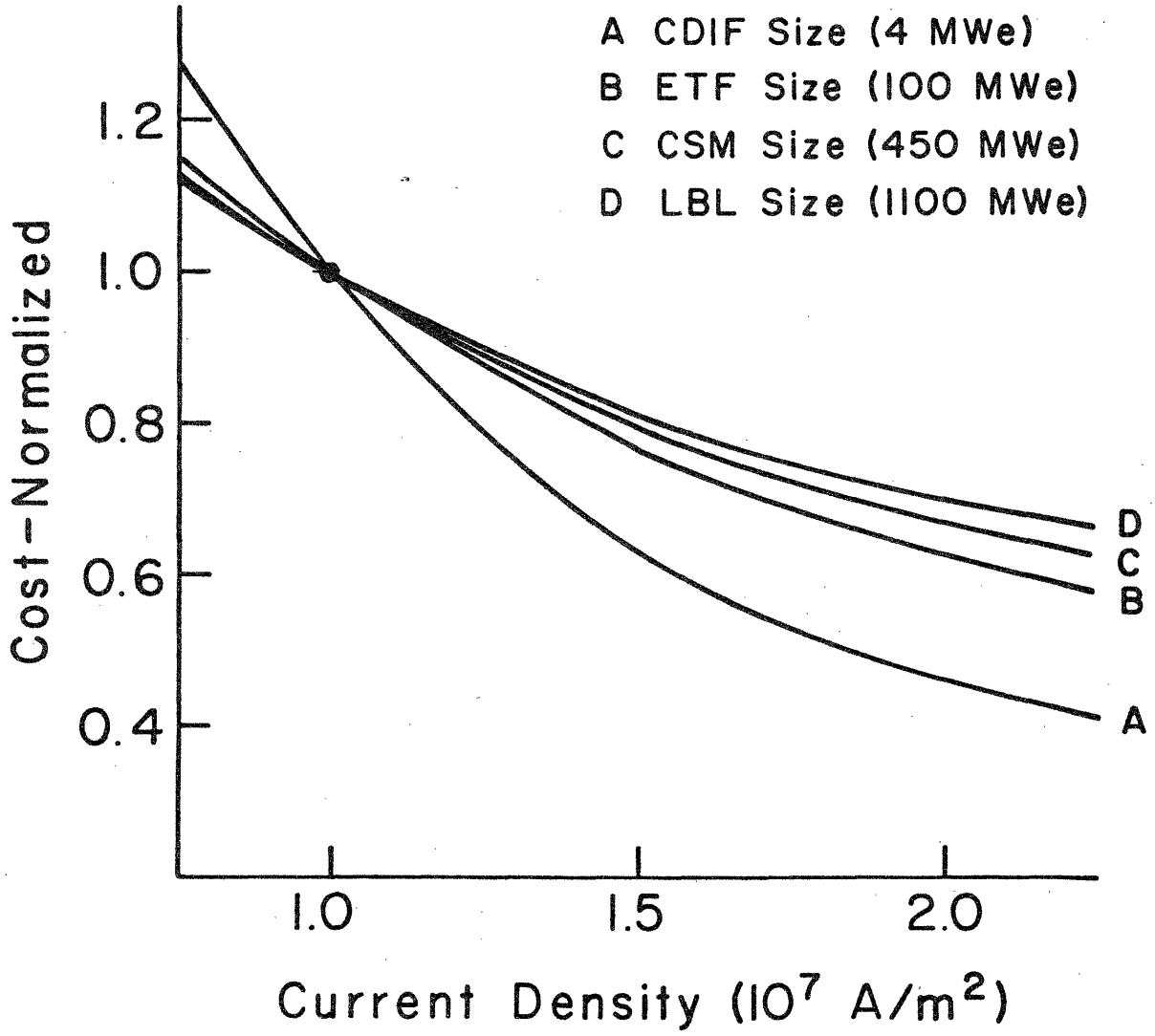

Fig. 4.2.2 Curves of normalized magnet system cost vs. design current density

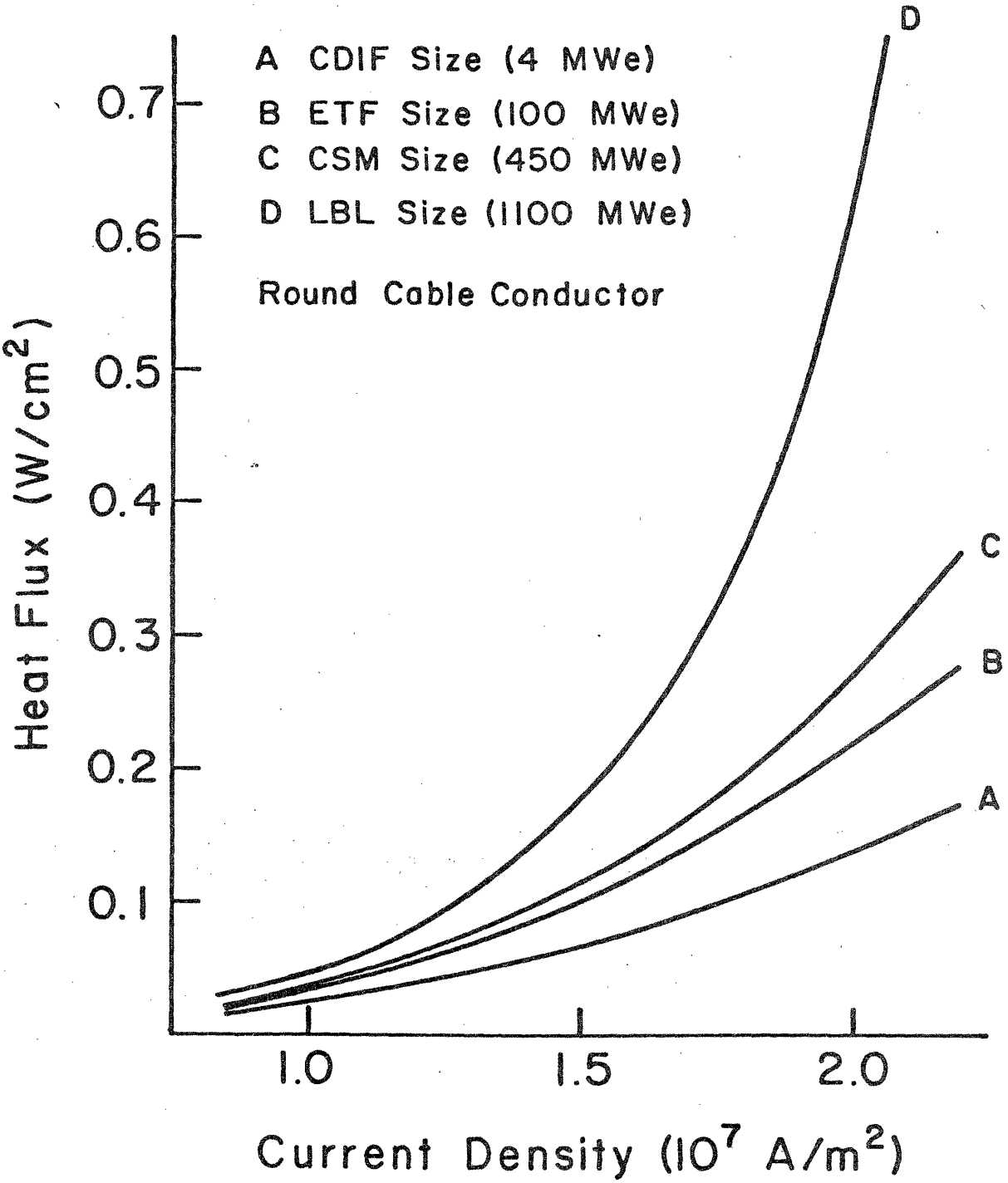

Fig. 4.2.3 Curves of heat flux vs. design current density

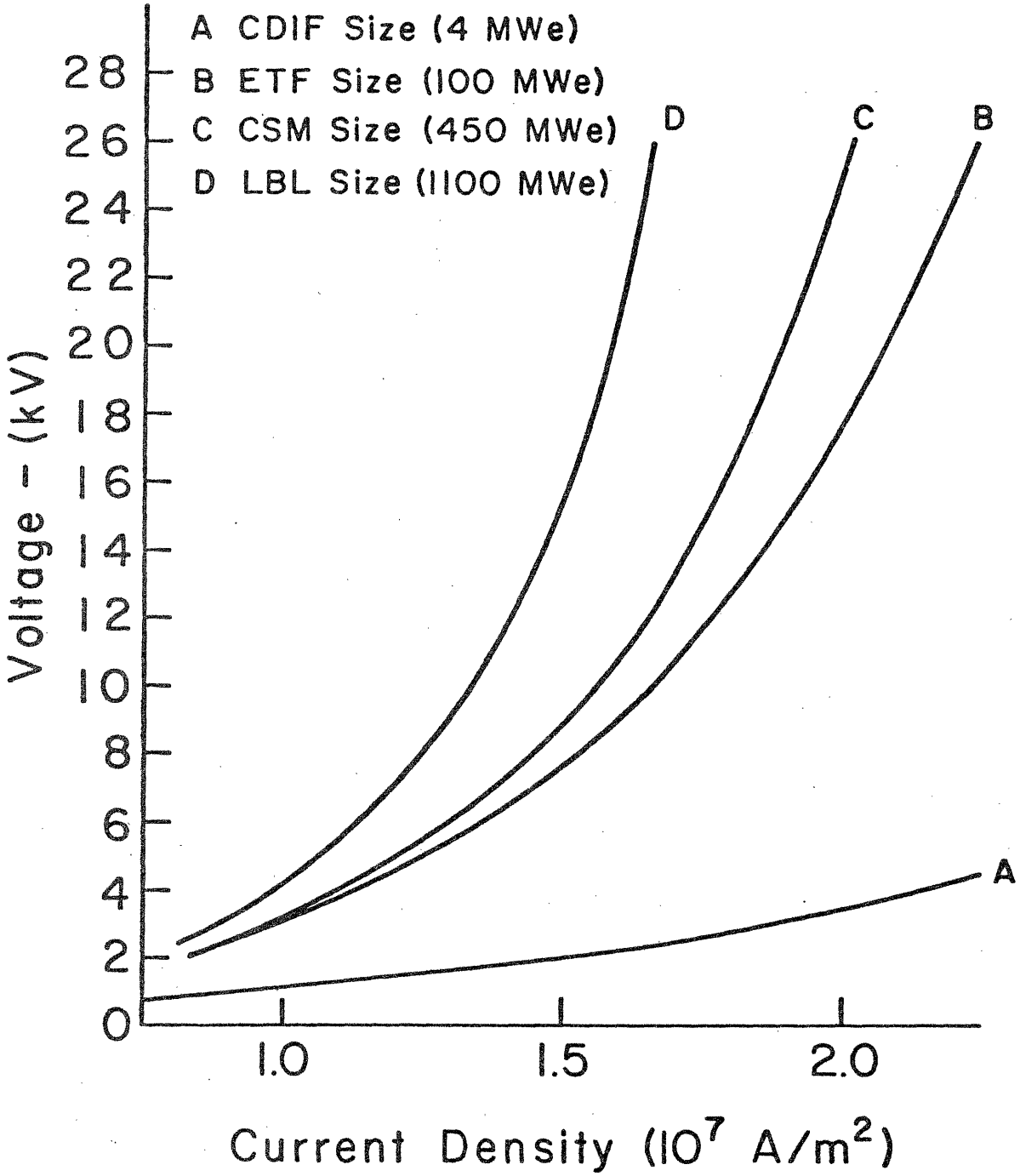

Fig. 4.2.4 Curves of emergency discharge voltage (initial) vs. design current density

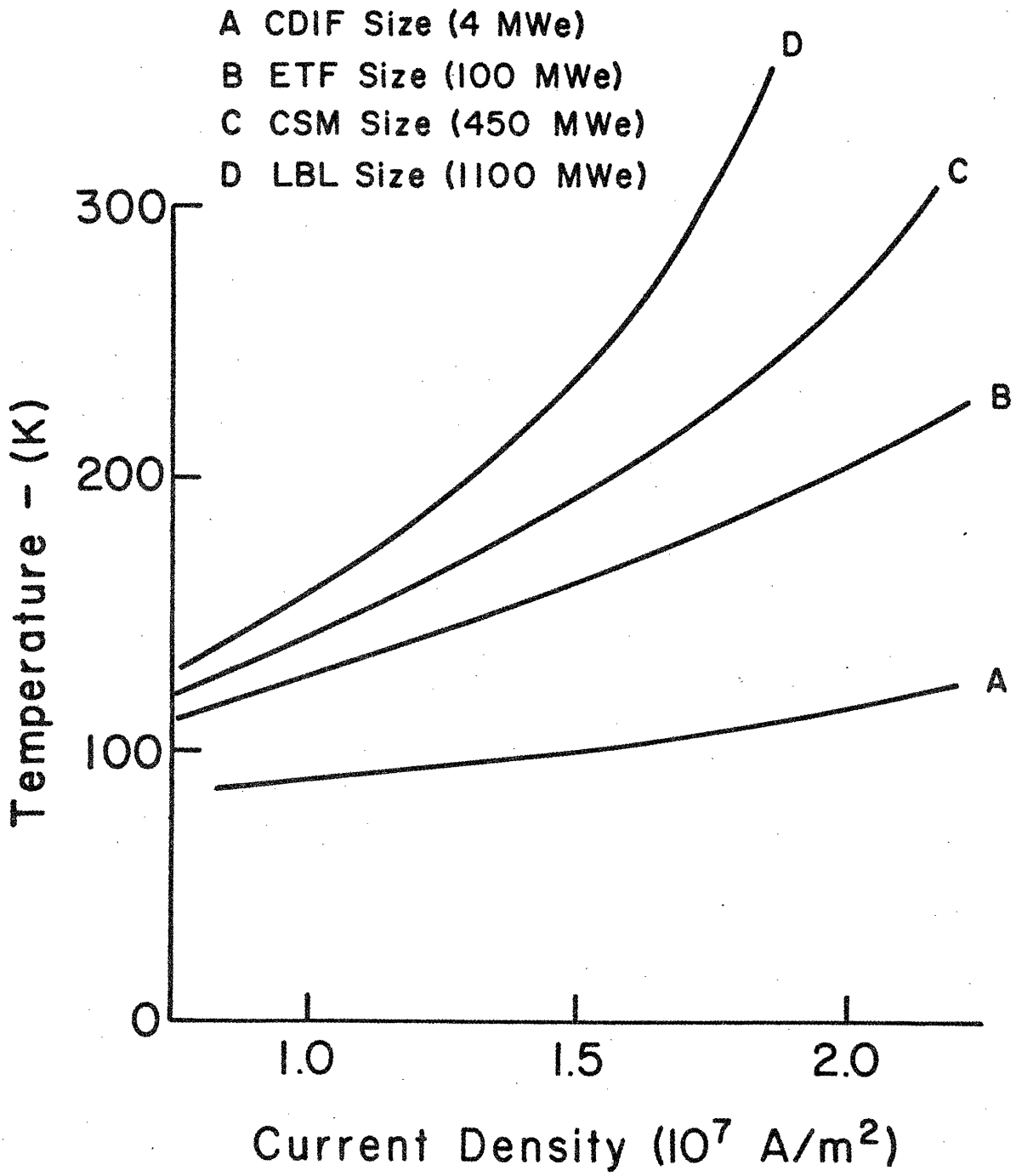

Fig. 4.2.5 Curves of final conductor temperature vs. design current density

It is of interest to note the range of design current densities used in past MHD magnet designs, as listed in Table 4.2-I. Here a definite trend toward lower design current density with increasing magnet size is observed. Values range from 2.82×10^7 A/m^2 for the relatively small U25 Bypass magnet to 1.15×10^7 A/m^2 for the commercial size CSM magnet. (However, current density in the conductor itself does not show the same trend, but varies erratically).

The observed trend to lower design current density with increased size is believed due in part to the instinctive desire of the designer to be generally more conservative as he enters the "unknown territory" of very large magnets, and in part to more specific influences such as the need for more conductor support material (substructure) in large windings and the tendency to provide extra copper and/or complicated extended surfaces to ensure that conductor surface heat flux is within acceptable limits. All of these factors make the winding pack bulkier and hence lower the average current density.

4.3 Study of Magnet Winding Design Improvements for Lower Cost and Increased Reliability

The study of the impact of design current density, described in Section 4.2, emphasized the need to improve winding designs with the objectives of reducing overall magnet cost while maintaining or improving reliability. The potential for substantial cost reduction by increasing design current density was quantified and was shown to be particularly attractive for smaller size (early commercial) magnets. Smaller magnets rather than large baseload magnets, were the focus of the initial design improvement effort described below.

The study of winding design improvements has only been started, and no definitive results have yet been obtained. The initial approach and some of the early data developed are summarized below.

Consideration was given to typical saddle coil windings having cross sections as shown in Fig. 4.3.1. The elements which occupy these winding cross sections are:

Superconductor
Stabilizer
Insulation
Substructure and/or cable sheath
Cooling passages

Fig. 4.3.2, containing sketches of typical winding cross sections, identifies these elements.

Higher design current density (and, one hopes, lower cost) can be achieved by reducing the overall winding cross-sectional area (while keeping the same area of superconductor). Since stabilizer and substructure are generally the largest elements in terms of area, it was necessary to consider design techniques to reduce these items without adversely affecting integrity, stability and protection.

As a first step, existing designs were reviewed. Table 4.3-I lists the relative amounts of stabilizer and substructure in the winding cross sections of four existing designs (CDIF/SM, ETF (6 T), CFFF and CASK). Fig. 4.3.3 is a sketch showing the ETF winding cross section. From the data shown, it appeared that the CDIF/SM and ETF designs had excessive amounts of substructure in the winding cross section. Also, it was seen that the ETF design had a minimal amount of stabilizer, partly the result of the poor space factor of the particular cable configuration chosen. The low stabilizer area was undesirable from the standpoint of protection.

As the next step, a series of winding designs was considered, including designs with higher strength substructures and more compact cable conductors, as well as designs using internally-cooled cable conductors without substructure (cable sheaths serving as substructure). For consistent comparisons, the designs were all related to a magnet reference design as shown in Fig. 4.3.4, intended for use with a 500 MWe channel

Table 4.2-I
Design Characteristics of
Representative MHD Magnet Designs of Various Sizes

Magnet Identification		U25 Bypass	CDIF	CFFF	ETF	CASK	CSM
Field	T	5	6	6	6	6	6
Warm bore inlet aperture	m	0.4 dia.	0.78× 0.97	0.8 dia.	1.5× 1.9	2.48 dia.	2.2× 2.8
Active length[a]	m	2.5	3.4	3.2	11.7	14.5	14.5
Stored energy	MJ	34	240	216	2900	6300	7200
Build	m	0.364	0.622	0.53	0.95	0.74	1.08
Design current	kA	0.89	6.13	3.675	24.4	50.0	52.2
Design current density, winding	10^7 A/m^2	2.82	1.87	2.0	1.42	1.28	1.15
Current density, conductor	10^7 A/m^2	5.0	6.28	2.63	8.16	2.2	5.7
Type of conductor		Rect. Built-up	Square Built-up	Rect. Built-up	Round Cable	Rect. Built-up	Round Cable
Substructure material		Fiber-glass & St. Steel[b]	Fiber-glass	Fiber-glass[b]	Fiber-glass	St. Steel	Fiber-glass

Notes:

a Active length for all magnets is distance between on-axis field points of 0.8 B_{peak} at inlet and 0.6 B_{peak} at exit.

b Banding between winding layers is used in place of a rigid substructure.

Table 4.3-I
Winding Cross Section Design Data for Four Representative MHD Magnet Designs

		CDIF/SM	ETF (6 T)	CFFF	CASK
Design current density	($\times 10^7$ A/m^2)	1.87	1.42	2.0	1.28
Type of conductor		Built-up	Round cable	Built-up	Built-up
Copper to superconductor ratio		11.1	6.0	21	34
Type of substructure		Individ. cond. support, G-10	Individ. cond. support, GRP	Banding only, GRP + st. steel	Group cond. support, st. steel
Cross-sectional areas, fraction of total conductor envelope		0.25	0.29	0.76	0.64
Stabilizer		0.17	0.13	0.69	0.58
Substructure		0.75	0.70	0.15	0.30

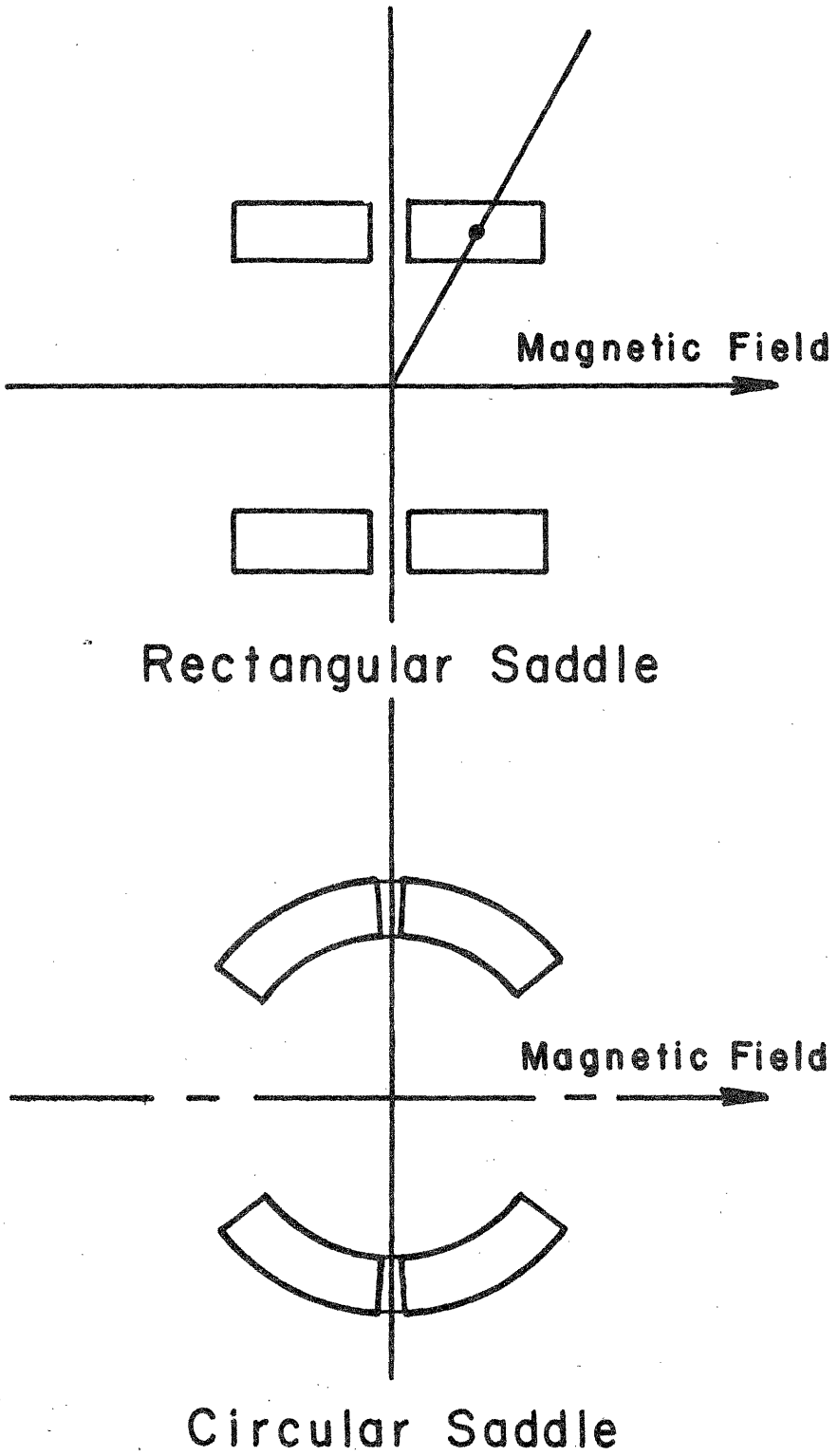

Fig. 4.3.1 Sketches of typical winding cross sections, rectangular and circular saddle configurations

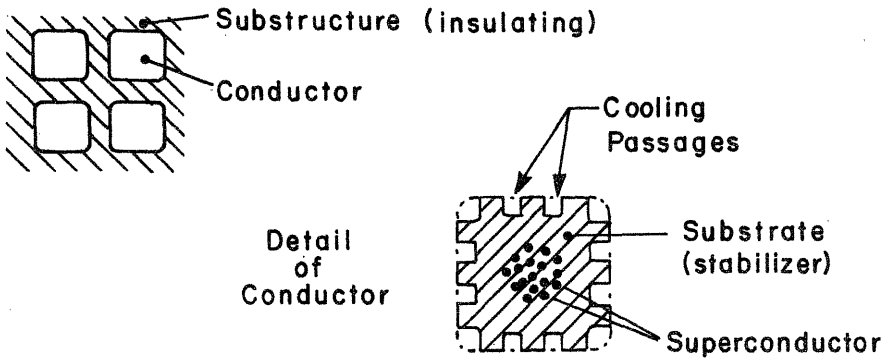

WINDING WITH INSULATING SUBSTRUCTURE

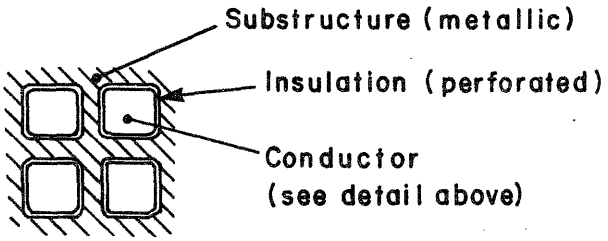

WINDING WITH METALLIC SUBSTRUCTURE

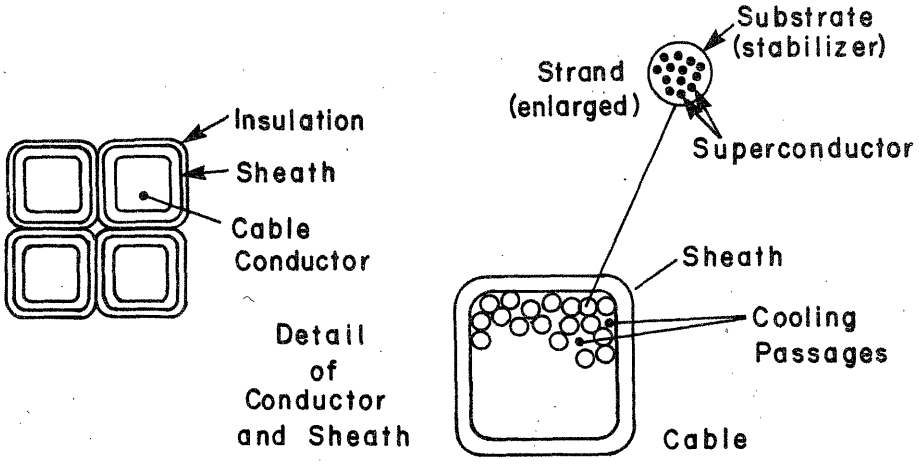

WINDING WITH ICCS CONDUCTOR, NO SUBSTRUCTURE

Fig. 4.3.2 Sketches of typical winding cross sections, detail

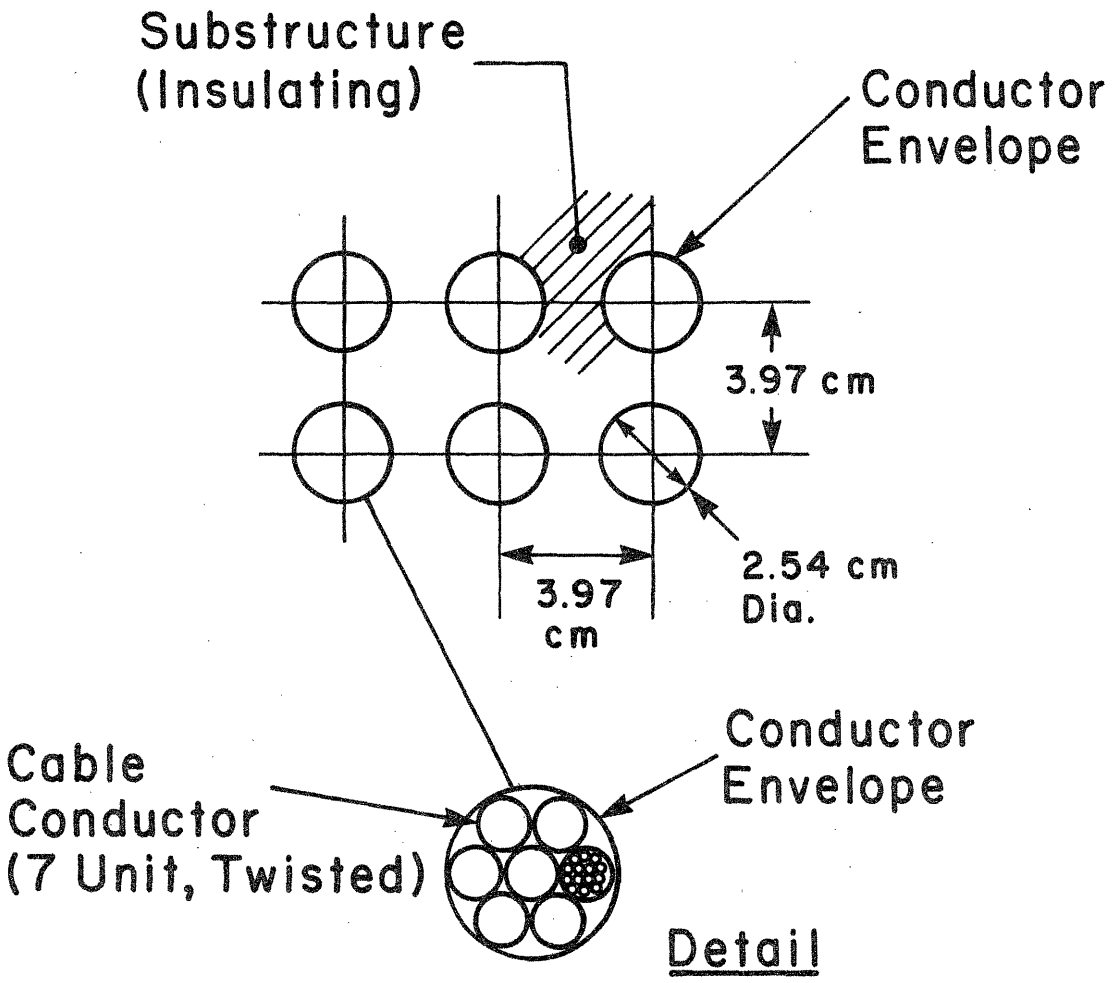

Space Factor, Cable

$$\frac{\text{Conductor Metal Area}}{\text{Conductor Envelope Area}} = 0.547$$

Fig. 4.3.3 Detail of ETF magnet winding cross section

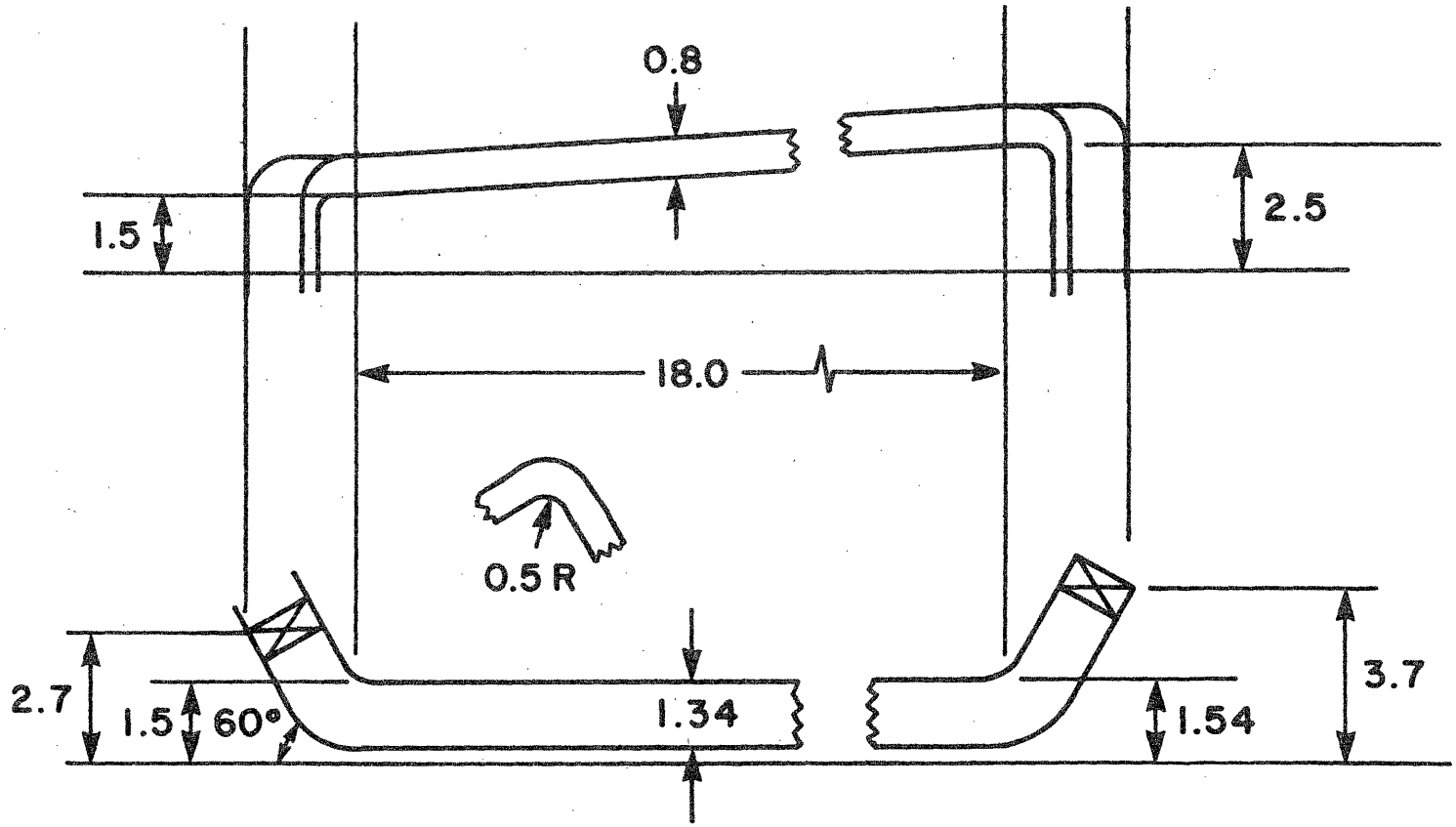

Fig. 4.3.4 Sketch showing reference design magnet winding used in winding design study (500 MWe channel)

similar to the largest channel being considered in the Advanced Power Train Study[8]. This size was selected to represent the upper size extreme with the expectation that data for this size would be safely scalable to smaller sizes. Winding designs considered, including computer-generated design characteristics, are shown in Fig. 4.3.5 and Table 4.3-II.

Tentative results showed that with appropriate winding design modifications, design current density could be increased to at least 2×10^7 A/m^2 while maintaining or improving stability and reliability criteria. The internally-cooled cabled superconductor (ICCS) configuration was identified as having the greatest potential for cost reduction. More work is required to verify these findings and to develop specific design improvement recommendations.

4.4 Review of HPDE Magnet Failure and Recommendations for Future Action

The magnet for the MHD High Performance Demonstration Experiment (HPDE) at the Arnold Engineering Development Center (AEDC), Tullahoma, TN, suffered a catastrophic failure in its force containment structure during channel performance testing on December 9, 1982. Following the failure, MIT personnel assisted in an in-depth investigation of the failure to determine its cause and to develop plans for future action.

The magnet was a large dual-mode (cryogenic/room temperature) unit with coils of hollow copper conductor, supported by a force containment structure of aluminum alloy and surrounded by a steel flux return frame. The bore dimensions and overall dimensions of the coil and steel are shown in Fig. 4.4.1 and the design characteristics of the magnet are listed in Table 4.4-I. The force containment structure is shown in Fig. 4.4.2.

Based on designs prepared by Magnetic Engineering Associates, the procurement and construction of the magnet was accomplished at AEDC in the period from 1975 through 1978. Prior to the structural failure, the magnet had been operated in the cryogenic mode on a number of test runs, most of which were at fields below 3.8 T, but several of which had attained or approached 4.1 T. The failure occurred at a field level of 4.1 T and led to brittle fractures in most of the structural components, significant displacements of some portions of the iron frame and substantial deformation of the winding with some conductor fracture. No personnel injury occurred because the operating procedures in force at the time of the incident restricted personnel access and required operating personnel to be in a remote control area.

MIT carried out a preliminary failure analysis which is summarized in Reference 3 and in Section 2 of "Safety and Protection for Large Scale Superconducting Magnets - FY 1983 Report" submitted to Idaho National Engineering Laboratory (INEL) (see Appendix B). This analysis concluded that the initiation of the failure was the result of severe overloading of interlocking structural fingers, in the ends of the longitudinal tension members where they penetrated the face plate, or in the collars (see Fig. 4.4.2). Calculations were made showing that at 4 T, the combined stresses due to sidewise bending and axial tension in the fingers exceeded the ultimate strength of the material at 77 K. A review of stress analyses performed during the design phase of the magnet indicated that the high local stresses in the fingers due to combined loading were not detected. It was also concluded that the use of a material having a low ductility may have contributed to the extent of the failure.

Subsequently, the detailed fields and forces were recalculated to check the original design calculations by using contemporary tools and techniques. This work is summarized in the FY84 update of Appendix B. It was found that the actual force values were somewhat less than had been used during the original failure analysis. However, this did not affect any of the conclusions.

Table 4.3-II
Characteristics of Alternative Winding Designs Studied
(see Fig. 4.3.5 for sketches of alternative designs)

Des. No.	Cond. Type	Cond. Curr.	Wind. Curr. Dens. (Av.)	Cu/Sc (λ_{Cu})	Heat Flux	Cu Curr. Dens. (Av.)	Voltage Emerg. Disch.	Stored Energy	Cost Index
		kA	A/cm^2	(λ_{Cu}	ω/cm^2	A/cm^2	kV	MJ	
I	Open Cable 55% void	50	1142	11.4 (0.21)	0.10	5390	5.4	9320	100
II	Open Cable 32% void	50	1544	9.3 (0.23)	0.15	6610	7.1	8150	87
III	Squared Cable 32% void	50	1680	10.3 (0.28)	0.12	5980	5.6	7870	84
IV	ICCS 32% void	50	1960	10.6 (0.34)	0.10	5800	5.0	7440	80
V	ICCS 32% void	25 wound two-in-hand	1960	10.5 (0.34)	0.08	5850	5.1	7440	80
VI	ICCS 32% void	25 wound two-in-hand	2800	6.6 (0.30)	0.16	9251	11.5	6660	71
VII	Built Up	50	3380	11.2 (0.62)	0.30 w/ext. surf.	5480	3.8	6400	69

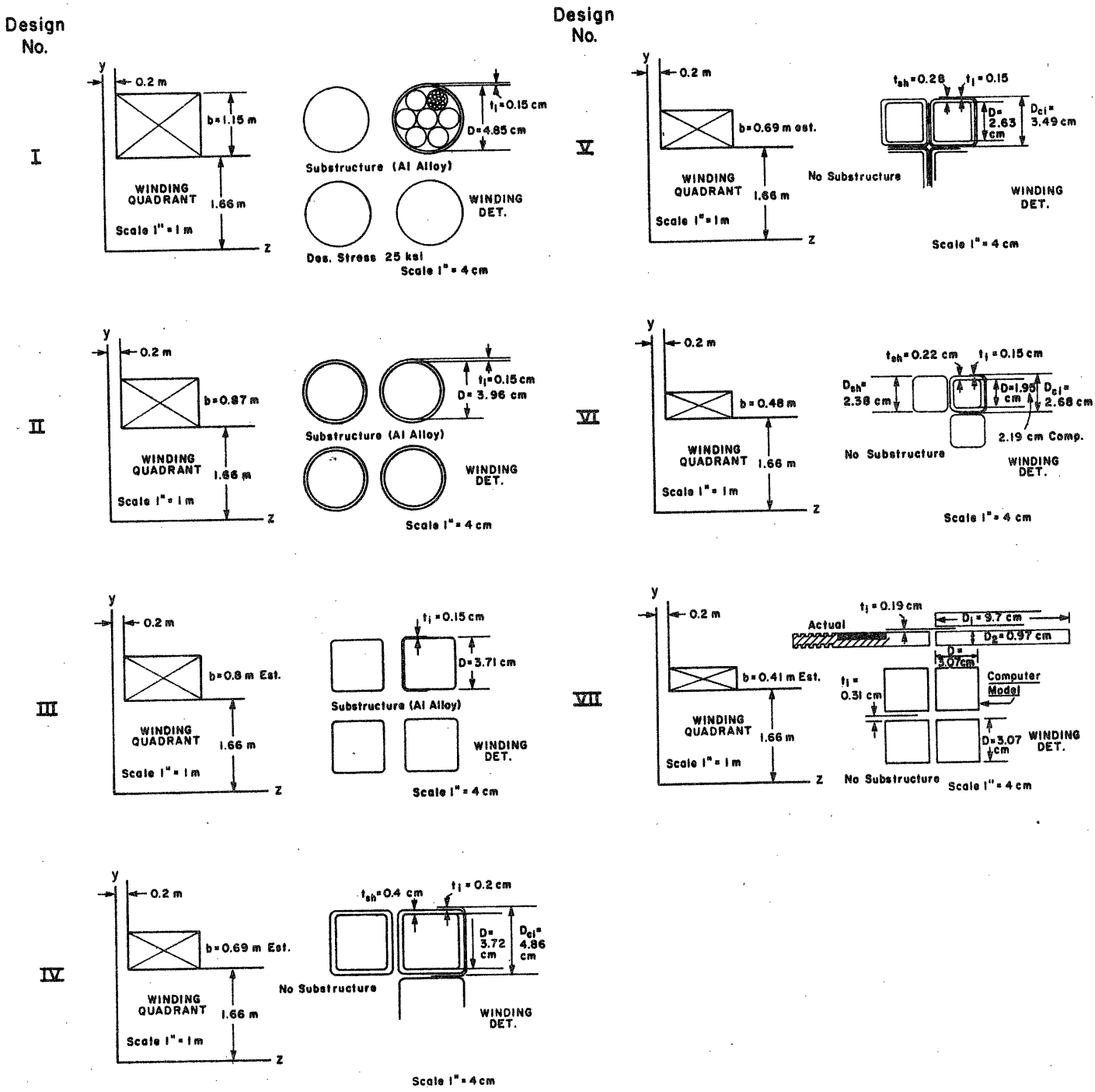

Fig. 4.3.5 Sketches of alternative winding cross sections studied (Note: Scales shown are listed on original copy, prior to reduction) (see Table 4.3-II for characteristics of alternative designs)

Table 4.4-1

Design Characteristics of the Dual Mode HPDE Magnet

Copper conductor weight	83,500 kg
Aluminum structure weight	54,100 kg
Steel weight	500,000 kg
Pole length	7.1 m
Entrance aperture	0.89 m wide × 0.71 m high
Exit aperture	1.40 m wide × 1.17 m high
Half-coil height	0.50 m
Coil width	0.53 m
Space factor	0.8
Turns (total)	720
Length of average turn	22 m
Conductor dimensions	0.025 m × 0.025 m
Cooling passages	0.0068 m ID
Overall length of coil	8.72 m
Cooling requirements	
Liquid nitrogen for initial cooldown	64,000 liters
Liquid nitrogen for recooling	<10,000 liters
Water (27 MW power in)	12.8 m^3/min
Peak axial fields	
Cold mode at pulse peak	6.0 T
Warm mode, continuous	3.7 T

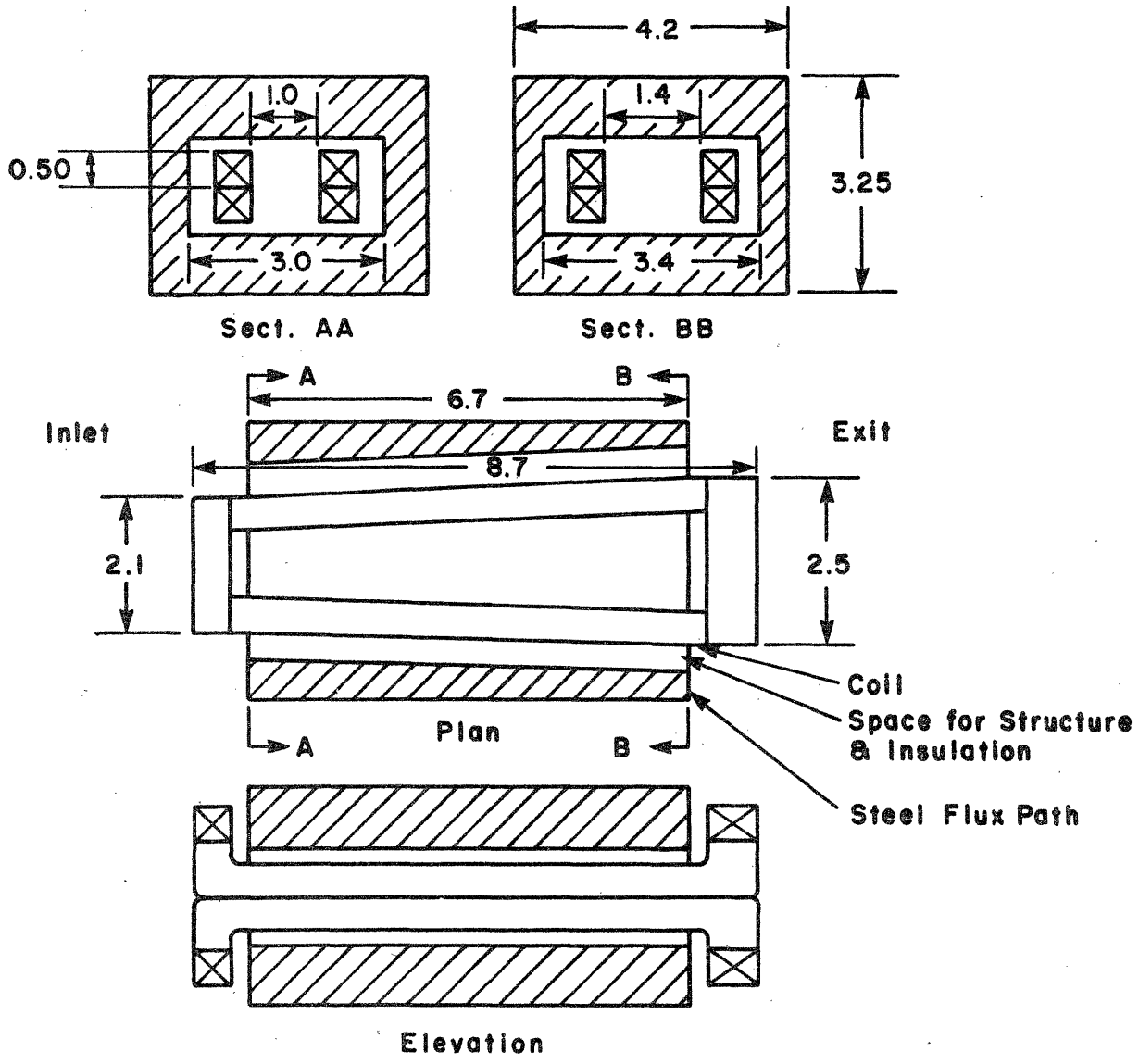

Fig. 4.4.1 Schematic of original HPDE magnet coil and steel flux path

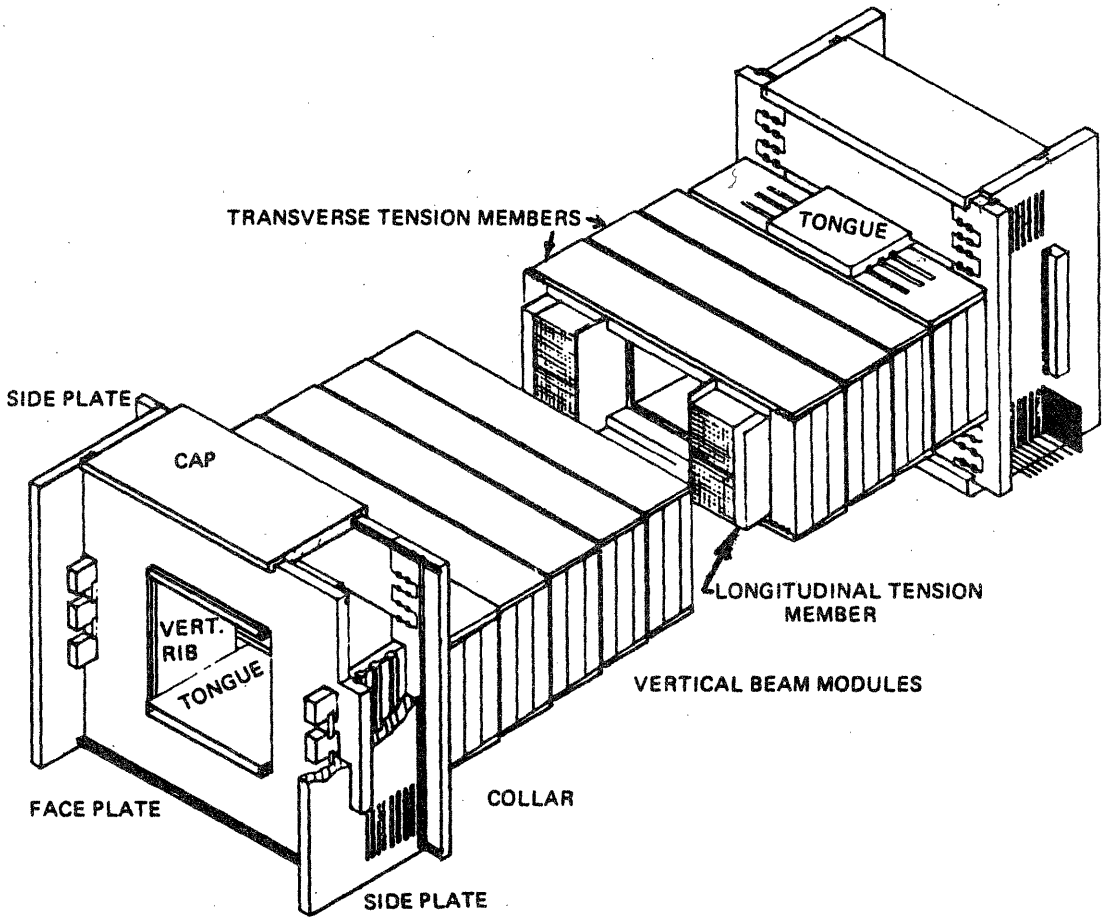

Fig. 4.4.2 Isometric view of original HPDE magnet force containment structure

The condition of the failed parts of the HPDE magnet was investigated by MIT to determine what would be involved in repairing and restoring the magnet to operating condition. It was concluded that the magnet could be restored to test use in the water-cooled mode only (field strengths to 4.0 T) with a reasonable expenditure of time and funds, and that this would be of overall benefit to the MHD program.

A schedule of rework was developed which included stripping, straightening and reinsulating the coils, and redesigning and rebuilding a simplified structure to provide a redesigned room temperature force containment system incorporating the existing steel flux path components, parts of the original aluminum structure and new carbon steel elements to replace aluminum elements damaged beyond repair. The proposed redesigned structure is shown conceptually in Fig. 4.4.3 with estimated weights listed in Table 4.4-II.

In preparing a cost estimate for the rework, vendors were contacted for estimates on stripping insulation from coils and reinsulating coils. The preliminary order of magnitude estimate for coil and structure rework and magnet reassembly was $ 1,500,000.

Observations from the HPDE failure were incorporated in a study of magnetic to kinetic energy conversion following structural failure, and how these considerations relate to safety and protection of large scale superconducting magnets. The study is summarized in Section 3 of the FY 1983 report to INEL (see Appendix B). A significant conclusion was that windings with low enough current density (probably exemplified by the HPDE magnet at 4.1 T) can absorb the total load following structural failure, thus limiting the kinetic energy conversion process (and reducing the extent of the potential damage zone) although this may involve substantial yielding and deformation of the winding itself.

Recommendations made by MIT at the conclusion of their investigation of the HPDE magnet failure included the following:

- Repair and rebuilding of the magnet with a modified structure for test operation in the room temperature mode (4.0 T max) should be accomplished.

- Work should continue toward the development of structural standards for MHD magnets and the eventual acceptance of such standards by the magnet community.

- The broad subject of magnet safety and protection should receive increasing attention in view of the rapid increase in size, stored energy and complexity of the magnet systems required for advanced energy conversion systems, and in view of the criticality of the magnet to such systems.

The HPDE magnet failure was a major incentive for the magnet failure workshop held at the Eighth International Conference on Magnet Technology (MT-8) in Grenoble, September, 1983 (Appendix C). It was pointed out during the introduction to the workshop that magnet "... technology is now adequately mature that future problems will result primarily from failure to use readily available information rather than from some hitherto unknown physical phenomenon." The HPDE magnet failure, together with other failures and problems in large magnets in both the United States and Europe were reviewed and discussed in this workshop.

Table 4.4-II

Estimated Weight of Redesigned Force Containment Structure for HPDE Magnet

Face plate, exit (Aluminum)	1	1,955 kg
Saddle caps, exit (")	2	2,091
Side plates, exit (")	2	1,775
Tongues, exit (")	2	954
Collar, exit (steel)	1	7,045
Face plate, inlet (Aluminum)	1	1,727
Saddle caps, inlet (")	2	1,682
Side plates, inlet (")	2	1,773
Tongues, inlet (")	2	545
Collar, inlet (steel)	1	6,364
Long. tens. members (steel)	set	3,0273
Side beam (Aluminum)	2 sets	15,000
Flux path & misc. (steel)	1 set	45,6363
Total (kg)		**527,548**

Fig. 4.4.3 Schematic of redesigned force containment structure for HPDE magnet

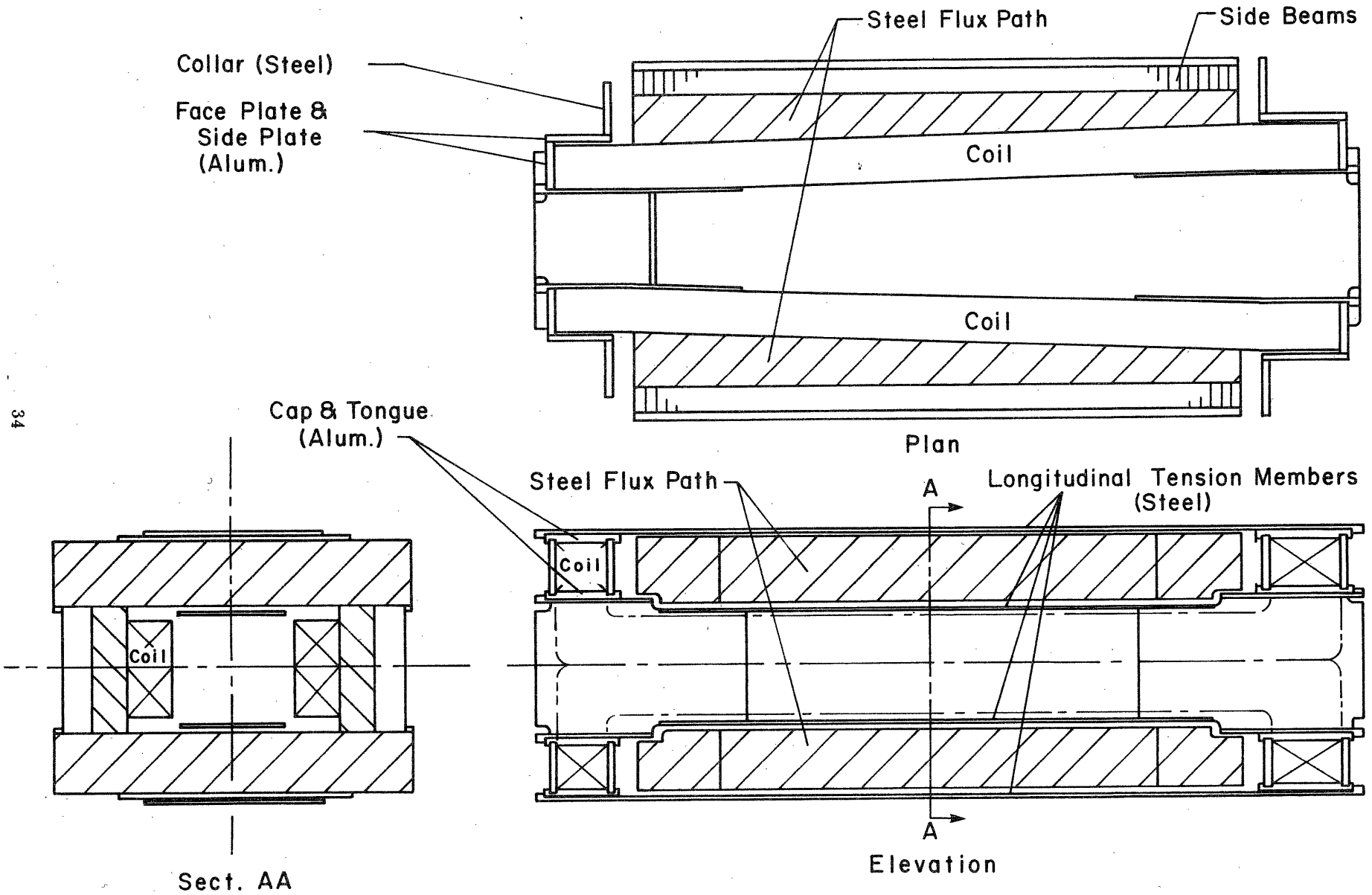

4.5 Development of Preliminary Magnet Designs and Cost Estimates in Support of the PETC MHD Program

Several preliminary designs and cost estimates were developed for magnets for use in alternative MHD flow trains under consideration by PETC. These were generally smaller scale and/or lower field systems that would be advantageous in providing commercial plant experience with MHD components at costs substantially below that of the MHD 200 MWe Engineering Test Facility (ETF) conceptual design developed in 1981.[4]

Major design characteristics and estimated costs for four preliminary designs are listed in Table 4.5-I. Estimated costs plotted vs. the size parameter, VB^2, are shown in Fig. 4.5.1, together with costs of other magnets (CDIF/CM, CDIF/SM, HPDE, ETF/SM4 and ETF/SM6) for comparison. The parameter VB^2 is explained in Appendix E.

The preliminary designs for the four alternative magnets are described in more detail in the following sections.

4.5.1 4.5 T Superconducting Magnet for MERDI MHD System (29 MWe)

A preliminary design and a cost estimate were developed in March 1983 for a 4.5 T superconducting MHD magnet system in response to a request from Multi-Tech Corporation of Butte, MT, representing Montana Energy Research and Development Institute (MERDI). Bore dimensions and active length, supplied by Multi-Tech, were intended to provide for a channel of 29 MWe output.

The MIT-developed design was similar in concept to the magnet of the MHD ETF 200 MWe Power Plant[4]. The winding consisted of rectangular saddle coils of copper-stabilized niobium titanium cable type conductor (bath-cooled), supported in an insulating (glass-reinforced plastic) substructure. The coils were mounted in a liquid helium filled stainless steel containment vessel. A stainless steel force containment structure surrounded the coils and containment vessel. The coil and structure assembly was mounted in a stainless steel cryostat. Accessories included cryogenic support equipment with refrigerator/liquefier and power supply and discharge equipment.

The design characteristics of the magnet are listed in Table 4.5.1-I. The estimated (budgetary) price for the system was $\$30 \times 10^6$.

A description of the magnet system design, including accessories and the budgetary price estimate was transmitted to Multi-Tech Corp. by letter on March 10, 1983 (see Appendix F).

4.5.2 4 T Water-Cooled Magnet for MHD ETF

A preliminary design and a cost estimate for a 4 T water-cooled magnet for an alternative flow train in the MHD Engineering Test Facility[4,5] (ETF) were developed in December, 1983. Bore dimensions and active length were taken to be the same as in the superconducting ETF magnets[4,5]. It was assumed that the full output of the channel would be available for powering the magnet.

The magnet was generally similar to the CDIF/CM and AVCO/CM test facility magnets[1]. It consisted of a pair of rectangular saddle coils of square, hollow copper conductor insulated with fiberglass tape and mounted in a steel yoke serving as both flux path and structural support for the center portion of the coils. Additional steel structure was provided to support the end turns. The coils and steel flux path diverged from inlet to exit end to provide a tapered field profile. Because of the relatively large size and high magnetic forces characterizing this magnet, the flux path structure combination was designed as a continuous assembly and the magnet did not have the roll-apart feature of the smaller CDIF/CM and AVCO/CM magnets.

Table 4.5-I

Major Design Characteristics and Estimated Costs of Alternative MHD Magnets

Magnet Type and Application		Super-conducting Magnet MERDI	Water Cooled Magnet ETF	Water Cooled Magnet Retrofit	Super-conducting Magnet Retrofit
Channel power, nominal	MWe	29	70-100	50	35
Peak on-axis field	T	4.5	4.0	4.5	4.5
Active field length	m	10	12.1	10	9.5
Warm bore aperture, start a.l.[a]	m	0.8×0.8	1.4×1.8	1.0×1.0	0.9×0.9
Warm bore aperture, end a.l.[a]	m	1.5×1.5	2.1×2.7	1.5×1.5	1.6 ×1.6
Conductor type		Cable NbTi/Cu	Hollow Cu	Hollow Cu	ICCS[b] NbTi/Cu
Average winding current density	$10^7 A/m^2$	1.4	0.84	0.87	1.63
Ampere turns	10^6 A	15	10.6	9.1	16
Stored energy	MJ	700	—	—	750
Estimated power loss in coil	MW	—	65	50	—
Weight conductor	tonnes	75	250	205	80
Weight steel flux path	tonnes	—	1890	1000	—
Weight total	tonnes	370	2260	1315	385
Size parameter, VB^2	m^3T^2	150	400	205	185
Estimated cost	10^6 $	30[c]	20-30[d]	15-20[d]	40[c]

a Active length

b Internally-cooled cable superconductor

c Including contingency allowance of 30 %

d Not including contingency allowance

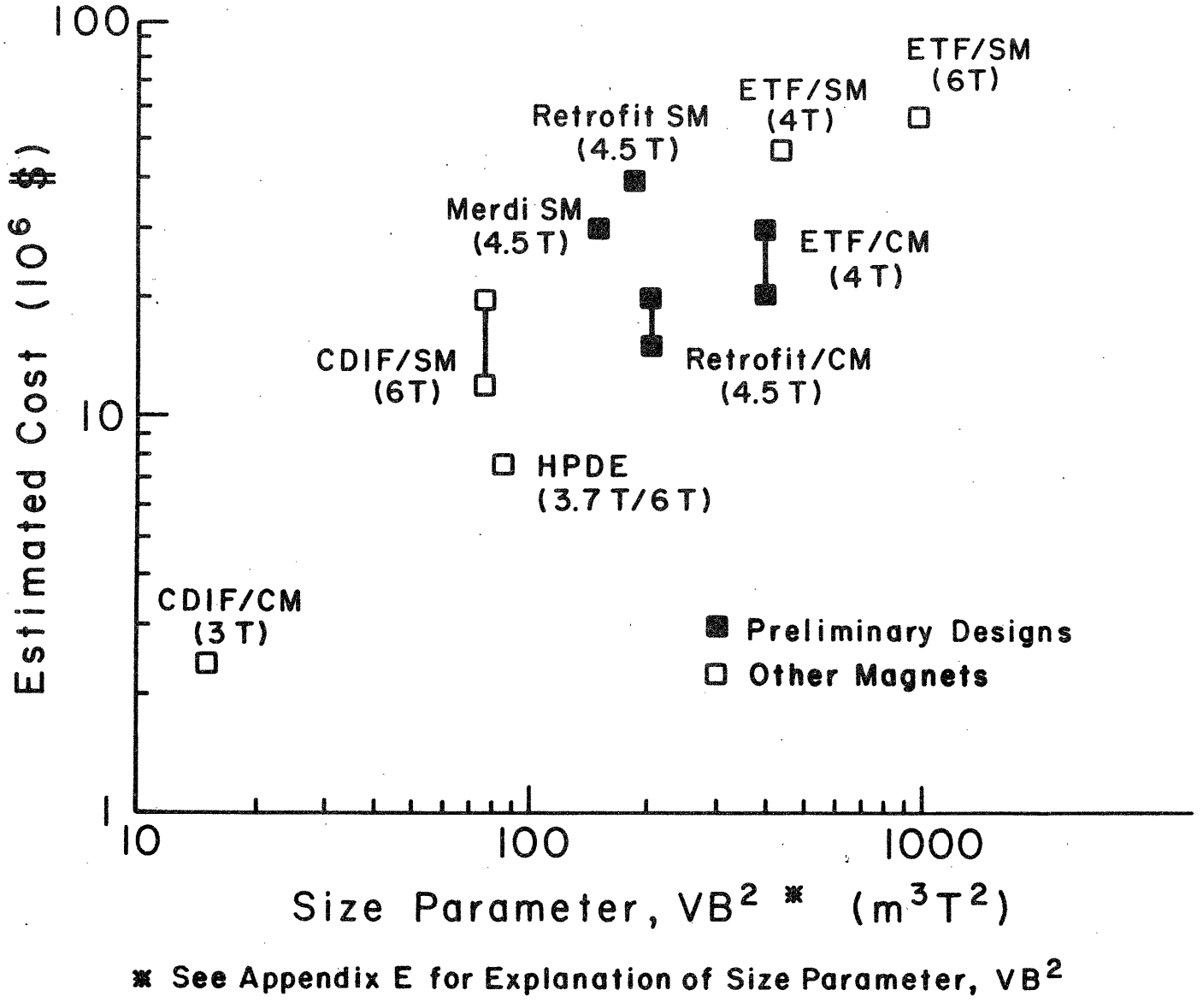

Fig. 4.5.1 Graph of estimated costs of alternative MHD magnet designs plotted vs. size parameter VB^2 (data for other magnets included for comparison)

Table 4.5.1-I

4.5 T Superconducting Magnet for MERDI MHD System (29 MWe)

Peak on-axis field	4.5 T
Active field length	10 m
Field at start of active length	3.6 T
Field at end of active length	2.7 T
Warm bore aperture, start of active length	0.8 m × 0.8 m
Warm bore aperture, end of active length	1.5 m × 1.5 m
Vacuum vessel overall length	14.2 m
Vacuum vessel outside diameter	6 m
Size parameter, VB^2	150 m^3T^2
Conductor type	Round cable
Conductor outside dimensions	2.85 cm (dia.)
No. of turns, total	760
Length mean turn	29.6 m
Length conductor, total	22.5 km
Design (operating) current	20 kA
Average winding current density	1.4×10^7 A/m^2
Ampere turns	15×10^6 A
Inductance	3.5 henries
Stored energy	700 MJ
Weights: Conductor	75 tonnes
Substructure	60 tonnes
Superstructure and coil containment vessels	125 tonnes
Thermal radiation shield, cold mass supports	20 tonnes
Vacuum vessel	80 tonnes
Miscellaneous	10 tonnes
Total Magnet Weight	**370 tonnes**

The design characteristics of the water-cooled 4 T ETF magnet are listed in Table 4.5.2-I. A sketch of the cross section of the coils and flux path steel at the plane of peak on-axis field is shown in Fig. 4.5.2.1. An order of magnitude cost estimate was made, indicating that the cost would be between $\$20 \times 10^6$ and $\$30 \times 10^6$ without contingency allowance.

After completion of the preliminary design, consideration was given to possible improvements that might result from further design and development effort. It was concluded that changing to an air core design (eliminating the large steel flux path) would greatly reduce overall size and weight and make installation much easier. In addition, the incorporation of the roll-apart feature and a reduction in bore size (made possible by providing radial access for pipes and wires) would further reduce size and weight and improve the effectiveness of the magnet system.

4.5.3 4.5 T Water-Cooled Magnet for Retrofit MHD System (50 MWe)

A preliminary design and a cost estimate for a 4.5 T water-cooled magnet for a 50 MWe MHD retrofit system were developed in March and April, 1984. Data used as a basis for the design were an iron length of 12 m and warm bore dimensions 1.0 m square at inlet and 1.5 m square at exit. It was assumed that the 50 MWe MHD output would be used to power the magnet.

The magnet was similar in concept to the 4 T ETF water-cooled magnet described in Section 4.5.2. The design characteristics are listed in Table 4.5.3-I. A sketch of the cross section of the coils and flux path steel at the plane of peak-on-axis field is shown in Fig. 4.5.3.1. An order of magnitude cost estimate was made indicating that the cost would be between $\$15 \times 10^6$ and $\$25 \times 10^6$ without contingency allowance.

4.5.4 4.5 T Superconducting Magnet for Retrofit MHD System (35 MWe)

A preliminary design and cost estimate for a 4.5 T superconducting magnet for a 35 MWe MHD retrofit system were developed in April 1984. Data used as a basis for the design were active length 9.5 m, field at the start of active length (inlet) 3.4 T, field at end of active length (exit) 2.6 T, inlet aperture 0.9 m square, exit aperture 1.6 m square.

The MIT-developed design incorporated a rectangular saddle coil configuration similar to that of the magnet for the MHD ETF 200 MWe Power Plant[4]. However, the conductor was internally-cooled, cabled conductor[7,10] (copper-stabilized NbTi) with a stainless steel sheath wrapped with continuous insulation instead of the open, bath-cooled cable used in the ETF design. Also, the substructure was aluminum alloy instead of the glass-reinforced plastic used in the ETF design.

The design characteristics of the magnet are listed in Table 4.5.4-I. Outline dimensions of the magnet assembly are shown in Fig. 4.5.4.1. The estimated budgetary price for the system, including design and analysis, supporting development, project management, accessories and a contingency allowance was $\$50 \times 10^6$.

A six-year program outline was prepared and submitted to PETC, the end-product of which was an installed magnet system for a 35 MWe power train. The outline included a summary of technology status, a discussion of technical problem areas, a list of magnet system characteristics and the estimated distribution and profile of the funding that would be required (see Appendix G).

4.6 Channel/Magnet Interfacing Support to APT Contractors

In communications between MIT and AVCO in December, 1983, the latter expressed a need for technical

Table 4.5.2-I

Design Characteristics of 4 T Water-Cooled Magnet for MHD Engineering Test Facility (ETF/CM)

Peak on-axis field (B_p)	4.0 T
Coil Contribution	2.75 T
Iron Contribution	1.25 T
Iron length	12.1 m
Active length (0.675 B_p to 0.6 B_p)	12.1 m
Field at start of active length	2.7 T
Field at end of active length	2.4 T
Warm bore aperture, start of active length	1.4 × 1.8 m
Warm bore aperture, end of active length	2.1 × 2.7 m
Magnet overall length	15 m
Magnet height and width, large end	6 × 5.6 m
Size parameter (VB^2)	400 m^3T^2
Conductor type	Hollow copper
Conductor outside dimensions	2.8 × 2.8 cm
No. of turns, total	928
Length mean turn	38.8 m
Length conductor, total	36 km
Design (operating) current	8150 A
Average winding current density	0.84×10^7 A/m^2
Packing factor (copper)	0.75
Current density in copper	1.12×10^7 A/m^2
Ampere turns	10.6×10^6 A
Weights: Conductor	250 tonnes
Insulator	10 tonnes
Steel flux path	1890 tonnes
Steel, other	110
Total	**2260 tonnes**

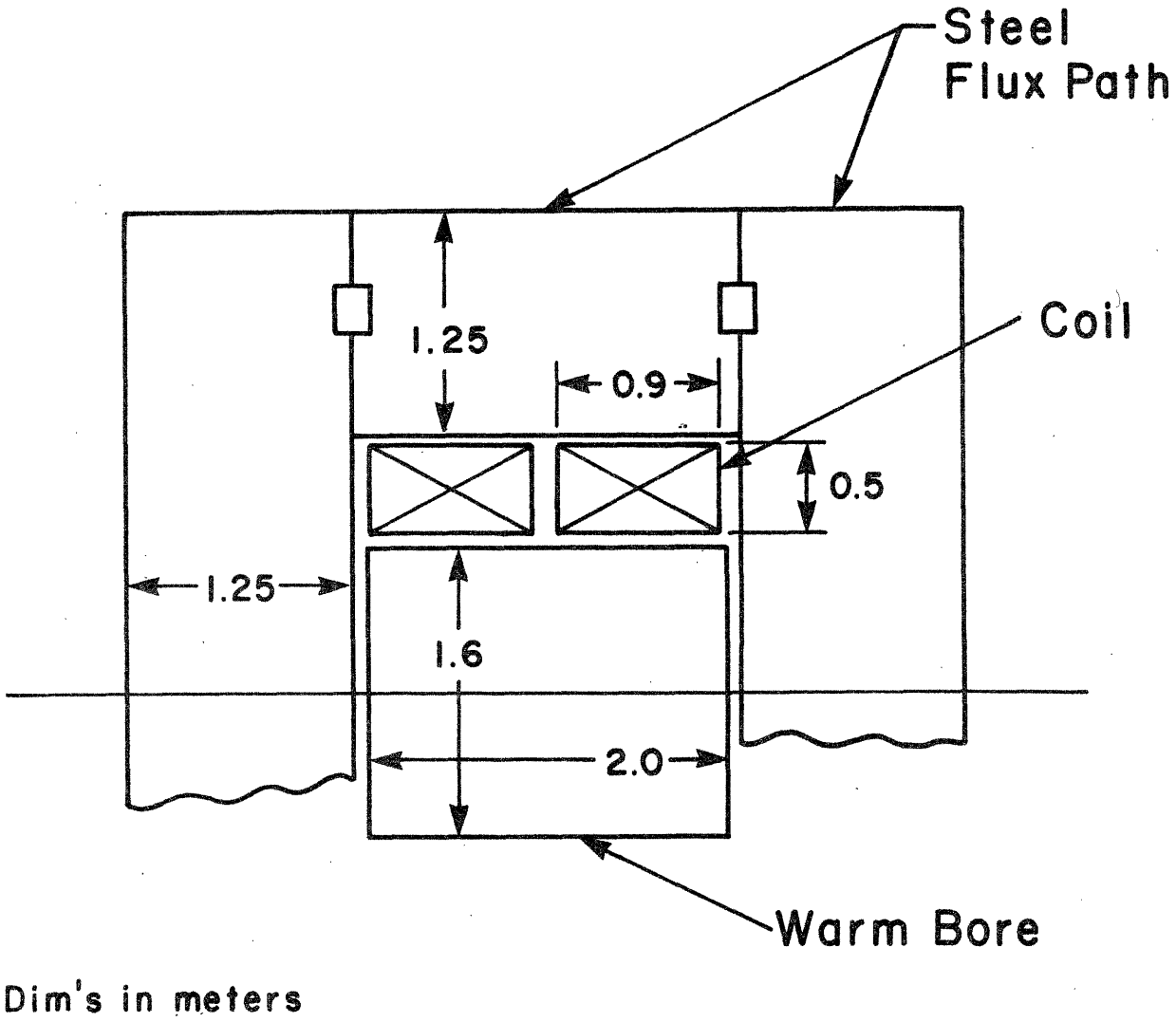

Fig. 4.5.2.1 Sketch of cross section of coils and steel flux path at plane of peak on-axis field, water-cooled magnet for ETF MHD system

Table 4.5.3-I

Design Characteristics of 4.5 T Water Cooled Magnet for Retrofit MHD System (50 MWe)

Peak on-axis field	4.5 T
Coil Contribution	3.25 T
Iron Contribution	1.25 T
Iron length	12 m
Active field length	10 m
Field at start of active length	3.6 T
Field at end of active length	2.7 T
Warm bore aperture, start of active length	1.0 × 1.0 m
Warm bore aperture, end of active length	1.5 × 1.5 m
Magnet overall length	15.5 m
Magnet height & width, large end	4.7 × 4.7 m
Size parameter (VB^2)	205 m^3T^2
Conductor type	Hollow copper
Conductor outside dimensions	2.8 × 2.8 cm
No. of turns, total	916
Length mean turn	32.2 m
Length conductor, total	30 km
Design (operating) current	9 kA
Average winding current density	0.87×10^7 A/m^2
Packing factor (copper)	0.75
Current density in copper	1.16×10^7 A/m^2
Ampere turns	9.1×10^6 A
Estimated power	50 MW
Cooling water flow	350 kg/s
Cooling water temperature rise	34 C
Weights: Conductor	205 tonnes
Insulator	10 tonnes
Steel flux path	1000 tonnes
Steel, other	100
Total	**1315 tonnes**

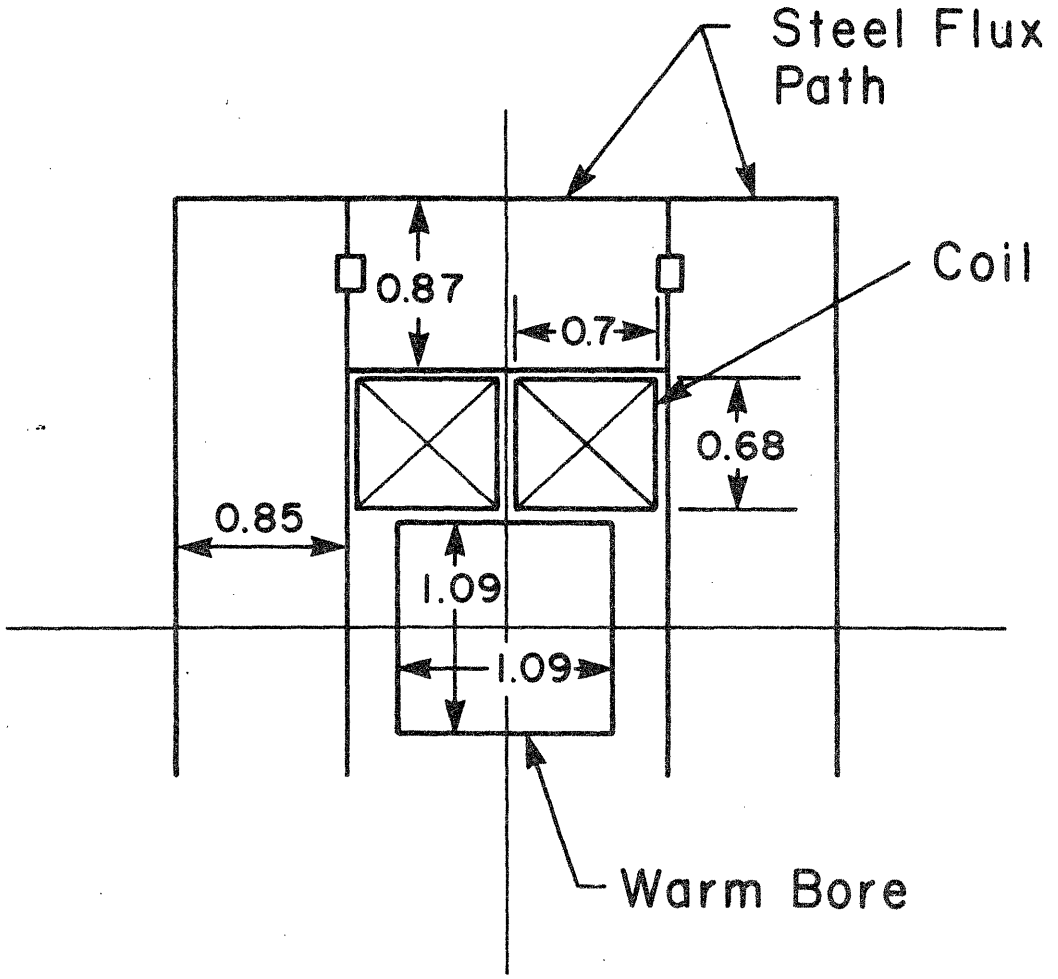

Fig. 4.5.3.1 Sketch of cross section of coils and flux path at plane of peak on-axis field, water-cooled magnet for retrofit MHD system (50 MWe)

Table 4.5.4-I

Design Characteristics of 4.5 T Superconducting Magnet for Retrofit MHD System (35 MWe)

Peak on-axis field	4.5 T
Active field length	9.5 m
Field at start of active length	3.4 T
Field at end of active length	2.6 T
Warm bore aperture, start of active length	0.9 × 0.9 m
Warm bore aperture, end of active length	1.6 × 1.6 m
Vacuum vessel overall length	13 m
Vacuum vessel outside diameter	6.6 m
Size parameter (VB^2)	185 m^3T^2
Conductor type	ICCS[a]
Conductor outside dimensions	2.5 × 2.5 cm
No. of turns, total	624
Length mean turn	29.8 m
Length conductor, total	18.6 km
Design (operating) current	25 kA
Average winding current density	1.63×10^7 A/m^2
Ampere turns	15.6×10^6 A
Stored energy	700 MJ
Weights: Conductor	70 tonnes
Insulator & misc	10 tonnes
Substructure	40 tonnes
Superstructure and containment vessels	150 tonnes
Cryostat	100
Total	**370 tonnes**

a internally-cooled cable superconductor

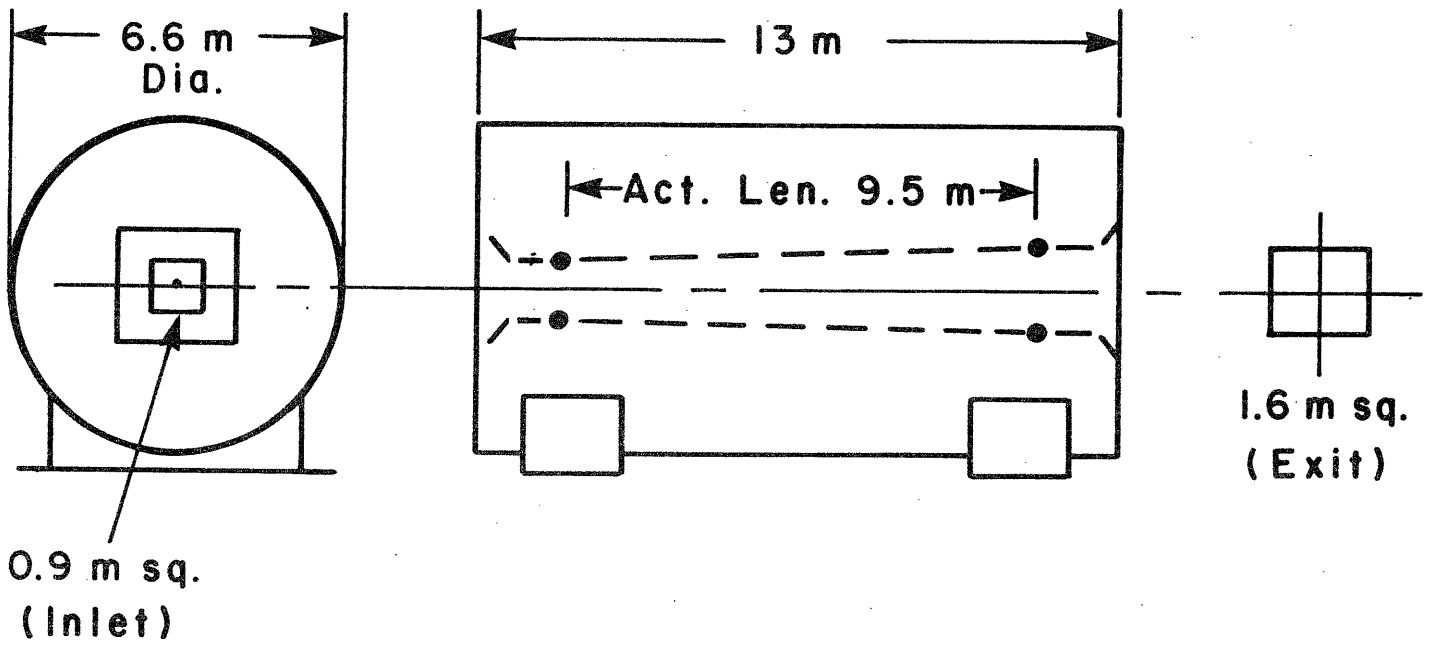

Fig. 4.5.4.1 Outline, 4.5 T superconducting magnet for retrofit MHD system (35 MWe)

and cost information on magnets for use in their Advanced Power Train (APT) studies. As a result, MIT representatives visited AVCO Everett Research Laboratory, Inc. on January 17, 1984 and discussed general aspects of channel/magnet interfacing with AVCO and GE representatives. Since the APT magnet requirements differ from earlier requirements (ETF, PSPEC, etc.) new magnet size, weight and cost estimates are needed. Also, channel/magnet interfacing should be an important part of the APT studies because careful integration of flow train and magnet is critical to the success of the system. Means of flow train support in the region of the magnet, and means of channel changeout (including consideration of magnet roll apart or roll aside) require conbined efforts of channel and magnet designers.

It was agreed that MIT support to APT contractors (GE and Westinghouse) would be in the best interests of the program. Packages containing channel/magnet interfacing information developed in the past were sent by MIT to GE, Westinghouse and PETC. Included were the following:

Interim Report - MHD Channel/Magnet Packaging Study, FBNML/MIT, July 1980

FBNML/MIT internal memo, MHD Magnet-Flow Train Interfacing Meeting (11/18/80), memo dated 12/3/80

Conference Paper, "Magnet-Flow Train Interface Considerations," P.G. Marston, et al., SEAM 1981

Report, "MHD Generator Superconducting Magnet Packaging Study," T.R. Brogan, MEPPSCO, August 1981

The MIT covering letter (Appendix D) contained a support program definition for collaboration with both AVCO and Westinghouse (individually) and provided an estimated cost for such an effort through the fiscal year.

4.7 Review of Cost Estimating, Cost Analysis and Cost Reduction Work on MHD Magnets, Including Comparison with Fusion Magnet Costs

Work relating to magnet system and component costs performed at MIT and by subcontractors in the period from 1976 to the present has been reviewed, and preparation of a report has been started. A rough draft of the report was about 80% complete when work was stopped due to lack of funds. The report, when completed, will be a valuable aid in improving the credibility of future magnet cost estimates and in implementing cost reduction measures. It should therefore be completed as soon as possible. The scope and outline of the report are given in the following sections.

4.7.1 Scope

The report summarizes cost estimating, cost analysis and cost reduction work done as a part of the MHD Magnet Technology Development Program at MIT from 1976 to the present. It describes cost estimating methods used by MIT and by subcontractors in estimating the costs of MHD magnet systems; it documents the estimated costs and in some cases, actual manufacturing costs of a number of MHD magnets and other large superconducting magnets designed in the past 8 years; and, it reviews cost analysis and cost reduction studies of MHD magnets that have shown ways by which significant cost reductions can be achieved.

4.7.2 Outline

The outline for the cost report which is now being written at MIT is given below:

1.0 Introduction

(Purpose and scope of report)

2.0 Discussion

(Importance of magnet costs in overall MHD program. Review of magnet program status)

3.0 Summary, Cost Estimating Work

- 3.1 Cost Estimating Using Empirical Cost Curves
- 3.2 Cost Estimating Using Magnet Overall Cost Algorithms
- 3.3 Cost Estimating Using Component Cost Algorithms
- 3.4 Cost Estimating Starting with Material, Labor and Overhead Costs (Detailed Estimates)
- 3.5 Estimate of Cost Reduction Resulting from Multiple Unit Production
- 3.6 Cost Estimates of Disk-Type Magnets
- 3.7 Comparative Costs of MHD Magnet and Fusion Magnet Components

4.0 Summary, Cost Analysis and Cost Reduction Studies

- 4.1 Relationship of Magnet System Cost to Overall Power Plant Costs
- 4.2 Comparison of Unit Costs ($ /kg) of Magnet and Other Items of Heavy Industrial Equipment
- 4.3 Identification of Major Cost Items in MHD Magnet Systems
- 4.4 Cost Reduction Through Improved Channel/Magnet Packaging
- 4.5 Study of Impact of High Current Operation on Magnet System Cost
- 4.6 Computer-Aided Study of Impact of Design Current Density on Magnet System Cost
- 4.7 Effects of Material Selection and Design Stress on Cost
- 4.8 Comparative Costs of Circular vs. Rectangular Saddle Coil Magnets
- 4.9 Comparative Analysis of Costs of CDIF/SM and CFFF Magnets

5.0 References

1. MHD Magnet Technology Development Program Summary, September 1982, Plasma Fusion Center, MIT, November 1983.

2. Hatch. A.M., et al., Design Current Density Impact on Cost and Reliability of Superconducting Magnet Systems for Early Commercial MHD Power Plants, Journal de Physique, Coll. C1, Supp. 1, Tome 45, C1-1984: C1-867. Jan. 1984.

3. Becker, H. et al., Failure of a Large Cryogenic Magnet, Journal de Physique, Coll. C1, Suppl. Tome 45, C1-1984; C1-603, Jan. 1984.

4. NASA/LeRC Conceptual Design Engineering Report - MHD Engineering Test Facility 200 MWe Power Plant, prepared for NASA/LeRC for DOE by Gilbert/Commonwealth, DOE/NASA/0224-1 Vol. I-V, September 1981.

5. MHD Magnet Technology Group, MIT, Conceptual Design of Superconducting Magnet System for MHD ETF 200 MWe Power Plant, Final Report, November 1981.

6. General Electric Co., Design Summary Report, Phase II, Detailed Design, Manufacture, Installation and Test of a Superconducting MHD Magnet (for CDIF), prepared for MIT/FBNML, PO ML65100, June 1979.

7. Hoenig, M.O., Internally-Cooled Cable Superconductors, Cryogenics, 20(7): 373-389 and 20(8): 427-434, 1980.

8. Hals, F.A., et al., Results from Comparative Analysis of Different MHD Generator and Power Train Designs for Early Commercial Power Plant Applications, 21st Symposium on Engineering Aspects of Magnetohydrodynamics, Argonne, IL, 1983.

9. Argonne National Laboratory, Design, Construction and Performance Test of a Six Tesla Superconducting Dipole Magnet System for Magnetohydrodynamic Energy Conversion Research, ANL/MHD-84-2.

10. Bobrov, E.S. and P.G. Marston, Theoretical and Engineering Aspects of Momentless Structures for MHD Magnets, 1980 Superconducting Magnet Design Conference, pp. 90-102, MIT, 1980.

Appendix A

Hatch, A.M., et al., Impact of Design Current Density on the Cost and Reliability of Superconducting Magnet Systems for Early Commercial MHD Power Plants

21st Symposium, Engineering Aspects of MHD

Argonne National Laboratory

June 1983

IMPACT OF DESIGN CURRENT DENSITY ON THE COST AND RELIABILITY OF SUPERCONDUCTING MAGNET SYSTEMS FOR EARLY COMMERCIAL MHD POWER PLANTS[a]

A. M. Hatch, P.G. Marston, R.J. Thome, A.M. Dawson, W.G. Langton, W.R. Mann

Plasma Fusion Center
Massachusetts Institute of Technology
Cambridge, Massachusetts 02139

ABSTRACT

The impact of the design current density on the estimated cost of large superconducting MHD magnet systems was investigated with the aid of design scaling and cost estimating computer codes. Major emphasis was placed on systems of the size required for linear MHD generators in the channel power output range of 100 to 1100 MWe. Copper-stabilized NbTi windings with average current densities from 0.75×10^7 A/m^2 to 2.5×10^7 A/m^2 were considered. Results indicated that design current density has a significant effect on system cost, particularly for systems in the lower range of powers considered. For example, a reduction of roughly 35% in overall magnet system cost would be expected when design current density is increased from 1.0×10^7 A/m^2 to 2.0×10^7 A/m^2 in magnets at the small end of the size range. A reduction of roughly 30% would be expected for the same current density increase in magnets at the large end of the size range.

The impact of design current on certain aspects of magnet reliability was also explored. Higher current density implies a smaller winding cross section with less space available for copper stabilizer, supporting substructure and insulation. Therefore, problems of stabilization become more critical. Practical limits for stability criteria including heat flux and ratio of liquid helium to conductor volume were examined in relation to overall winding current density. Quench protection was also investigated, in particular the problem of dumping stored magnetic energy into external resistors fast enough to prevent overheating of regions of normal conductor. Results indicated that provisions to assure adequate stability and protection become more complicated for higher current densities and larger magnet sizes, and reliability is reduced.

In final designs for large MHD magnets, selection of average current density should be based on careful consideration of its effects both on magnet cost and on criteria affecting reliability. Results of the overall investigation are summarized in curves of various parameters vs winding average current density, including magnet weight, magnet system estimated cost, conductor stabilizer current density, conductor copper-to-superconductor ratio and maximum terminal voltage under emergency discharge conditions.

[a]Supported in part by the Office of Fossil Energy, MHD Division, U. S. Department of Energy.

INTRODUCTION

High reliability and long service life are prerequisites for superconducting magnets for commercial MHD power plants. These prerequisites dictate conservatism in magnet design, which can be achieved more easily if design current densities are kept low. Low capital cost is also an important consideration for commercial size MHD magnets, because the cost of the magnet system represents one of the largest component costs in the MHD topping cycle.

In developing designs for commercial MHD magnets, tradeoffs must be made between the cost advantages of higher design current densities and the resulting greater risks and/or special design provisions associated with the higher current densities.

The main purpose of the study reported here was to obtain quantitative information on the effect of design current density on magnet cost. It was intended that the results of the study would be useful in future design work on commercial-size MHD magnets, particularly with regard to the tradeoffs between the cost advantages of high current density and the adverse effects on other aspects of the design.

For the limited number of computer-generated designs covered in this paper, characteristics at the extremes of the parametric range, though believable, do not necessarily represent good design practice. The fact that certain computed characteristics tend to exceed practical limits emphasizes the importance of careful cost/risk assessment when final designs are developed.

APPROACH

In reviewing MHD magnet designs developed in the past, it is noted that winding (average) current densities become lower as magnet size is increased. This trend is shown in Table I, which lists representative MHD magnet designs, both commercial-size and test-facility size, with current densities ranging from 1.15×10^7 A/m^2 for the largest to 2.85×10^7 A/m^2 for the smallest. Based on these data, the range from 0.75×10^7 A/m^2 to 2.5×10^7 A/m^2 was selected as appropriate for this study.

A series of magnet reference designs of different bore sizes, representing magnets for power plants in the 100 to 1100 MWe range, and all embodying the same design concepts, were used as a basis for the study. For each magnet size, at least three current densities between 0.75×10^7 A/m^2 and 2.5×10^7 A/m^2 were considered. With the aid of computer programs and using scaling techniques, the characteristics and estimated costs of magnets of each bore size and current density were calculated. Curves were then plotted to show how cost, weight and other characteristics varied with design current density.

Particular attention was given to characteristics relating to reliability and safety. For typical winding designs, the impact of increased current density on stability criteria such as copper-to-superconductor ratio, heat flux and helium-to-conductor volume ratio were considered. Also considered were items such as the temperature rise in the winding when all stored magnetic energy is dumped into the winding as heat, and the peak terminal voltage when the magnetic energy is dumped into external resistors fast enough to prevent overheating of limited regions of normal conductor.

SIZES AND DESIGNS OF MAGNETS STUDIED

To cover the MHD channel power size range from 100 to 1100 MWe, three magnet bore sizes and active lengths were selected, based on the conceptual designs for the Engineering Test Facility (ETF)[1], the Commercial Demonstration Plant (CSM) [2] and a Large Baseload (LBL) system. The first two designs were developed in 1979-1981 as a

TABLE I

DESIGN CHARACTERISTICS

REPRESENTATIVE MHD MAGNET DESIGNS

Magnet Identification		U25	CDIF	CFFF	ETF	CASK	CSM
Field	T	5	6	6	6	6	6
Warm bore inlet aperture	m	0.4 dia.	0.78 x 0.97	0.8 dia.	1.5 x 1.9	2.48 dia.	2.2 x 2.8
Active length [a]	m	2.5	3.4	3.2	11.7	14.5	14.5
Stored energy	MJ	34	240	216	2900	6300	7200
Build	m	0.364	0.622	0.53	0.95	0.74	1.08
Design Current	kA	0.89	6.13	3.675	24.4	50.0	52.2
Current density, winding	10^7 A/m^2	2.82	1.87	2.0	1.42	1.28	1.15
Current density, conductor	10^7 A/m^2	5.0	6.28	2.63	8.16	2.2	5.7
Type of conductor	---	Rect. Built-up	Squ. Built-up	Rect. Built-up	Round Cable	Rect. Built-up	Round Cable
Substructure material	---	Fiber-glass & St. Steel [b]	Fiber-glass [b]	Fiber-glass [b]	Fiber-glass	St.Steel	Fiber-glass

Notes: a. Active length for all magnets is distance between on-axis field points of 0.8 B_{peak} at inlet and 0.6 B_{peak} at exit.

b. Banding between winding layers is used in place of a rigid substructure.

part of the DOE Magnet Technology Development Program. [3] The basic characteristics of the third design (LBL) were developed specifically for this study by scaling from the CSM design.

In addition to these three relatively large designs, a smaller magnet design, based on the Component Development and Integration Facility (CDIF) superconducting magnet [4] was also included in the study for comparative purposes. Basic characteristics of the four magnet designs considered are listed in Table II.

For consistency in the study itself, all designs used are of the rectangular saddle-coil type with rectangular warm bores, copper-stabilized NbTi conductor and rectangular frame winding support structures of stainless steel. Designs of other types, such as circular saddle coils with circular warm bores, would be expected to show the same trends with regard to the impact of current density on magnet cost and other characteristics.

For uniformity in comparing overall magnet characteristics, all magnet designs used in the study incorporated round cable conductors and insulating (fiberglass) substructures of the type used in the ETF magnet conceptual design [1] and shown in Fig. 1. For the purpose of determining copper and superconductor volumes, it was assumed that magnet windings were ungraded.

CALCULATION METHOD

A model to serve as a basis for the calculation of magnet characteristics was established as follows:

The winding configuration used was a rectangular saddle coil winding as shown in Fig. 2, generally similar in shape to the windings of the ETF, CSM and CDIF/SM designs[1,2,4]. A section through the winding, perpendicular to the axis and in the plane of peak-on-axis magnetic field (Plane P in Fig. 2) is shown in Fig. 3.

Design (winding) current density as referred to in this paper is the average current density in the winding cross section, shown in Fig. 3, required to produce the design field at the MHD channel axis.

To lower (or raise) the design current density while maintaining constant magnetic field on axis (at point 0), the area of the winding cross section is increased (or decreased) by varying the build, b, and width, d, as illustrated in Fig. 3.

For purposes of the study the following relationships were used:

$$I = 2aj \tag{1}$$

$$B = \frac{4It}{t^2 + s^2} \times 10^{-7} \tag{2}$$

where:

I = total ampere turns in winding (A)

a = area of winding cross section, one quadrant (m^2)

j = design current density (A/m^2)

B = peak on-axis field (T)

t = distance from Z axis to coil center, one quadrant (See Fig. 3)

s = distance from Y axis to coil center, one quadrant (See Fig. 3)

Combining (1) and (2)

$$j = \frac{B(t^2 + s^2)}{8at} \times 10^7 \qquad (3)$$

When varying b, it was assumed that good field uniformity in the channel cross section would be assured by restricting the center of coil quadrant cross section to lie on the radial line O-A. It was assumed also that the dimensions e and m would remain constant for a given magnet bore size to provide necessary space for structure and vacuum insulation.

Equation (2) calculates the field produced by infinitely long, parallel current filaments. It is therefore a means only of obtaining an approximation of the field at the axis of the saddle coil system, which is finite in length, tapered and has crossovers. However, experience has shown that results using Eq. (2) and an empirical correction factor are sufficiently accurate for the purposes of a study such as this.

An initial computer program, Scaler 1, was written to calculate the characteristics of a series of windings of different current densities for given bore sizes, active lengths and field strengths.

The input to Scaler 1 included data defining the basic geometry (size) of the magnet and specifying the general characteristics of the conductor, insulation and substructure. Winding current density was established by specifying the winding build (dimension b in Fig. 3).

The output included winding current density, ampere turns, insulation and substructure volume, superconductor volume, copper-to-superconductor ratio, winding overall dimensions and scaling factors.

A second computer program, Scaler 2, was written to calculate stored magnetic energy, component weights and budgetary costs using scaling techniques. The input included dimensions, volumes and scaling factors from the output of Scaler 1 together with baseline magnet characteristics (for scaling) and empirical cost data obtained from past experience in the costing of MHD magnets[1,6,7].

The output included stored energy, component weights and costs, and weights and costs for the assembled and installed magnet systems.

INPUT DATA

Specific data input to Scaler 1, used to arrive at the results reported in the following sections, are listed in Table III. For the 4, 100, and 450 MWe sizes, the data listed are consistent with the actual designs of the CDIF/SM, ETF and CSM magnets[4,2,1] respectively. For the 1100 MWe size, the data are extrapolations from CSM data.

The level of design currents used in the larger magnets is consistent with an earlier study[8] to investigate the impact of design current on magnet system cost. The study showed magnet system cost to be minimum for design currents in the range of 50

TABLE II

BASIC CHARACTERISTICS OF MAGNET REFERENCE DESIGNS USED IN STUDY

Magnet Identification	MHD Channel Power Output	Warm Bore Size		Active Length
		Inlet	Exit	
	MWe	m	m	m
CDIF/SM	4	0.78 x 0.97	0.97 x 0.97	3.4
ETF	100	1.5 x 1.9	2.2 x 2.8	11.7
CSM	450	2.2 x 2.8	4.0 x 4.2	14.5
LBL	1100	3.3 x 4.2	6.1 x 6.4	16.0

Note: Field strengths for all magnets are taken as 6 T peak on-axis, 4.8 T inlet, 3.6 T exit.

TABLE III

SPECIFIC DATA INPUT TO SCALER 1

Magnet size (nominal MHD channel power)	MWe	4	100	450	1100
Reference		CDIF	ETF	CSM	LBL
Conductor type assumed	--	Cable	Cable	Cable	Cable
Conductor shape factor*	--	0.785	0.785	0.785	0.785
Conductor metal space factor**		0.547	0.547	0.547	0.547
Substructure design stress	10^8Pa	1.03	1.03	1.10	1.25
Design current	kA	6.13	25	50	80

* conductor shape factor = $\frac{\text{conductor envelope area}}{\text{area of square enclosing envelope}}$

** conductor metal space factor = $\frac{\text{conductor metal cross-sectional area}}{\text{conductor envelope cross-sectional area}}$

to 150 kA.

The substructure for all magnets was assumed to be a glass-reinforced plastic, designed to transmit magnetic loads from individual conductors to the surrounding coil containment vessels and superstructure without any accumulation of loading on the conductors themselves.

The superstructure for all four magnet sizes was assumed to be similar in design to that of the ETF magnet, made of stainless steel with design stress not exceeding 4×10^8 Pa.

Data input to Scaler 2 included the winding dimensions, volumes and scaling factors generated by Scaler 1 together with material densities, unit cost data and empirical cost factors derived from past experience. Typical data input to Scaler 2, common for all four sizes, are given in Table IV.

Unit cost of conductor was obtained from the curve of cost vs copper-to-superconductor ratio, Fig. 4. This curve was based on engineering estimates of unit costs of conductors of various copper-to-superconductor ratios, using the round cable conductor of the ETF magnet[1] as a model.

OUTPUT DATA

Partial Scaler 1 and Scaler 2 outputs are shown in Table V, which lists the computed major characteristics and costs for a particular magnet size (450 MWe) at two current density levels.

Computer output data were used to plot curves of magnet weight, cost and other characteristics vs design (winding) current density for four magnet designs with current densities varying from 0.75×10^7 A/m^2 to over 2.5×10^7 A/m^2. These data are discussed in the following sections.

WEIGHT AND COST

Curves of normalized magnet weight vs current density are shown in Fig. 5 for all four magnet sizes studied. Curves of normalized magnet cost vs current density are shown in Fig. 6. In both cases, normalizing is on the basis of the 1.0×10^7 A/m^2 designs.

It will be noted that the impact of design current density on magnet cost is significant. The curves indicate that increasing current density from 1.0×10^7 A/m^2 to 2.0×10^7 A/m^2 results in a decrease in magnet cost of about 30% in the case of the large baseload (1100 MWe) magnet and about 35% in the case of the (smaller) engineering test facility (100 MWe) size.

The decreases in total magnet weight and cost as current density increases are the result of accumulated decreases in weight and cost of all major components and associated decreases in winding and assembly costs. Higher current density implies a more compact winding which in turn means fewer ampere turns, decreased stored energy and total force, decreased volume of conductor and substructure and smaller helium containment vessel, superstructure and vacuum vessel. These trends for a particular magnet are shown in Table V, which lists calculated component weights for two current density levels in the CSM size (450 MWe) magnet.

STABILITY CRITERIA

Copper-to-superconductor ratio, heat flux and helium-to-conductor-metal volume ratio

TABLE IV

TYPICAL DATA INPUT TO SCALER 2

Density, stabilizer (copper)	8900	kg/m^3
Density, superconductor (NbTi)	6380	kg/m^3
Density, substructure (fiberglass)	1800	kg/m^3
Unit cost, substructure	10.35	\$/kg
Unit cost, helium vessel	18.00	\$/kg
Unit cost, superstructure	18.00	\$/kg
Unit cost, thermal shield , piping, etc.	58.00	\$/kg
Unit cost, vacuum vessel	14.00	\$/kg

TABLE V

MAJOR CHARACTERISTICS OF COMPUTER-GENERATED MAGNET DESIGN, 450 MWe SIZE, DESIGN CURRENT DENSITIES 1.2×10^7 A/m^2 AND 2.0×10^7 A/m^2

Peak on-axis field (input)	(T)	6	
Inlet aperture size (input)	(m)	2.2 x 2.8	
Active length (input)	(m)	14.5	
Design current (input)	(kA)	50	
Design current density	(10^7 A/m^2)	1.2	2.0
Ampere turns	(10^6 A)	38.6	34.8
Stored energy	(10^6 J)	7560	6100
Weight of conductor	(10^3 kg)	274	96
Weight of superstructure	(10^3 kg)	704	567
Total weight, magnet assembly	(10^3 kg)	2220	1580
Vacuum jacket overall length	(m)	21.7	21.1
Vacuum jacket overall diameter	(m)	12.8	11.5
Cost of magnet assembly installed, not including design costs, accessory costs, mark-up, etc.	10^6 \$	62.4	45.4
Total cost of magnet system including design, accessories, mark-up, etc.	10^6 \$	91.3	68.2

are criteria often used as measures of the stability, and hence the reliability of magnet windings. In the past, conservative winding designs for MHD magnets have usually involved copper-to-superconductor ratios in the range of 6 to 30, heat fluxes of less than 0.4 W/cm^2 and helium-to-conductor ratios of at least 0.2.

The effect of increasing design current density on stabilizer current density, copper-to-superconductor ratio and on heat flux, for the four magnet sizes studied, is shown in Figs. 7, 8 and 9.

It will be noted in Fig. 8 that copper-to-superconductor ratio decreases rapidly as winding current density is increased. The situation is compounded because the computer program keeps substructure stress constant, thus causing the absolute volume of substructure to drop only very slowly and the ratio of substructure to conductor to increase substantially as winding current density increases. This occurs because as the winding becomes more compact, there is less room for copper. Above 1.5×10^7 A/m^2 average current density, the copper-to-superconductor ratio in the larger magnets becomes lower and the current density in the stabilizer becomes higher than is usually considered acceptable. It should be kept in mind that the study is based on a specific type of conductor and winding design (round cable, uncompacted, with relatively low stressed substructure, see Fig. 1). By altering the conductor and winding designs and increasing substructure design stress, it is possible to increase the copper-to-superconductor ratio (with resulting decrease in stabilizer current density) but other factors such as cooling and substructure stress will be affected, and the designer must take these tradeoffs into account. The particular design selected for the study is not considered optimum, but is sufficiently representative to show trends.

The curves of Fig. 9 show heat flux at a very conservative level for the lower design current densities but rising rapidly, above a current density of 1.5×10^7 A/m^2. The heat fluxes shown were calculated assuming all strands in the cable conductor to be cooled on 100% of their surface. This is probably an optimistic assumption. Therefore, the heat flux curves should be considered primarily as indicators of trends.

Helium-to-conductor metal volume ratio does not vary with current density in the designs covered in this study, because all designs use a cable-type conductor with a metal-to-void ratio of about 0.55. The amount of helium in close contact with the conductor strands is therefore about 0.45 of the conductor (envelope) volume. Since this is well above the 0.2 value often considered satisfactory, the designs studied are conservative in this respect. However, one means of improving the undesirably low copper-to-superconductor ratio mentioned earlier is to substitute a compacted cable or monolithic conductor in place of the ordinary cable used. Such a substitution would involve reducing the helium-to-conductor metal volume ratio and would require careful consideration.

SAFETY AND PROTECTION

Important factors in the safety of a magnet system are the emergency discharge characteristics and the thermal inertia of the winding.

In the event of an MHD flow-train emergency or a fault in the magnet itself, it may be necessary that the MHD magnet be discharged very rapidly for safety reasons. Therefore, MHD magnet systems include external (dump) resistors and switches which, when activated, connect the magnet coils in series with external resistors designed for the emergency discharge function.

Under certain magnet fault conditions, emergency discharge may take place with only a very small (poorly cooled) section of magnet winding in the normal state. This normal section will heat up rapidly, and it is necessary that discharge to the external resistors be accomplished rapidly to prevent overheating of the conductor.

Rapid discharge involves high initial voltage at the coil terminals and voltage may become a critical factor in the coil design.

Curves of initial emergency discharge voltage vs design current density are shown in Fig. 10. The curves are based on the assumptions that all energy is dissipated in the external resistors and discharge is rapid enough to prevent the normal section of conductor (under adiabatic conditions) from exceeding 300 K temperature.

The voltages shown on Fig. 10 for the larger magnets at higher current densities appear excessive. For a given winding current density, the discharge voltage may be lowered by several design means, including adding of copper to the conductor, increasing the design current (reducing inductance) and dividing the winding into sections with separate power supplies. The designer must make tradeoffs between these design measures (and their possible adverse effects on the system) and the indicated cost savings associated with higher design current densities.

If a normal (resistive) region could be made to propagate very rapidly throughout the entire magnet winding, nearly all the magnetic energy would be absorbed as heat in the winding itself. To illustrate what would happen under this special condition, curves of final winding temperature vs design current density are shown in Fig. 11. For these curves, it is assumed that all the magnetic energy is dissipated uniformly throughout the winding as heat. The curves show that for all magnet designs studied except the largest, the windings are capable of absorbing, as heat, all of the stored magnetic energy without exceeding room temperature. The curves are conservative in that they assume adiabatic heating of copper, with no allowance for heat absorbed by helium, NbTi and substructure, or for conduction of heat into vessel walls and main structure.

WINDING SUBSTRUCTURE

The effect of winding substructure on the results discussed earlier deserves attention.

All magnet designs used in the study incorporated substructures providing individual support for the conductors and transmitting magnetic loads from conductors to containment vessels (superstructure) without accumulation of loading on conductors themselves. Substructure design stress ranged from 103 MPa for the smallest design to 125 MPa for the largest.

By eliminating substructures and adding relatively thin insulation to separate conductors from each other electrically, a substantial amount of extra space would be made available for additional copper in the conductor. In a final magnet design, the advantages of the structural support provided by the substructure must be weighed against the advantages of higher copper-to-superconductor ratio which can be achieved if substructure is eliminated.

CONCLUSIONS

1. Increasing design current density causes a significant decrease in the cost of superconducting MHD magnets, although the effect is not as great in larger magnets as in smaller ones. For a specific design studied, the estimated cost of a 1100 MWe size MHD magnet system was reduced by about 30% (roughly \$20 x 10^6) when design current density was increased from 1.0 x 10^7 A/m^2 to 2.0 x 10^7 A/m^2.

2. Increasing design current density from 1.0 x 10^7 A/m^2 to 2.0 x 10^7 A/m^2 has a significant adverse effect on the ability to achieve winding stability and safety. This effect is particularly pronounced in the larger size

magnet designs.

3. In anticipation of future large MHD magnet construction, it is important that analysis, development testing and design studies be performed to enable the use of higher winding current densities with acceptable stability and safety, so that magnet designs will be more cost effective.

REFERENCES

1. Conceptual Design Engineering Report - MHD Engineering Test Facility 200 MWe Power Plant, prepared for NASA/LeRC for DOE by Gilbert/Commonwealth DOE/NASA/0224-1, Vol. 1-V, September 1981.

2. MHD Magnet Technology Development Program Summary, prepared for DOE by Plasma Fusion Center, MIT, 1982 (to be issued).

3. A.M. DAWSON, P.G. MARSTON, R.J. THOME, Y. IWASA, and J.M. TARRH, "The United States Superconducting Magnet Technology Development Program," *IEEE Trans. Mag.*, MAG-17(5): 1966-1969, 1981. (MT7-Karlsruhe).

4. A.M. DAWSON, ed., Proc. 1980 Superconducting Magnet Design Conference, MIT, Cambridge, MA, March 1980.

5. General Dynamics Convair Division Report No. CASK-GDC-031, Cask Commercial Demo Plant MHD Superconducting Magnet Systems: Conceptual Design Final Report, MIT PO ML-67466, December 1979.

6. General Dynamics Convair Division Report No. PIN78-182 Cask Commercial Demo Plant MHD Magnet: Budgetary (Cost Estimate) and Planning, Final Report, MIT PO ML-68221, February 1980.

7. A.M. HATCH, "MHD Magnet Cost Analysis and Estimation" (Course Notes), MHD Magnet Design Course, MIT, Cambridge, MA, July 1980.

8. R.J. THOME, R.D. PILLSBURY, JR., H.R. SEGAL, and B.O. PEDERSEN, "Impact of High Current Operation on the Cost of Superconducting Magnet Systems for Large-Scale MHD Operation," *Adv. Cryogenic Eng.*, 25: 12-18, 1981.

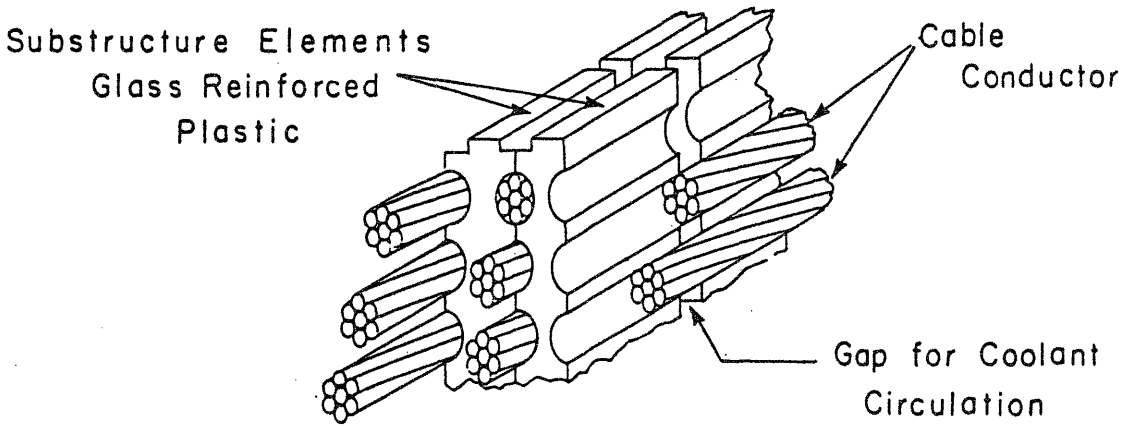

Figure 1 Magnet winding detail--round cable conductor supported in insulating substructure

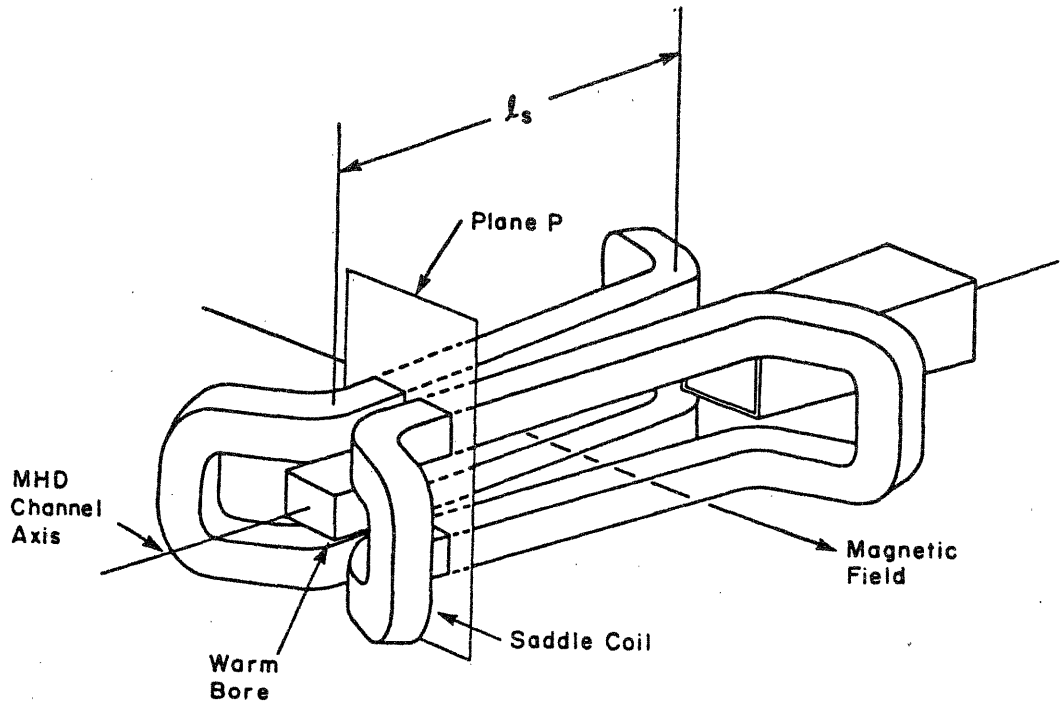

Figure 2 Rectangular saddle coil configuration

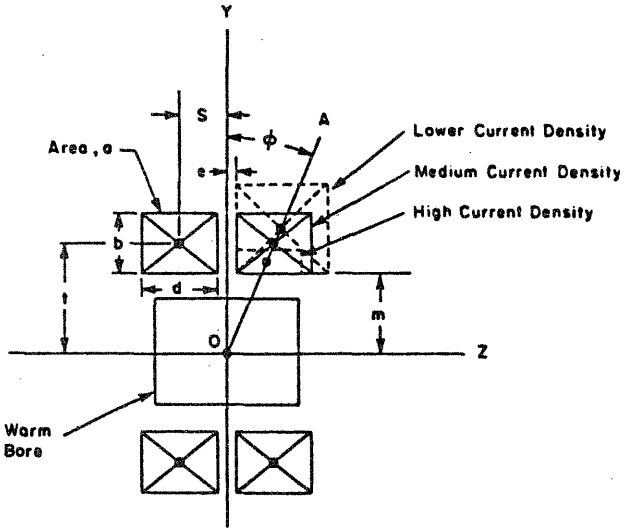

Figure 3 Winding cross section in plane of peak on-axis field

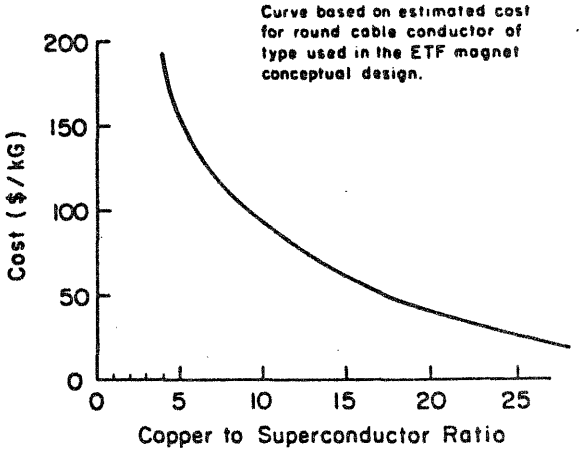

Figure 4 Curve of conductor unit cost vs copper-to-superconductor ratio

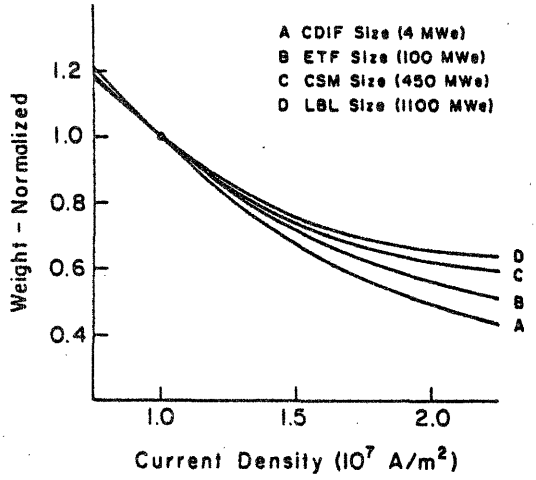

Figure 5 Curves of normalized magnet weight vs design current density

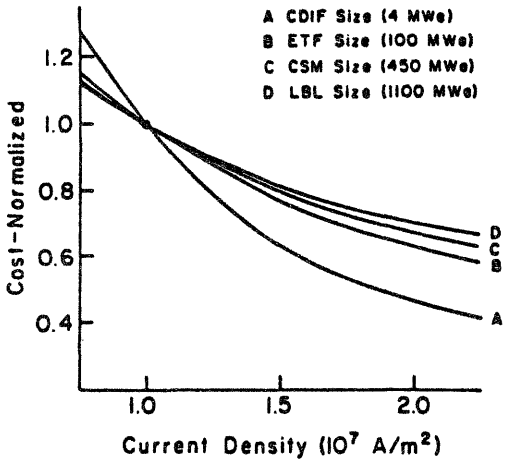

Figure 6 Curves of normalized magnet cost vs design current density

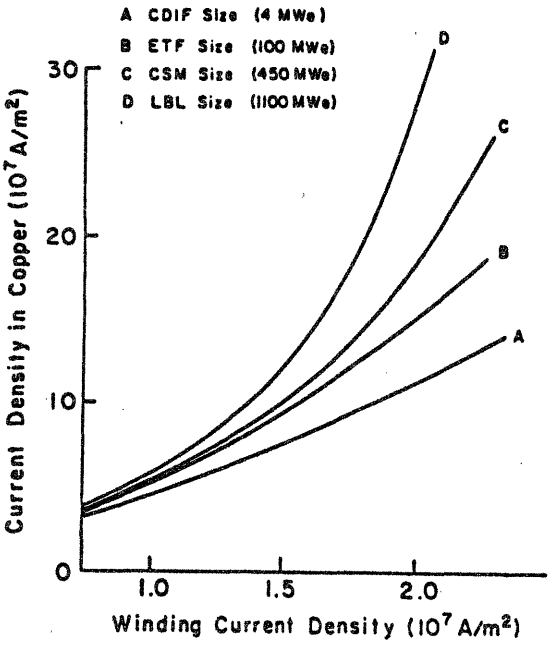

Figure 7 Curves of stabilizer (copper) current density vs design winding current density

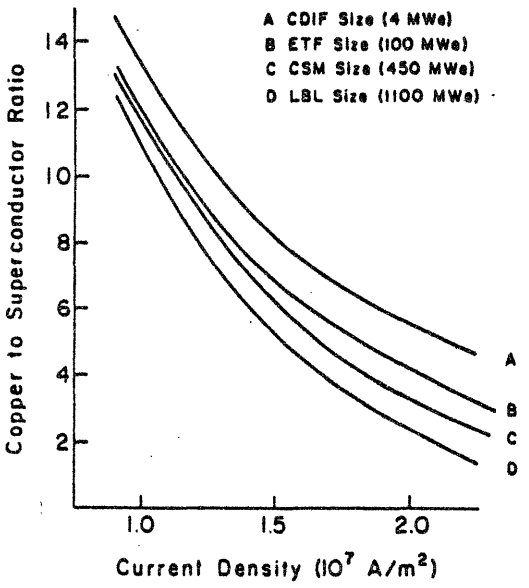

Figure 8 Curves of copper-to-superconductor ratio vs design current density

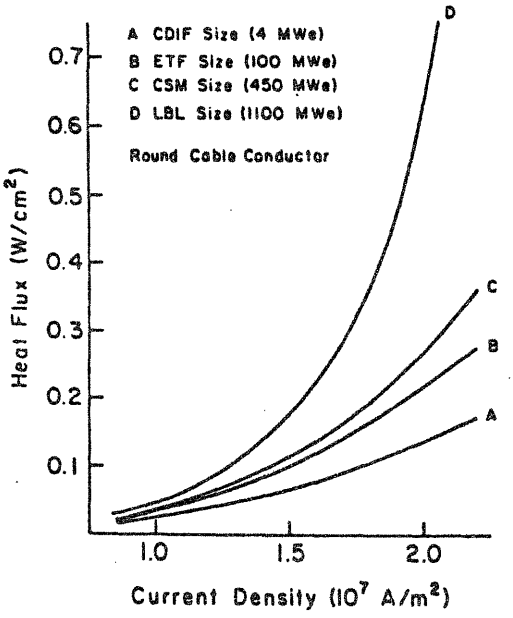

Figure 9 Curves of heat flux vs design current density

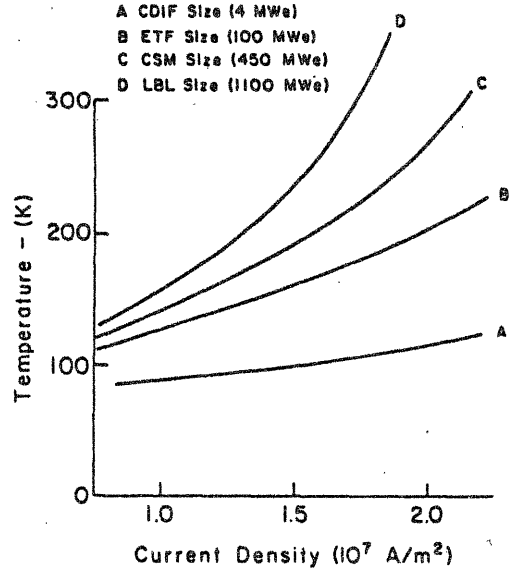

Figure 10 Curves of emergency discharge voltage (initial) vs design current density

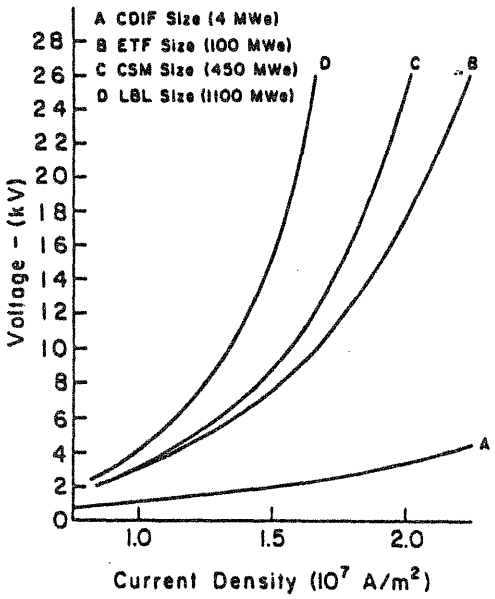

Figure 11 Curves of final conductor temperature vs design current density

Appendix B

Safety and Protection for Large Scale Superconducting Magnets

FY1983 Report (pages 1 - 81) submitted to Idaho National Engineering Laboratory

Plasma Fusion Center Report PFC/RR-83-33

December 1983

PFC/RR-83-33 DOE/ET/51013-104

Safety and Protection for Large Scale Superconducting Magnets — FY1983 Report

by

R.J. Thome, J.M. Tarrh, R.D. Pillsbury, Jr., W.G. Langton, W.R. Mann, H. Becker, A. Hatch, P.G. Marston, Y. Iwasa, A.M. Dawson, J. Borzikowski, and T. Ishigohka
Plasma Fusion Center
Massachusetts Institute of Technology
Cambridge, MA. 02139

December 1983

Submitted to Idaho National Engineering Laboratory

TABLE OF CONTENTS

1.0 INTRODUCTION

R.J. Thome

The rapid increase in size, stored energy, and complexity of the magnet systems required for advanced energy conversion applications such as fusion demands a thorough understanding of safety and protection for personnel and other systems. Toward this end, MIT has been carrying out a program for INEL oriented toward safety and protection in large scale superconducting magnet systems. The program involves collection and analysis of information on actual magnet failures, analyses of general problems associated with safety and protection, and performance of safety oriented experiments. This report summarizes work performed in FY83.

In December 1982, a massive structural failure occurred in a large magnet at the Arnold Engineering Development Center (AEDC). The magnet utilized about 8.4×10^4 kg of copper conductor, 5.4×10^4 kg of aluminum structure, and 5×10^5 kg of steel in a flux return frame. The failure occurred at a field level of 4.1 T and led to brittle fractures in most of the structural components, significant displacements of some portions of the iron frame, and substantial deformation of the winding with some conductor fracture. Chapter 2 describes this system before and after failure and summarizes the structural failure analyses which were performed by MIT in parallel with the investigation by a team from AEDC.

The magnet failure was catastrophic in the sense that most structural components were fractured and the winding suffered extensive plastic deformation. However, operating procedures prevented possible injury to personnel and the rugged nature of the winding limited deformations to

large but safe values, and restrained conversion of magnetic to kinetic energy of failed components. This suggests that it may be desirable to limit operating current densities in magnet design to levels whereby the winding could act in this structurally fail-safe manner even if it sustained substantial deformation in the event of a failure in its primary structure. A general analysis of this problem was, therefore, performed and is presented in Chapter 3.

The model and examples in Chapter 3 are based on an infinitely long solenoid configuration. Although the geometry is simple, this shape allows the important parameters to become apparent. The preliminary conclusions are:

(a) A protective circuit reaction involving dissipation in resistive elements following a major structural failure is unlikely to be effective on a fast enough time scale to limit the mangetic to kinetic energy conversion process in magnets using high current density windings.

(b) Windings with low enough current densities can absorb the total load following structural failure, thus limiting the kinetic energy conversion process, although this might involve substantial yielding and deformation of the winding. This is not usually a design requirement, but might form the basis for one criteria for large magnet design.

(c) Protective circuits involving inductive energy transfer can respond fast enough to limit the kinetic energy conversion process in high or low current density configurations. The range of coupling coefficients and time constants to allow this method to be effective are under study. This is the source of our interest in the use of multiple circuits for discharge of a TF coil system as begun this year and as discussed in Chapter 4.

Chapter 3 closes with a simple model which illustrates the ability of an inductively coupled secondary circuit to be effective in restraining magnetic to kinetic energy conversion in the event of a structural failure in a primary circuit. In Chapter 4, the use of multiple circuits in a TF

coil system was studied since it presents a means for limiting another process, that is, the magnetic to thermal energy conversion in a superconducting winding in the event of a quench. Typically, results show that only a small fraction of the total energy needs to be removed if only one of k circuits is discharged because the bulk of the energy is retained by the (k-1) circuits which maintain constant flux throughout the transient. This procedure allows the first circuit to be discharged more rapidly for a given initial voltage and final temperature limit, thus allowing for a longer delay time before the dump is initiated or for operation at a higher current density. The remaining coils could then be discharged on a longer time scale. However, if the remaining circuits require rapid discharge shortly after the first, then the necessary voltage per coil may or may not be higher than that required for the first circuit depending on the discharge sequence, number of coils and aspect ratio. The voltage to ground can be considerably lower than if a single system circuit was used. The general criteria governing the different reactions will be developed further next year.

Chapter 5 describes the experimental activity under this program during FY83. This involved a continuation of earlier activity regarding measurements of arc extinction voltages between electrodes in 300 K and 4.2 K (Section 5.1). Section 5.2 describes a small "football" experiment involving internally cooled cable conductor. Because of delays in delivery of the conductor the test was not carried out in FY83 as planned, but will be performed in FY84 together with another small football test as originally planned for FY84. Section 5.3 gives an update on the hybrid magnet status at FBNML as a continuation of our interest in the short

circuit in the superconducting section of that system. In summary, the short persists, but has minimal impact on operations because of the well cooled, highly stable design of this coil. Other types of design could experience a much more serious impact.

The report closes with a summary of safety related activities partially supported by this program. In FY83 this included participation in a Fusion Safety Workshop in Japan and involved a presentation regarding programs in magnet safety in the United States, participation in workshop discussions on other fusion systems, and tours of the fusion facilities at JAERI.

2.0 HPDE MAGNET FAILURE

(Subject to review and update in FY84)

2.1 System Description and Summary - R.J. Thome and J.M. Tarrh

The High Performance Demonstration Experiment (HPDE) at the Arnold Engineering Development Center (AEDC) employed a large (active bore approximately 1 m square x 7 m long) iron-bound copper magnet designed to operate in either of two modes: (1) as a 3.7 T (continuous) water cooled magnet, or (2) as a 6 T (long pulse) nitrogen precooled, cryogenic magnet. In either mode, coolant would flow through conventional hollow copper conductor windings. A unique force containment structure of 2219 aluminum alloy was selected on the basis of thermal considerations (77 to 350 K operating temperature range; coefficient of thermal expansion permitting dimensional matching to the coil) and cost. In December 1982 a catastrophic structural failure occurred at a field level of 4.1 T which led to massive brittle fractures and failure of most of the structural components, significant displacements of some of the iron frame components, and substantial deformation of the winding with some conductor fracture. Although the failure occurred at a fraction of the design field level, no personnel injury occurred because of the operating procedures in force at the time of the incident which restricted personnel access and required operating personnel to be in a remote control area. At present, the structure is considered beyond repair. The windings are considered to be reparable without prohibitive time and effort assuming a reduced performance requirement (single mode, pulsed from room temperature).

Following the incident a detailed investigation was performed by AEDC personnel.[1] In parallel with this effort, MIT carried out a preliminary failure analysis which is summarized in Section 2.2. Although there is general agreement,

more than one failure scenario is possible from the standpoint of the early sequence of events. The evidence indicates a localized structural failure leading to sequential overloading and fracture of other structural components. The primary cause appears to have been design flaws relative to structural details and the load distribution in localized areas. A contributing factor was utilization of structural materials having low ductility. The conversion of the stored magnetic energy to kinetic energy of the fractured components was limited because of the large cross-section of the winding and the ability of the windings to deform to a configuration which could accept the magnetic loads while the coil discharged. This has led to the simplified modeling and analyses for magnets in general which is described in Chapter 3.0.

The remainder of this section will describe the system characteristics before and after failure. Section 2.2 will describe the failure analyses and summarize the fault scenarios. Further analyses of effects such as the deflection limiting nature of the clamping between components of the iron flux return frame will be carried out in FY84 together with a review of the preliminary failure analysis. This chapter, will therefore, be updated in our FY84 report.

The HPDE magnet utilized a saddle coil pair typical of an MHD experiment in which a magnetic field is required in a direction perpendicular to the axis of a long channel. The shape of the coils is shown in Fig. 2.1 which also indicates the direction and magnitude of the electromagnetic loads on the coils at the design field level. The scale of the device is indicated by Fig. 2.2 which shows the coils before addition of the aluminum structure or side and top

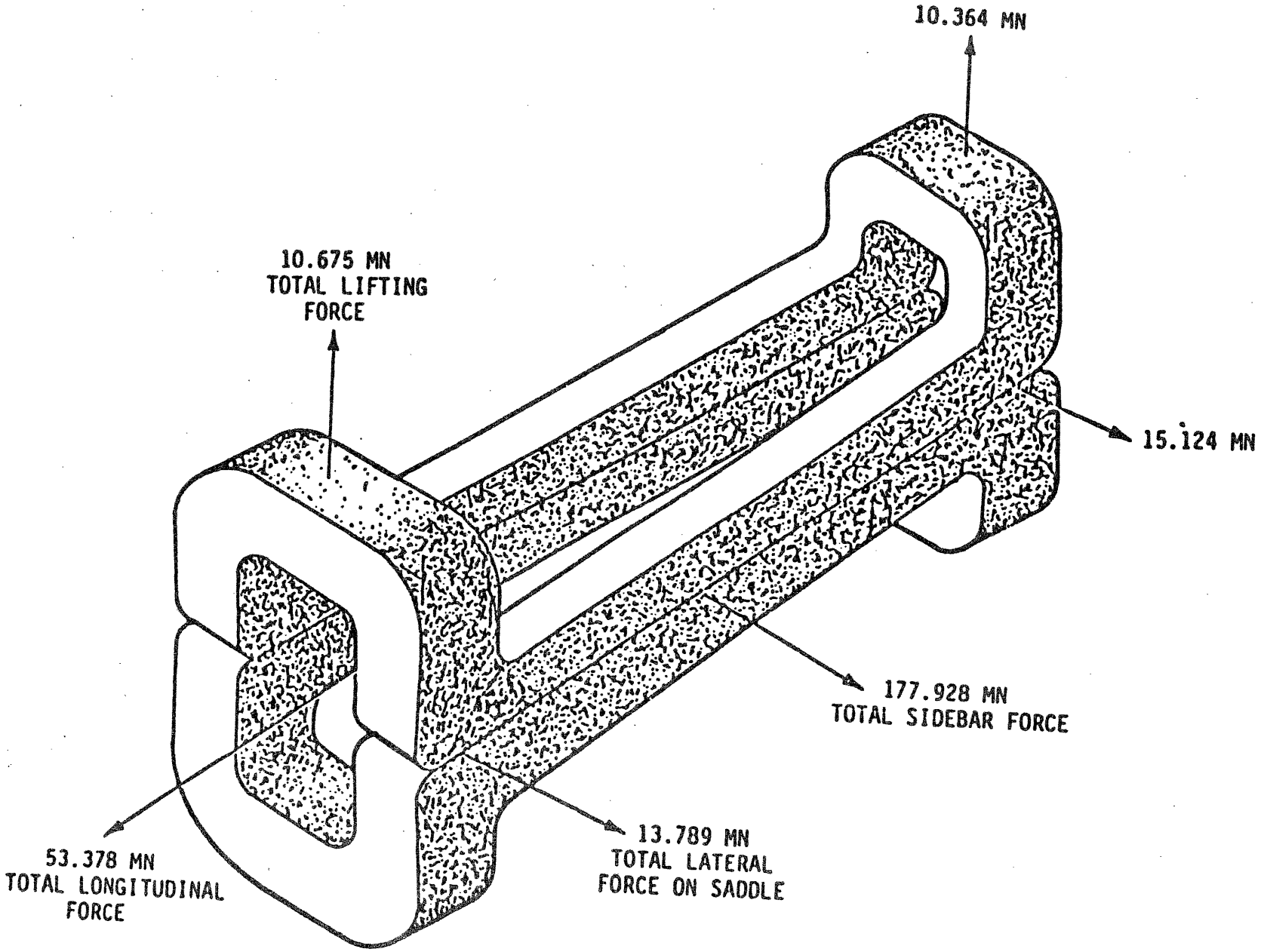

Figure 2.1 HPDE Saddle Magnet Coils

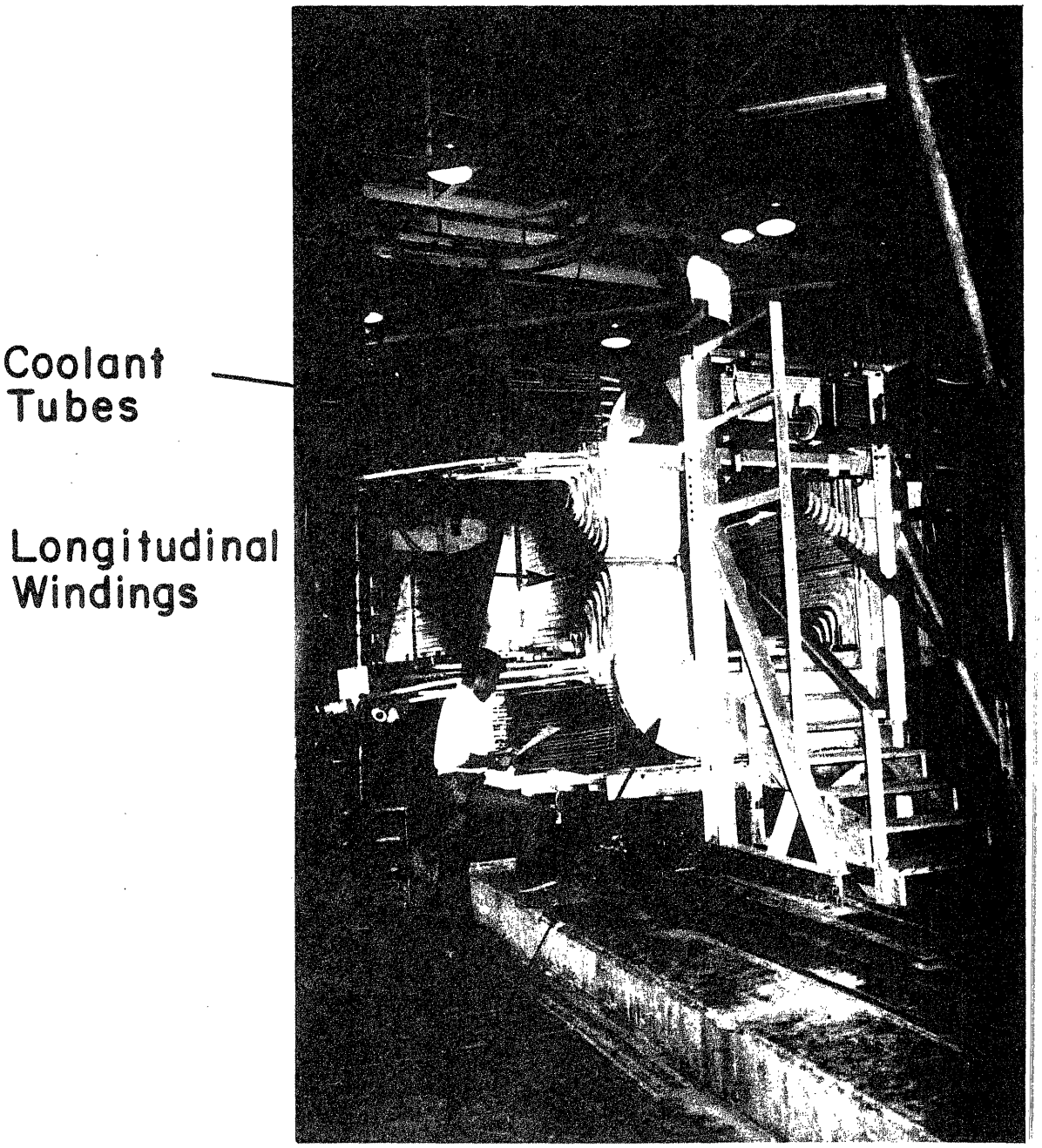

Figure 2.2 HPDE Magnet Coils before addition of structure or top and side components of iron flux return frame.

components of the iron flux return frame. The figure indicates the longitudinal section of the windings which lie parallel to the MHD channel axis and the end turns of the saddle coils which pass over and under the MHD channel (not shown).

The structure was composed of aluminum plates which enclosed the windings as shown in Fig. 2.3 and were primarily held in place by a system of keys and bolts. The "sidebar loads" in Fig. 2.1 were carried by the vertical beam modules on each side of the magnet. These modules were held in place by the transverse tension members. Near the ends of the coils, portions of this load were carried by the collars which were composed of four plates at each end, held together with keyed fingers.

The longitudinal forces in Fig. 2.1 were carried partly by the longitudinal windings but predominantly by the longitudinal tension members (LTM). These plates (having cross-sections of 1.0 x 0.13 m each) ran the length of the windings and had fingers at their ends which passed through the face plates to pick up a portion of the loads from the face plates. Figure 2.4 shows details of the fastening approach which uses keyblocks between the LTM fingers on the outside of the face plate. The fingers and keys between the collar components are also evident in this view. Analyses indicate that one or the other of these finger areas failed as the initiating event, followed by failure of the other area and subsequent sequential overload and failure of the transverse tension members and their connections to the vertical side beam modules along the entire length of the magnet. Table 2.1 summarizes the fractured structural components based on a visual inspection.

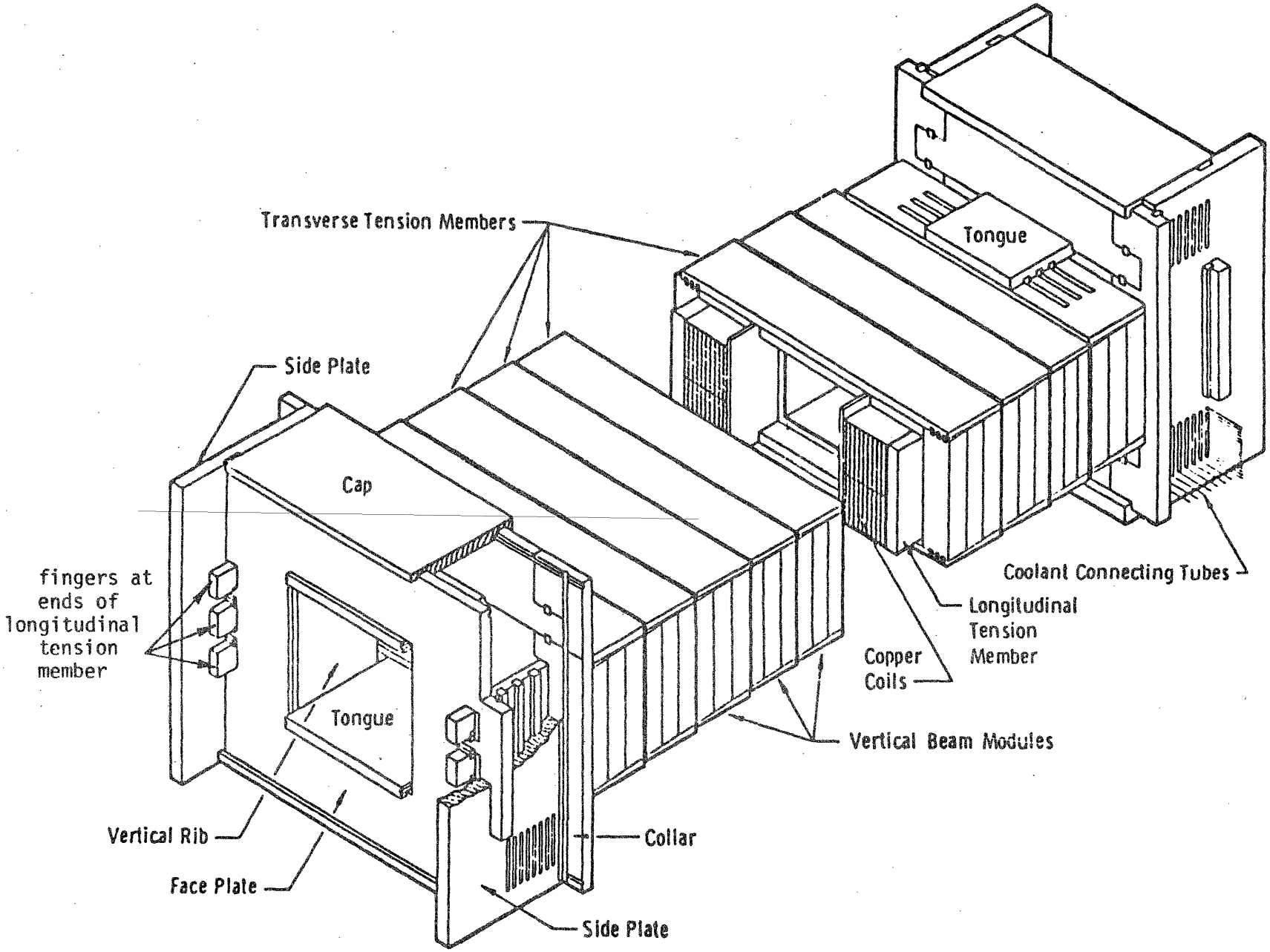

Figure 2.3 Aluminum Force Containment Structure (FCS)

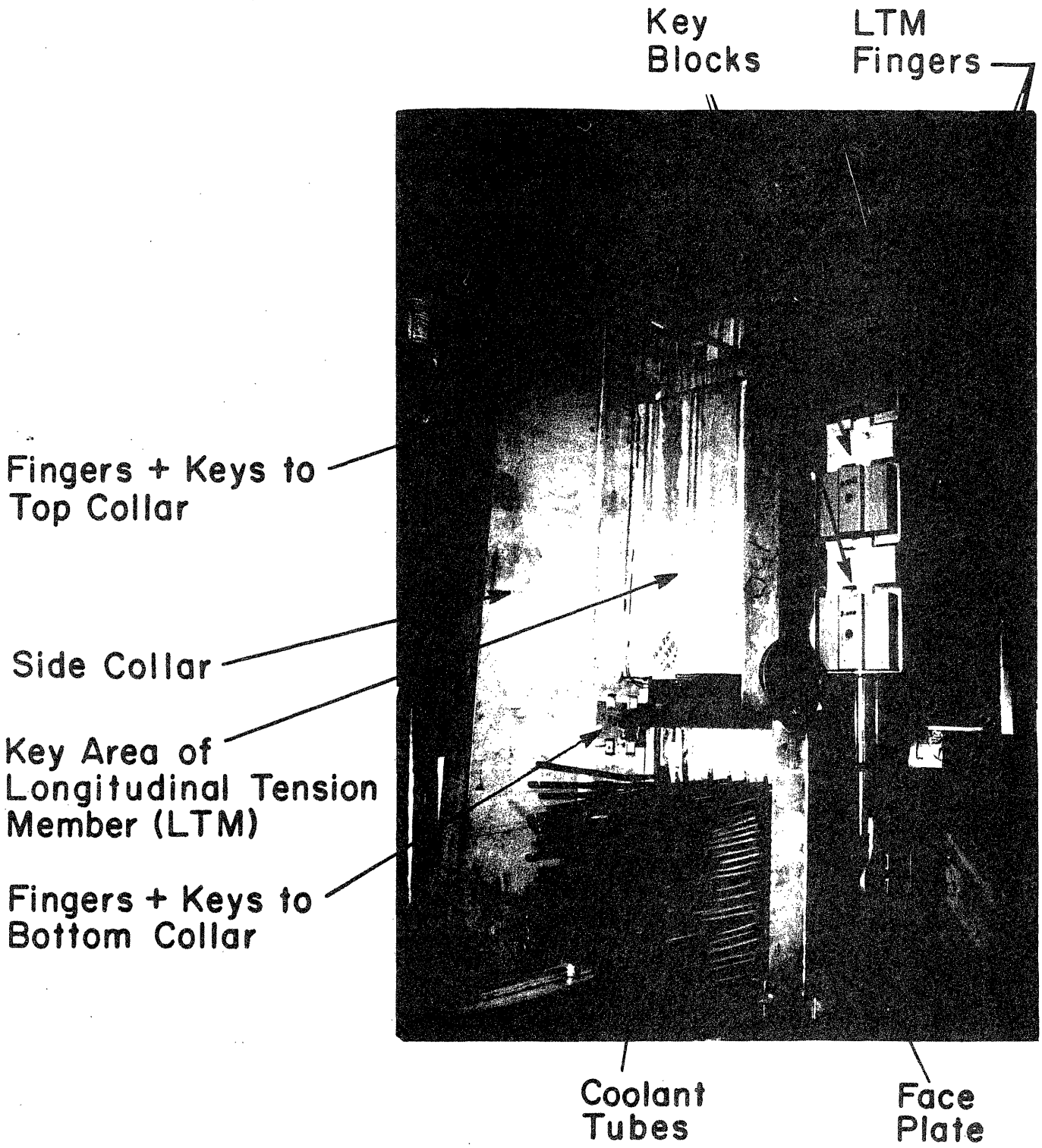

Figure 2.4 Partial Structure in the end turn region; LTM fingers and fingers and keys on the collar components are evident in this view (note: sideplate not in place).

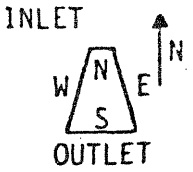

TABLE 2.1
HPDE MAGNET FCS

Damage Status Based on Visual Inspection

COMPONENTS	LOCATION	CONDITION
Face Plates	N, S	No failures
Side Plates	SW, NW	Failed through slotted regions
	SE, NE	No failure
Longitudinal Tension Members	W	Fingers failed at both ends. Plate fractured and separated at N collar region. Bend at S collar region.
	E	No failure evident at present
Collars	SW, NW	All fingers failed
	SE	Fingers failed at bottom
	NE	No failure
Vertical Side Beams	W	All connections to transverse tension members failed at top and bottom. Central regions intact.
	E	Failed along bottom at connections to the transverse tension members at ends.
Transverse Tension Members	W	All failed, top and bottom, at or near side beam connections.
	E	All failed or cracked along bottom except for one in center. Failure in several top members at each end.
Saddle Caps	N S	No failure, top or bottom
Tongues	S	Rotated about fore - aft axis but no failure
	N	Lips broken off
Vertical Edge Stiffeners	N S	No failure Failed

The relationship and scale of the iron flux return frame (magnet steel yoke) relative to other magnet components is shown in Fig. 2.5 and an overall view of the fully assembled magnet is shown in Fig. 2.6. The outer case (also called the thermal enclosure) in the end turn region was provided for thermal isolation. Overall characteristics of the magnet system prior to failure are summarized in Table 2.2.

TABLE 2.2
HPDE MAGNET CHARACTERISTICS

Copper conductor weight	83,500 kg
Aluminum structure weight	54,100 kg
Steel weight	500,000 kg
Pole length	7.1 m
Entrance aperture	0.89 m wide x 0.71 m high
Exit aperture	1.40 m wide x 1.17 m high
Half-coil height	0.50 m
Coil width	0.53 m
Space factor	0.8 m
Turns (total)	720
Length of average turn	22 m
Conductor dimensions	.025 m x .025 m
Cooling passages	.0068 m dia.
Overall length of coil	8.72 m
Cooling requirements	
LN_2 for initial cooldown	64,000 liters
LN_2 for recooling	<10,000 liters
Water (27 megawatts)	12.8 m^3/min
Peak axial fields	
Cold mode at pulse peak	6.0 tesla
Warm mode	3.7 tesla

On December 9, 1983 the magnet was being charged in a routine manner prior to an MHD channel test. It had been cooled to 105 K which was lower than any previous run. The coil was energized for 39 seconds and the field strength had reached 4.1 T (several earlier runs had attained or approached this level) when the force containment structure failed.

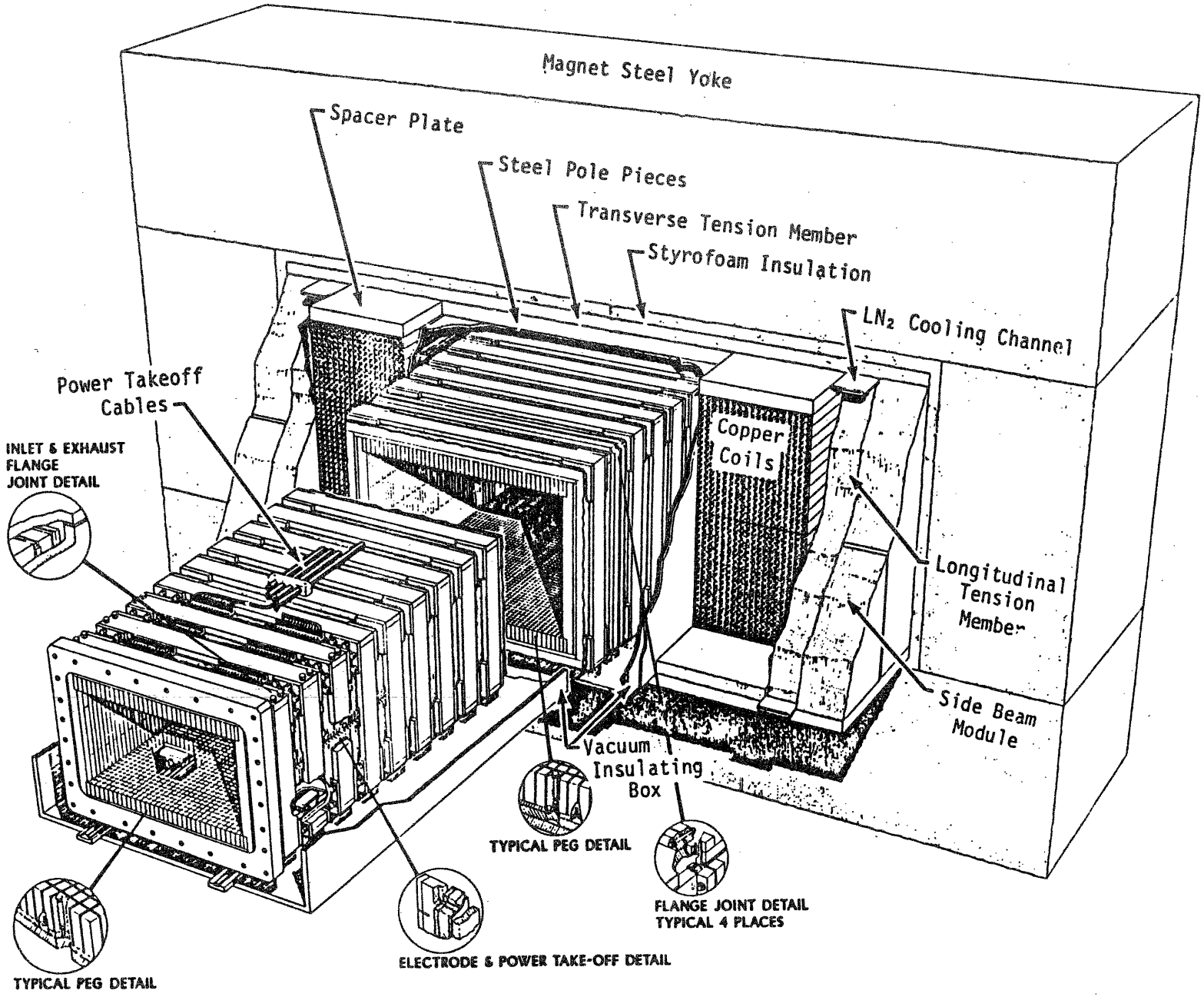

Figure 2.5 Schematic of HPDE magnet and MHD channel.

Figure 2.6 Overall View of the assembled magnet system.

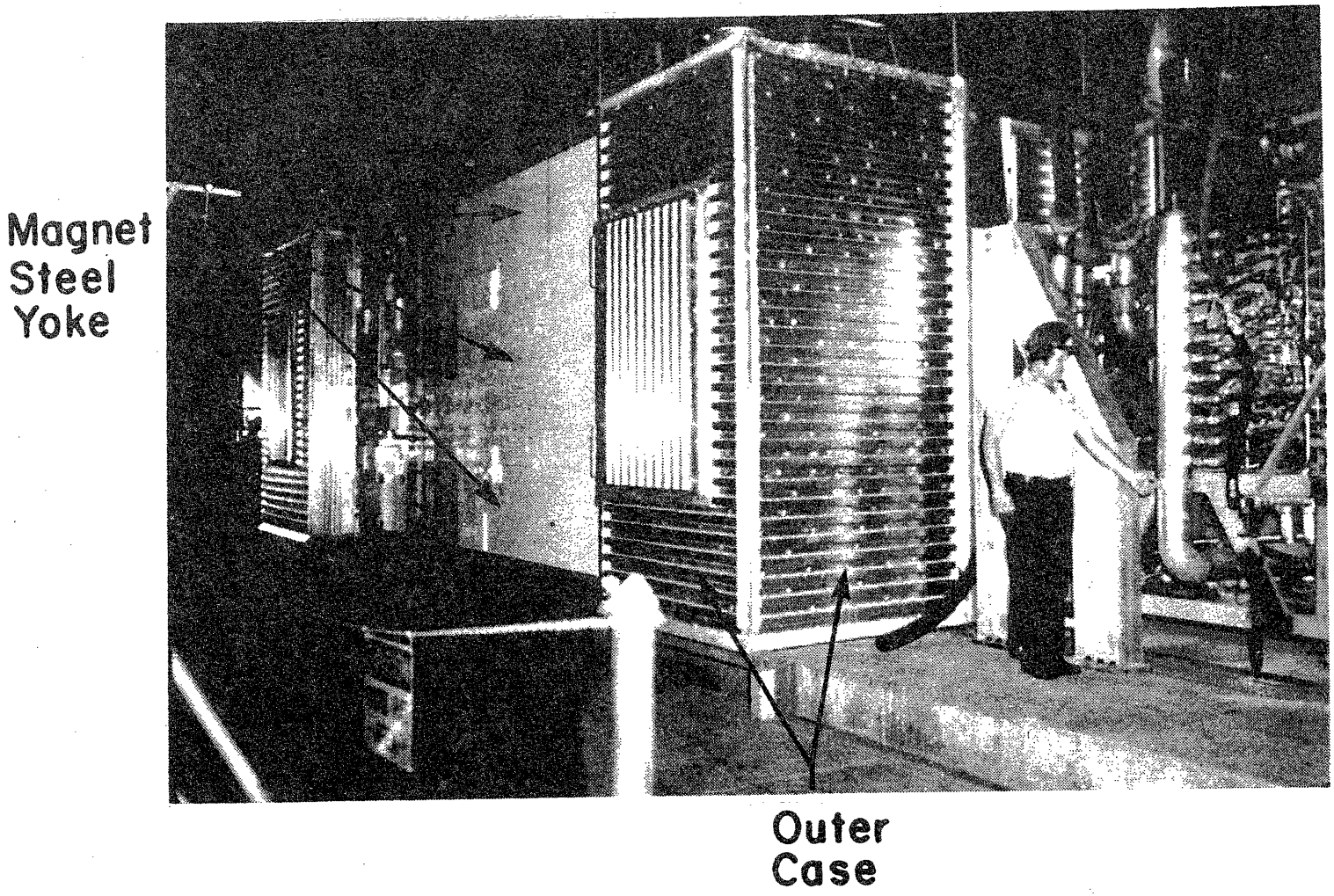

The sequence of events during the failure is shown in Fig. 2.7, as reconstructed from the data systems and witnesses.[1] The time scale of the failure is shown to be very short in comparison to the electrical time constant (inductance divided by resistance) of the magnet. Observers described the failure as earthshaking and producing a loud boom which, although short, had a perceptible duration (time) and contained two peaks. A discussion of the sequence of events and the time scale of the failure based on analysis is given in Section 2.2.4.

The figures described in the following were taken at various stages in the disassembly process. Figure 2.8 shows the fracture at the base of the LTM fingers. A closeup of the fracture at the base of a finger is shown in Fig. 2.9. Note that the presence of the finger and the keyways in the finger represent significant stress concentrations and a significant reduction of the LTM load carrying ability relative to its full size cross-section which existed over most of its length. The failure in this region was accompanied (either immediately before or immediately after) by failure of the fingers which key the four components of the collar assembly together.

Failure of the collar in the end turn region led to a sequential overload and failure of each transverse tension member and vertical side beam subassembly along the length of the magnet. Figure 2.10 shows several fractured vertical side beam modules after removal and placement side-by-side on the floor.

After failure of the transverse support structure, the longitudinal coil windings moved outward under the action of the sidebar forces. Figure 2.11 schematically illustrates the manner in which the outward deformation was

Figure 2.7 Reconstruction of events HPDE run 007-018

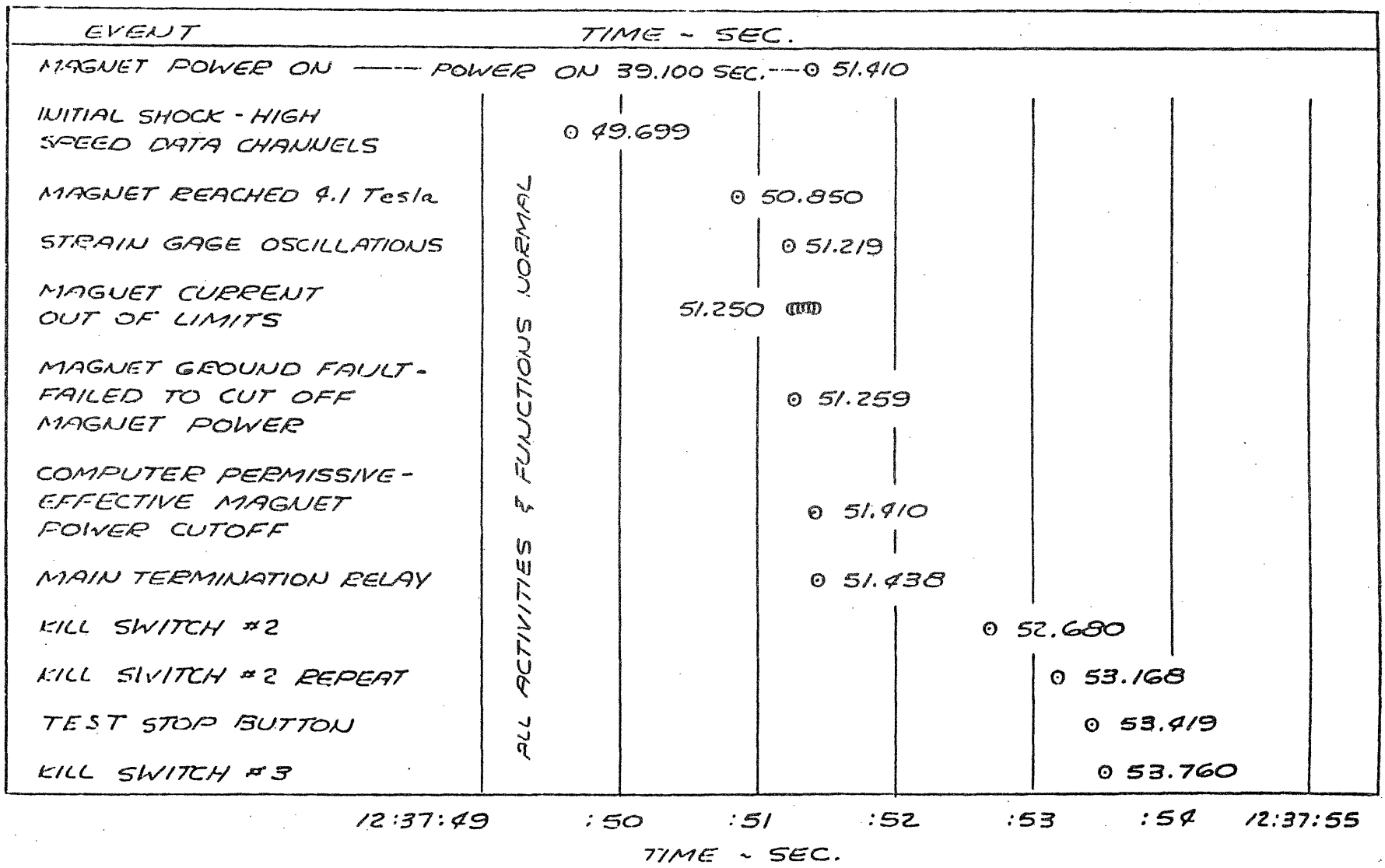

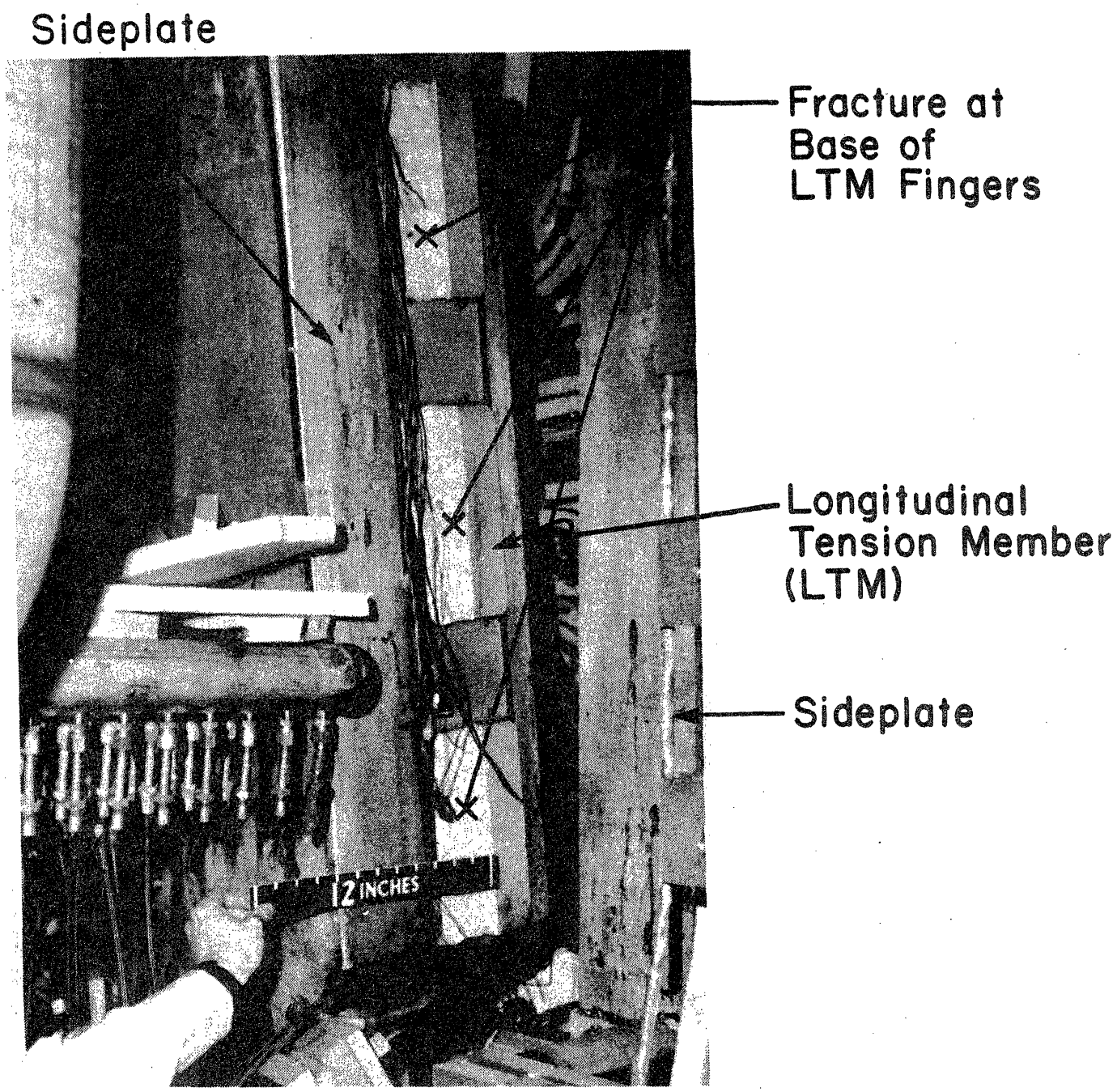

Figure 2.8 Fractures at base of LTM fingers.

Figure 2.9 Close-up of the fracture of an LTM finger.

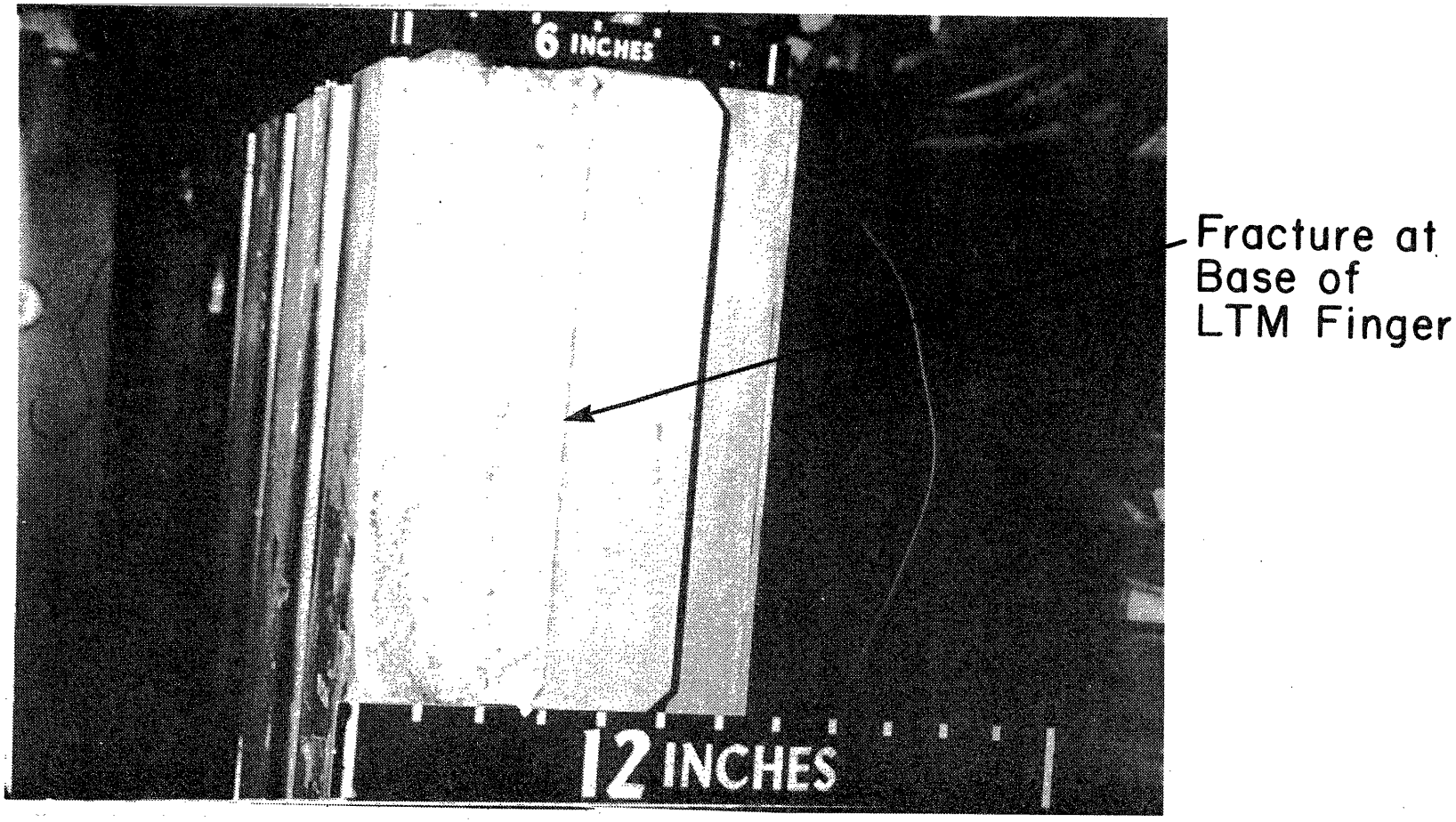

Figure 2.10 Several vertical side beam modules with typical fractures at locations where they connect to the transverse tension members.

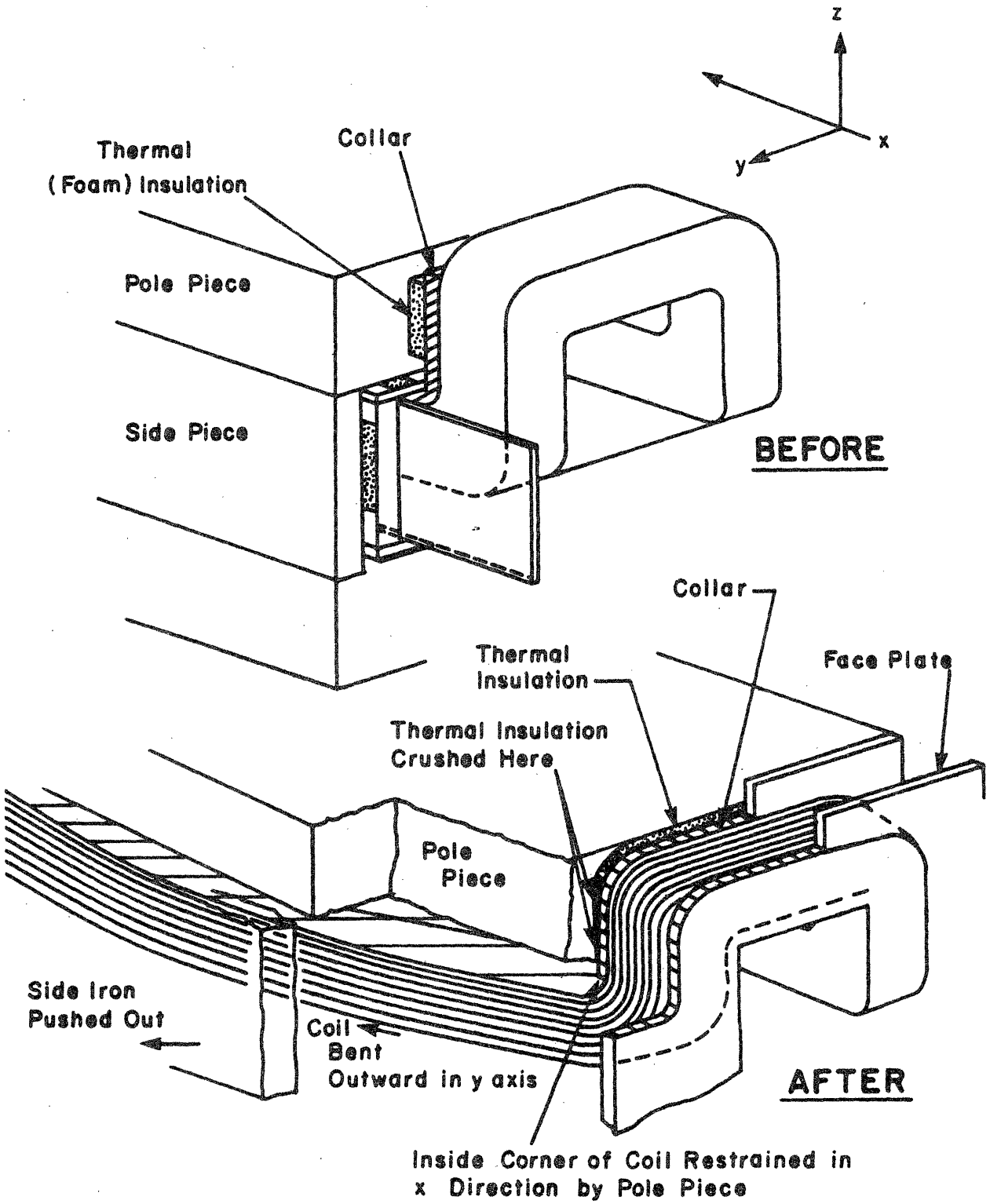

Figure 2.11 Schematic illustrating manner in which coil outward displacement was restrained by pole piece.

ultimately restrained. This occurred because the coil cross-section was large enough to carry the load as an outwardly loaded arch anchored at its ends by the end turns pulling in towards the pole piece. In a winding designed with a high enough current density (i.e., small cross-section), the windings would not necessarily be capable of this restraint and could have fractured. This effect is studied with a simplified model in Chapter 3.0 to illustrate the ability of a winding to absorb the load and restrain the conversion of magnetic to kinetic energy.

Figures 2.12 is a view looking down the side of the magnet from the top before removal of side components of the iron flux return frame. The view indicates the displacement of the iron from between the top and bottom magnet steel yokes by the outward movement of the windings. The displacement and arch formed by the windings as well as the anchoring of the windings at the ends is shown in Fig. 2.13.

Despite the relatively large winding deformation, very few turns were actually severed. Damage to the winding was most severe in the ends of the top and bottom two layers which were adjacent to the steel yokes and subjected to substantial loading as a reaction to the arch formed by the windings when they moved outward. A view in this region is given in Fig. 2.14.

Figure 2.15 shows the winding deformation at the "far" end of the magnet from the point where the failure initiated. Note the broken LTM fingers lodged in the faceplate and the winding deformation relative to the flatness of the faceplate.

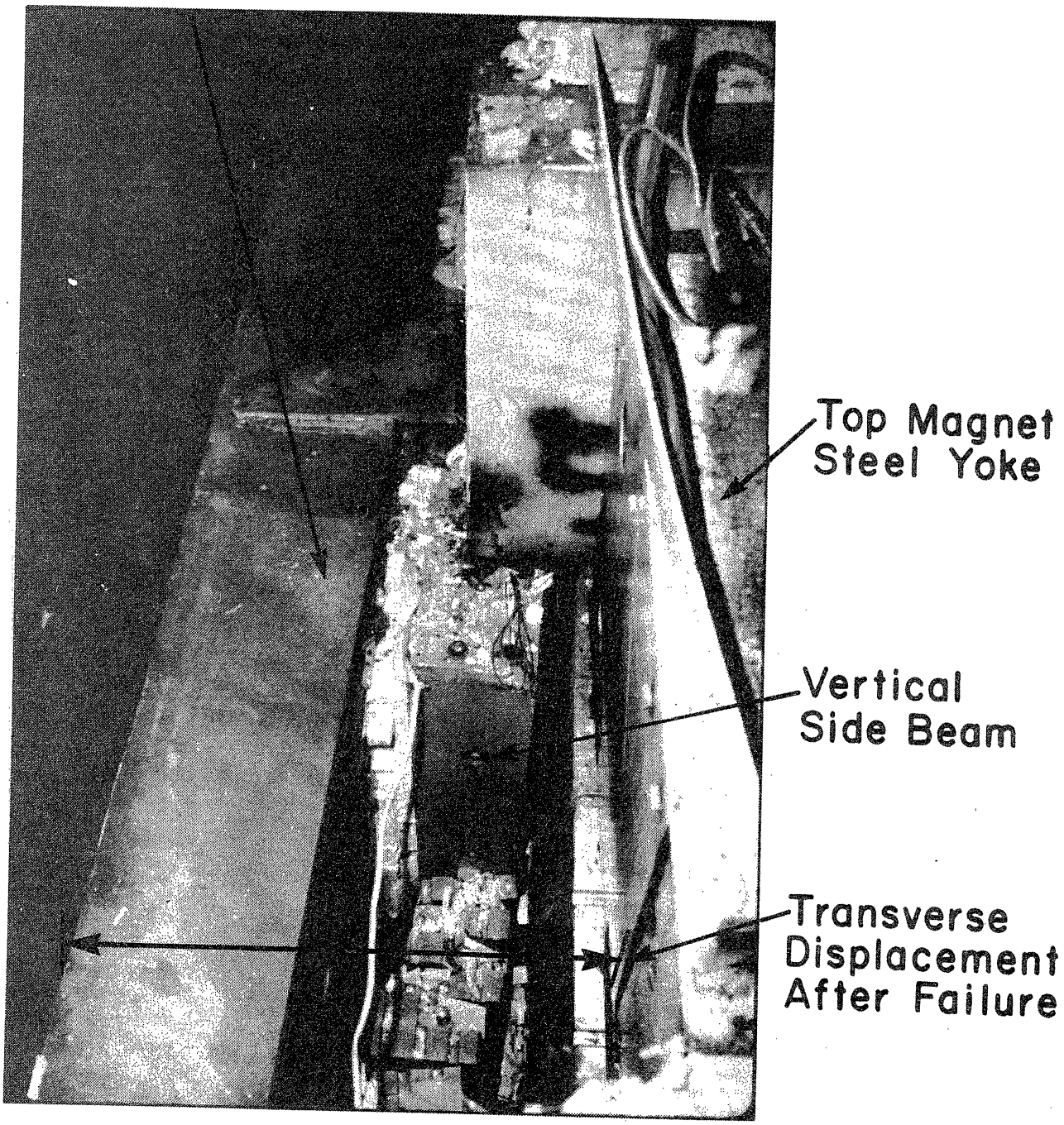

Figure 2.12 View looking down the side of the magnet from the top.

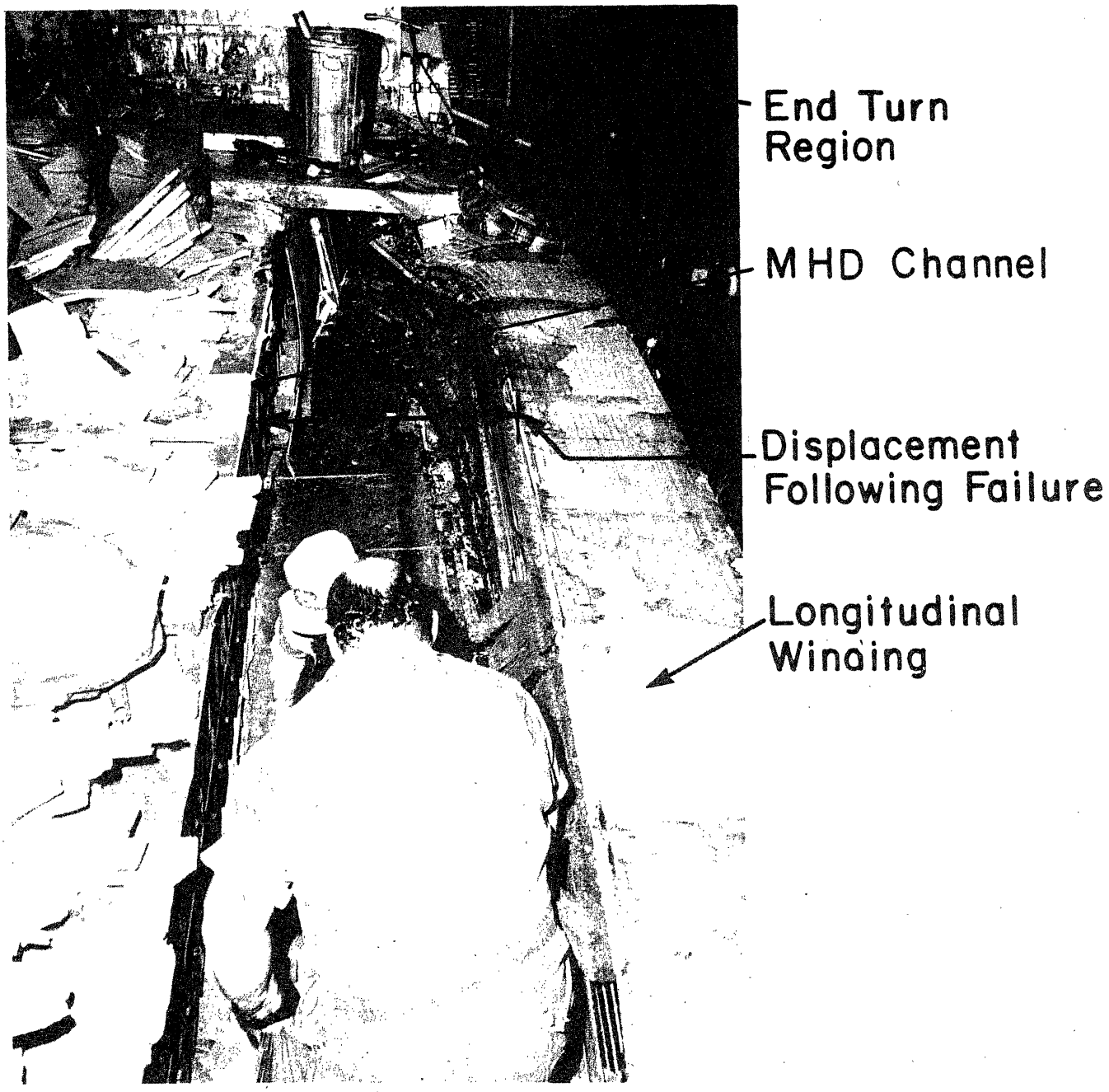

Figure 2.13 View showing outward movement and arch formed by winding.

Figure 2.14 Turn and insulation damage in top layer adjacent to steel yoke.

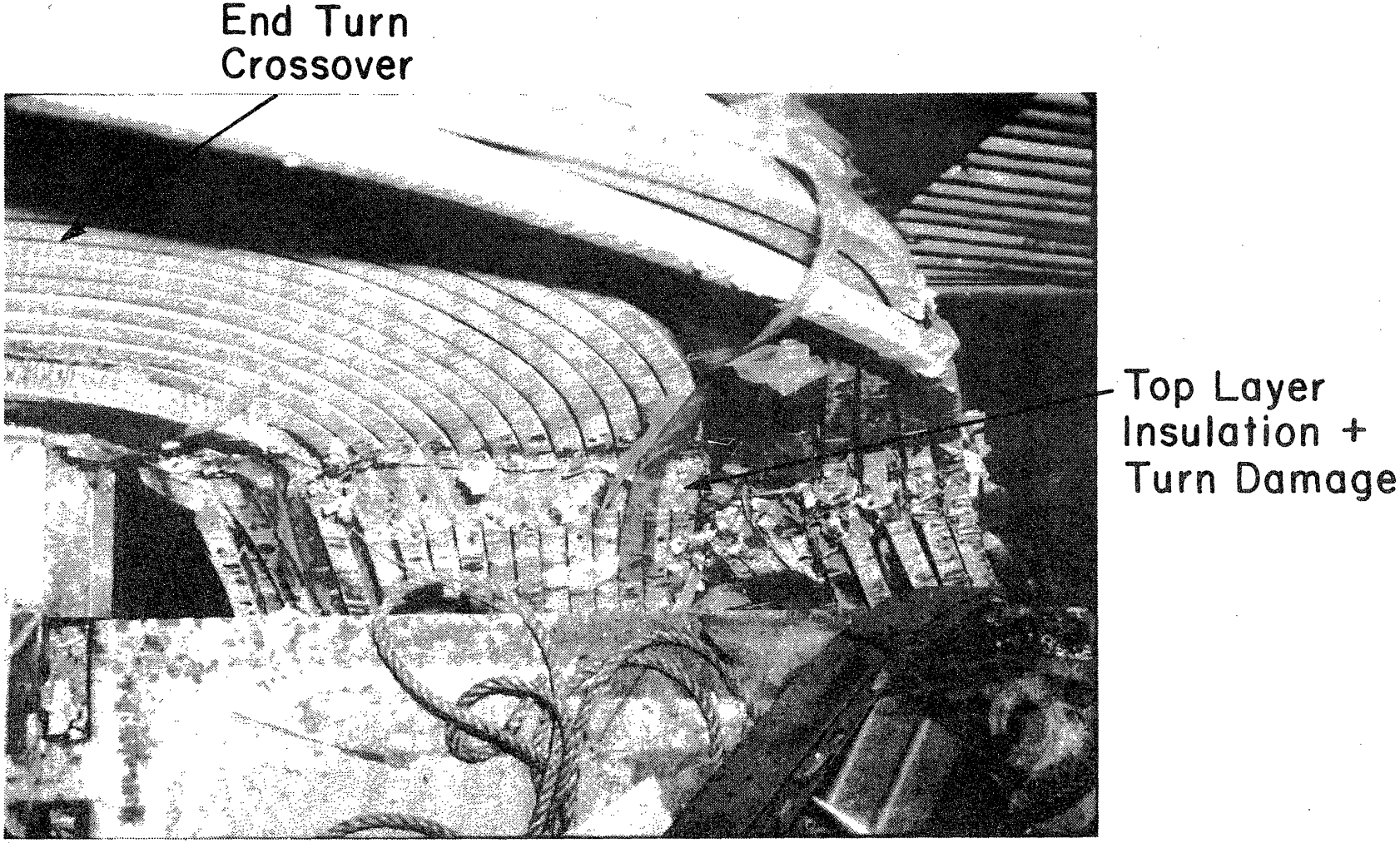

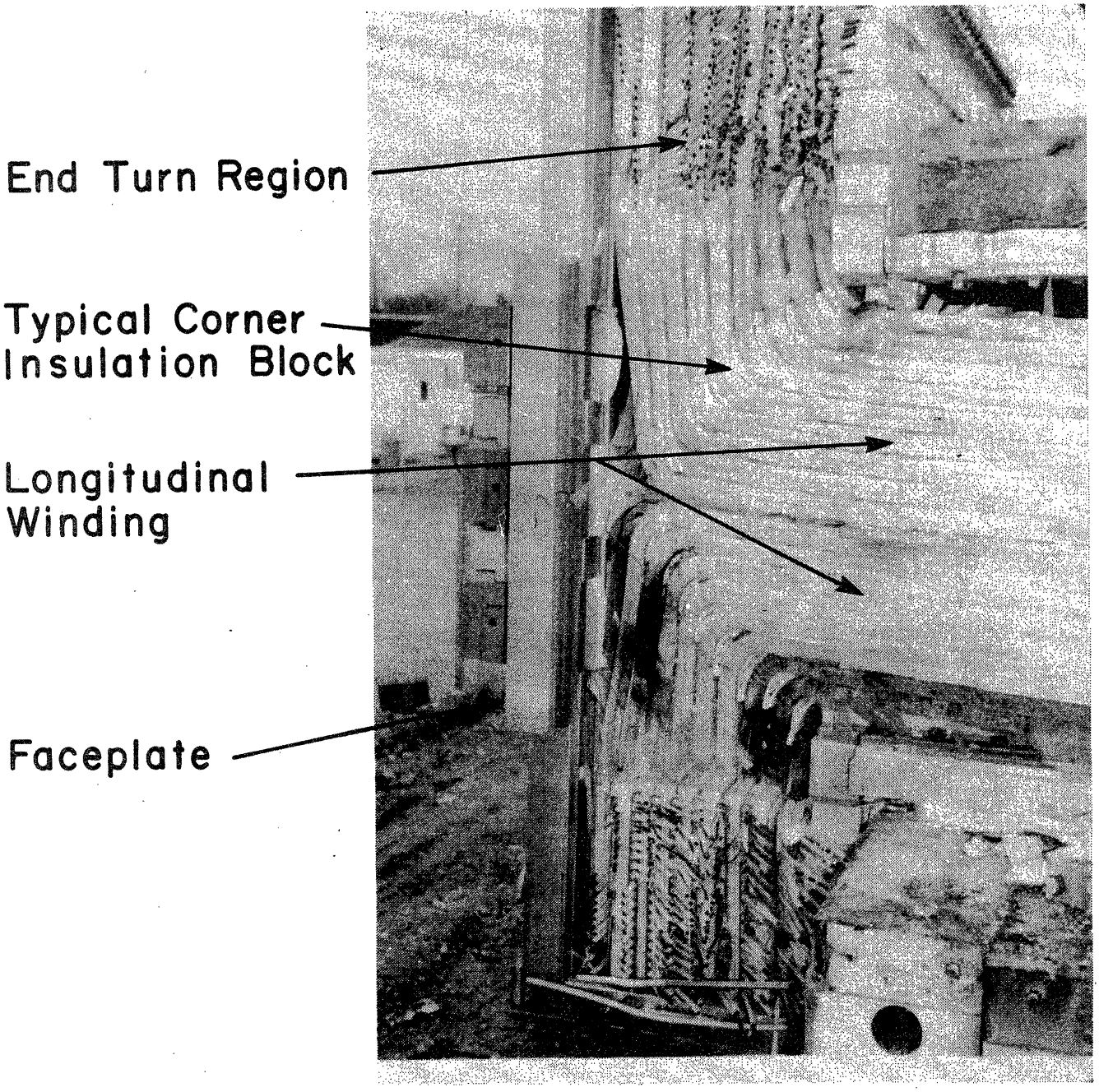

Figure 2.15 End turns with iron side structure removed. Note LTM fingers entrapped in faceplate.

The HPDE magnet failure was catastrophic in the sense that most structural components were fractured and the winding suffered extensive plastic deformation. However, operating procedures prevented possible injury to personnel and the rugged nature of the winding limited deformations to large but safe values, and restrained conversion of magnetic to kinetic energy of failed components. This suggests that it may de desirable to limit operating current densities in magnet design to levels whereby the winding could act in this structurally fail-safe manner even if it sustained substantial deformation in the event of a failure in its primary structure.

2.2 Preliminary Structural Failure Analysis (May 1983) - H. Becker, A. Hatch, P. Marston and J. Tarrh

Strength-of-materials calculations have been performed on the HPDE magnet at AEDC to assist in determining the nature and cause of the failure that occurred in the force containment structure (FCS) on December 9, 1982. From a structural standpoint, the broad basis for the failure appears to have been design flaws, particularly of structural details. Initiation of the failure was the result of severe overloading of the fingers in the ends of the "longitudinal tension members" where they penetrate the "face plate" and also of the fingers in the collar" (See Fig. 2.16). These very high local stresses were not detected in either of the previous stress analyses performed. The use of materials having low ductility may have contributed to the extent of the failure.

The results of the calculations are summarized and the most probable failure scenario is identified based on the calculations. The conclusions must be considered tenetative since they are founded on structural mechanics only,

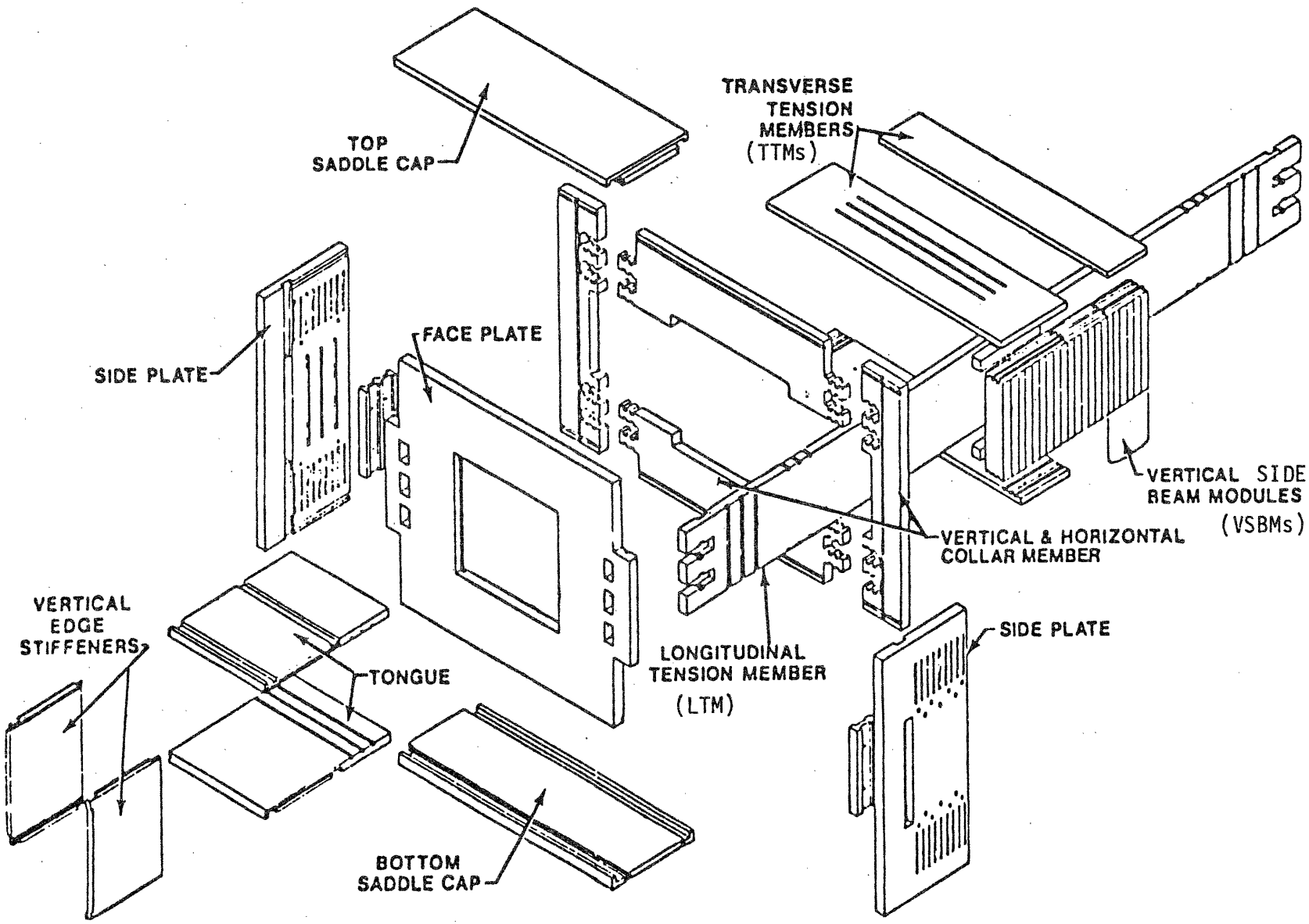

Figure 2.16 Expanded view of force containment structure (FCS) and key to abbreviations

although at present the locations and shapes of the visible fracture surfaces appear to substantiate the conclusions.

2.2.1 Failure Sources

The structural failure of the magnet, which occurred at only 2/3 of design field (less than half load), may be attributed to inadequate structures engineering. Four related aspects are discussed in this section: the design concept, the stress analysis, inspection, and the materials selection.

Design Concept

One of the design criteria for the force containment structure was ease of assembly and disassembly. One of the results of this criterion was the use of the vertical notches that cut through the fingers at the ends of the longitudinal tension members (LTMs). The consequent reduced section is among the prime candidates for the failure initiation site; however, a thorough analysis of the stresses in these areas had not been done previously.

The basic concept for the force containment structure requires the use of four load paths to transmit the major portion of the axial Lorentz load from the end structural plate/collar system into the LTMs, which react the axial forces. None of these load paths was considered stiff enough (by analysis) to transmit more than 40 percent of the axial force. Furthermore, the stiffest axial path would not begin to act until the remainder of the system were to deform to half the design value. Since the magnet never was loaded beyond that value, it is possible that the stiffest load path was inactive at the time of failure. However, this axial load condition appears to have had little influence on the mode of failure initiation.

Lorentz loads in all directions are transmitted through fingers, keys and key blocks. Tolerances among these structural elements and deformations during loading could alter the design load paths. As a result, local structural behavior could have become the most important factor in controlling the magnet's structural integrity.

Stress Analysis

Prior to this analysis, no calculations appear to have been made of the stresses induced by the transverse Lorentz forces on the LTMs and the surrounding structure at the magnet ends. That is, the longitudinal force supports were thoroughly analyzed, but no consideration was given to the effects of the transverse deflections of the structure (due to the transverse Lorentz loads) on the stresses in the longitudinal force supports. As will be shown, the axial stresses in the LTM fingers due to longitudinal forces alone are trivial compared with the actual stresses when the transverse deflections are taken into account. Conclusions about fatigue life were drawn from a fatigue curve constructed using an artificial procedure instead of test data. No fracture mechanics studies were performed.

Inspection

There is no record of inspection of critrical areas identified in the previous stress analyses, although ice formation was observed in areas where a crack might have been initiated. While the magnet was extensively instrumented, the strain gauges were located in such a way that critical stresses were not detected.

Material Selection

Aluminum alloys, which have low fracture toughness, were used for the force containment structure. They tend to propagate a fatigue crack rapidly when the crack length is of the order of 1/10 inch (a nominal minimum observable size) if the peak theoretical elastic stress exceeds 100,000 psi, as predicted would occur. In addition, the high strength 2000 series aluminum alloys commonly are corrosion sensitive.

All of these areas were working together against successful operation of the magnet. However, had adequate stress analysis of the structural details been performed, the inadequacy of the structure would have been apparent.

2.2.2 Stress Analysis

Summary

An analysis was conducted by MIT primarily to identify regions of high stress, the conditions that induced that stress, and the possible impact upon a failure scenario. Hand calculations were used since high precision was unnecessary. A number of dimensions were scaled from drawings. The results of the analysis appear to indicate the probable structural failure site and failure mode.

The dynamic behavior following failure initiation also was considered. In addition, a structural energy budget was prepared. A simplified fracture mechanics analysis was performed to supplement a fatigue life calculation.

The calculations were performed for nominal 4 tesla forces. Loads were actually assumed to be approximately 45 percent of the calculated forces shown in Fig. 2.1 (from Reference 2). The same fraction was used for the pressure

distributions given in Reference 3.

The structural behavior was assumed to be symmetric from side to side and from top to bottom.

The highest stresses were found at the outlet end of the magnet in the fingers of the LTMs and in the fingers at the corners of the collar (Figs. 2.17 and 2.18). The numerical magnitudes of the calculated stresses in these locations were of the order of twice the measured ultimate strengths of the aluminum alloys used in the FCS. Stresses at selected other locations were found to be in the range between yield and ultimate.

The presence of stress concentrations, ice pressure (if present), and temperature gradients would amplify these stresses. However, these effects were not included in the stresses calculated by MIT and reported herein.

The axial load paths were assumed to follow those shown in Reference 2. As mentioned above, however, calculations indicate that small tolerances at the various keys in the system could alter the Lorentz load distribution and possibly, in an extreme case, eliminate one or more thereby overloading the others. Furthermore, the use of a gap in the spacer bar (between LTM and TTM) indicated that below 4 T the potentially stiffest load path for longitudinal forces was out of action.

Results of Calculations

The peak stresses were found to occur in the downstream fingers of the LTMs (Fig. 2.17) and in the corner fingers of the collars (Fig. 2.18).

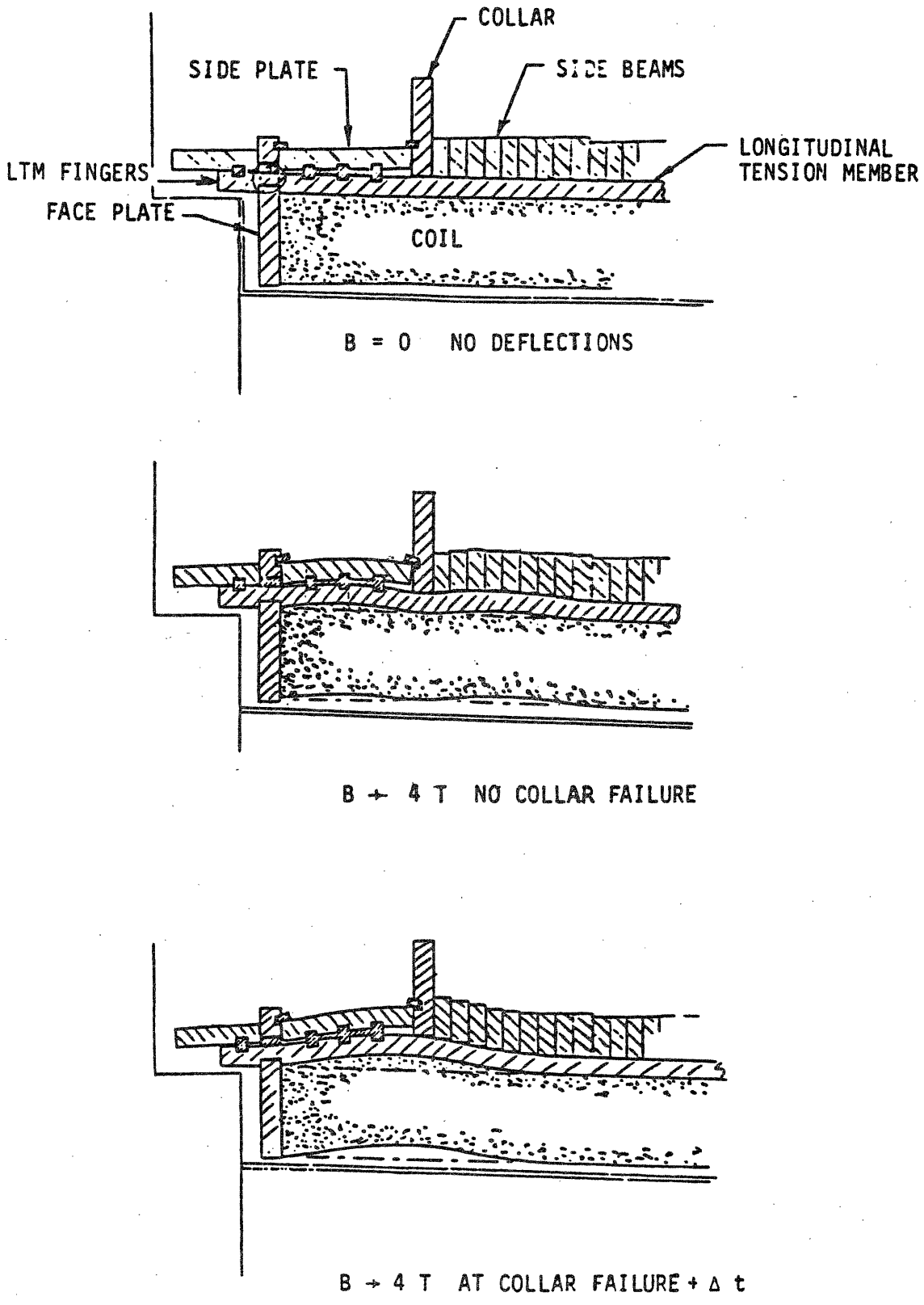

Figure 2.17 Exaggerated depiction of LTM-related deflections at the magnet midplane

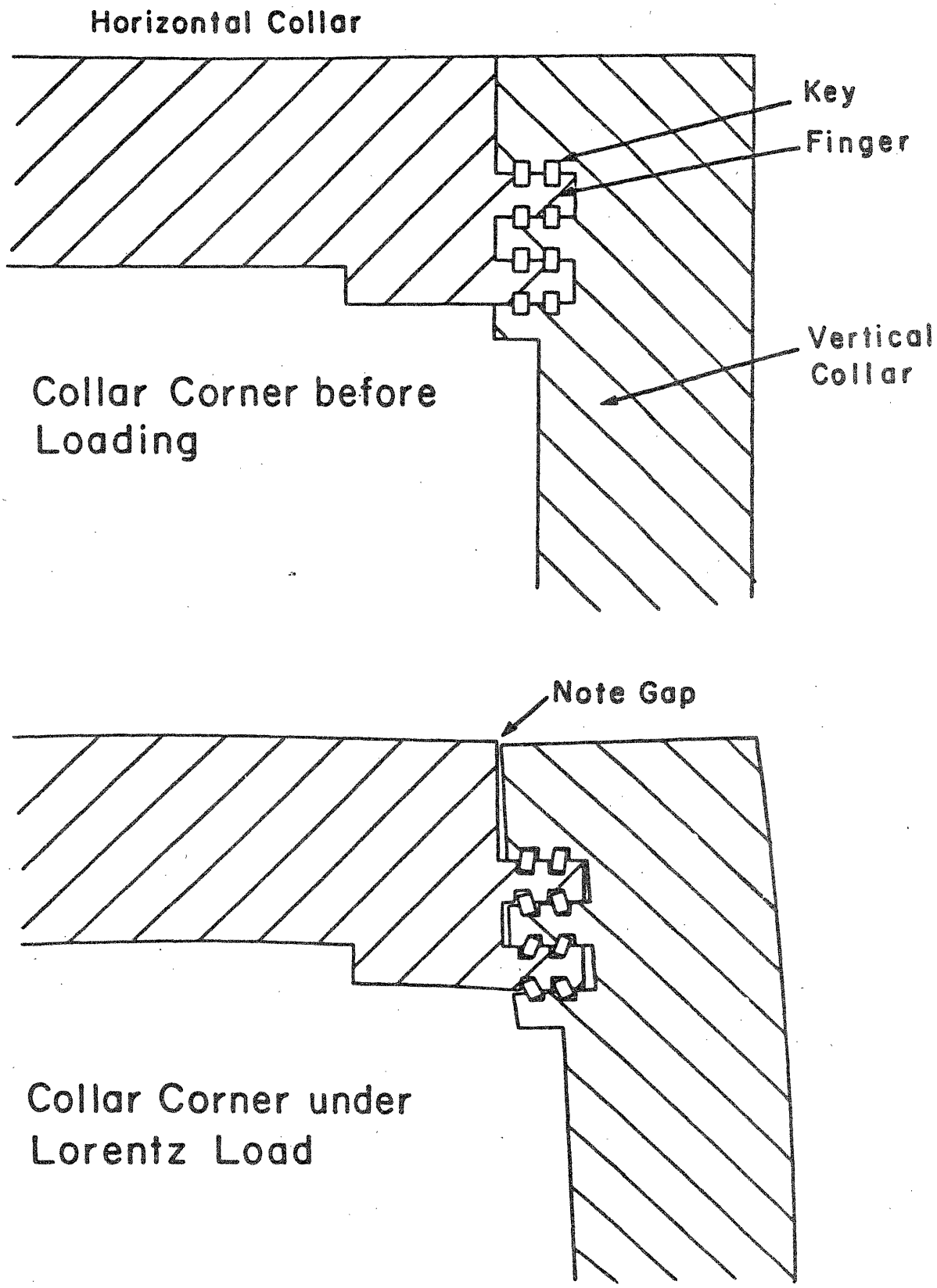

Figure 2.18 Collar corner behavior

The major stresses in the LTM fingers were due to sidewise bending of all the fingers about a vertical axis and vertical bending about a horizontal axis in the top and bottom fingers only. As mentioned herein above, the axial tension was small. Figure 2.19 depicts the stresses due to each component. Combined values appear in Fig. 2.20.

In addition to the high normal stresses (nominally twice the 86 ksi ultimate tensile strength of 2219 aluminum alloy at 77 K) a twisting shear stress of the order of the ultimate strength can act on the plane of the nominal fracture surface. It would arise from resistance to the anticlastic (saddle shape) curvature induced by the horizontal bending of the LTM (Fig. 2.21). (It should be noted that anticlastic curvature was observed at the LTM downstream end where the fingers broke.)

The neutral axis orientation in each finger is shown in Fig. 2.20. Each is rotated slightly from the vertical. The sense of rotation is different from that measured at AEDC (Fig. 2.22). However, the discrepancy is slight and may be due to the torsional shear and to details of the key/block/faceplate fitup at each finger.

The sidewise deflection shape of the LTM is shown in Fig. 2.17. The cause of the large horizontal bending stress is depicted. It arises from LTM bending (induced by the transverse Lorentz forces) between the faceplate and collar, together with bending from the outward deflection of the collar. The sideplate was found to be too flexible to support more than 20 percent of the Lorentz pressure on the LTM. Furthermore, the collar was found to react some of the transverse Lorentz pressure that would be expected to act on the VSBM/TTM

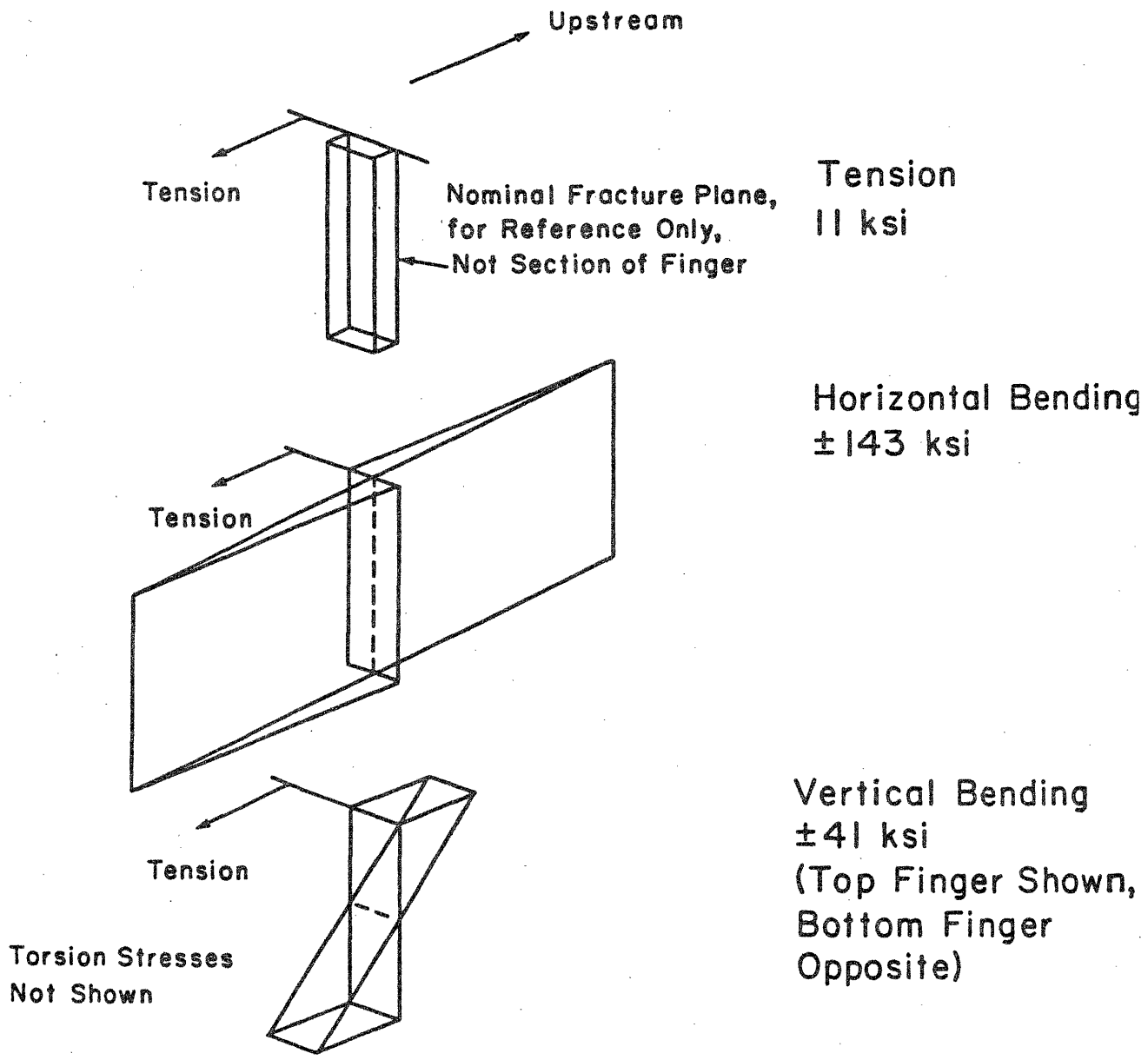

Figure 2.19 Stress components acting perpendicular to nominal fracture plane of LTM downstream fingers at groove.

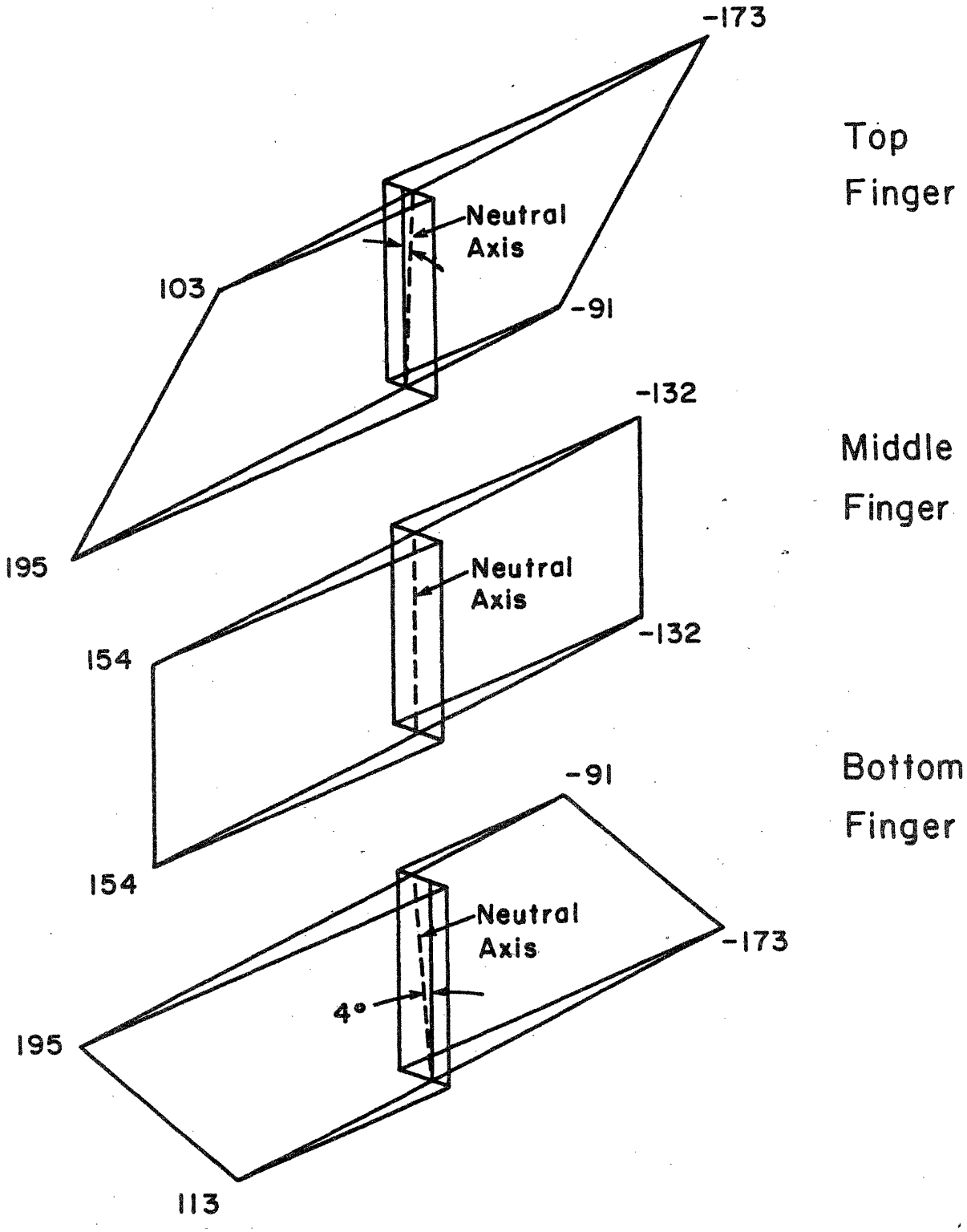

Figure 2.20 Combined stresses (ksi) in sections of LTM downstream fingers

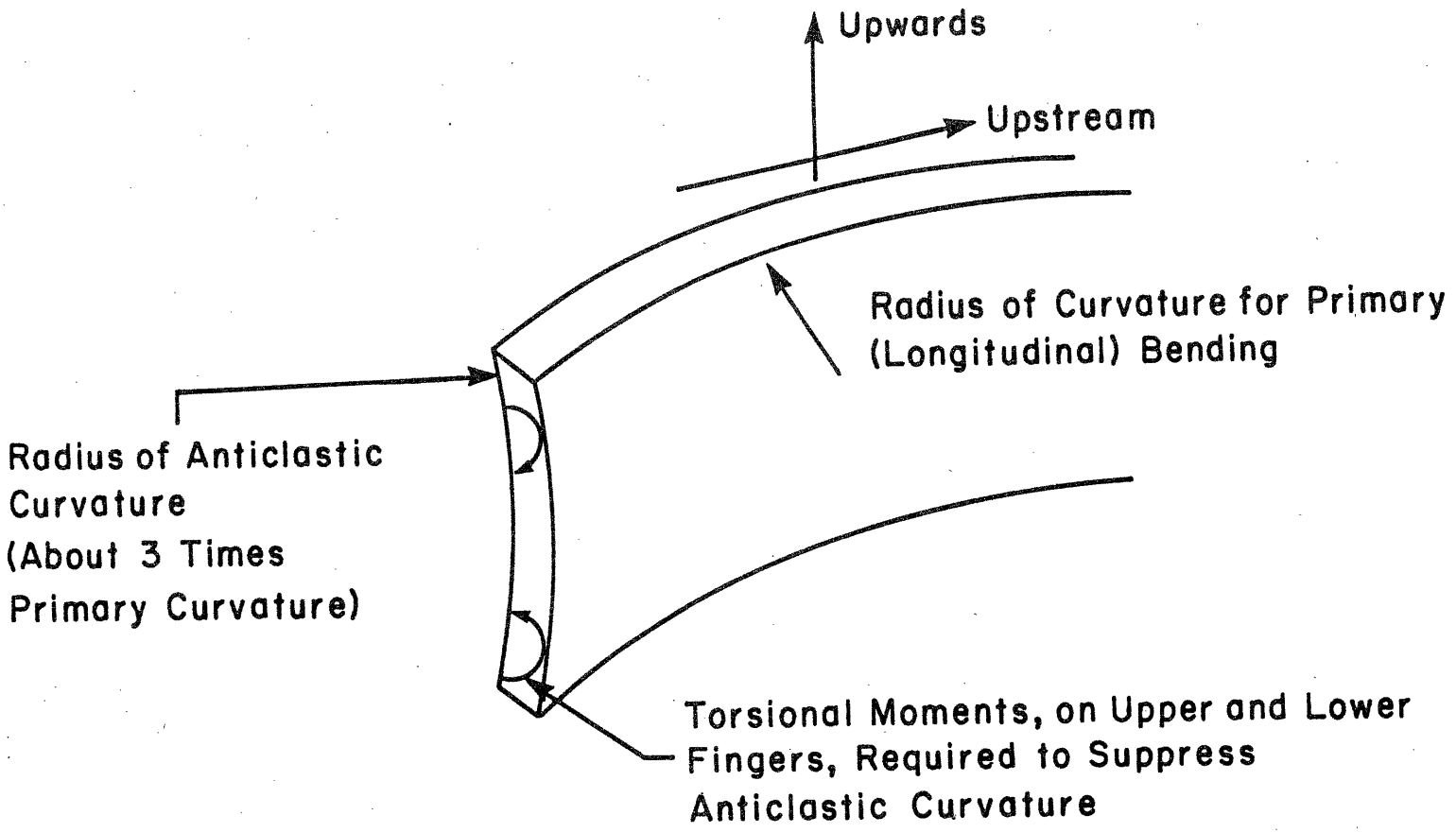

Figure 2.21 Anticlastic curvature effects at ends of LTM

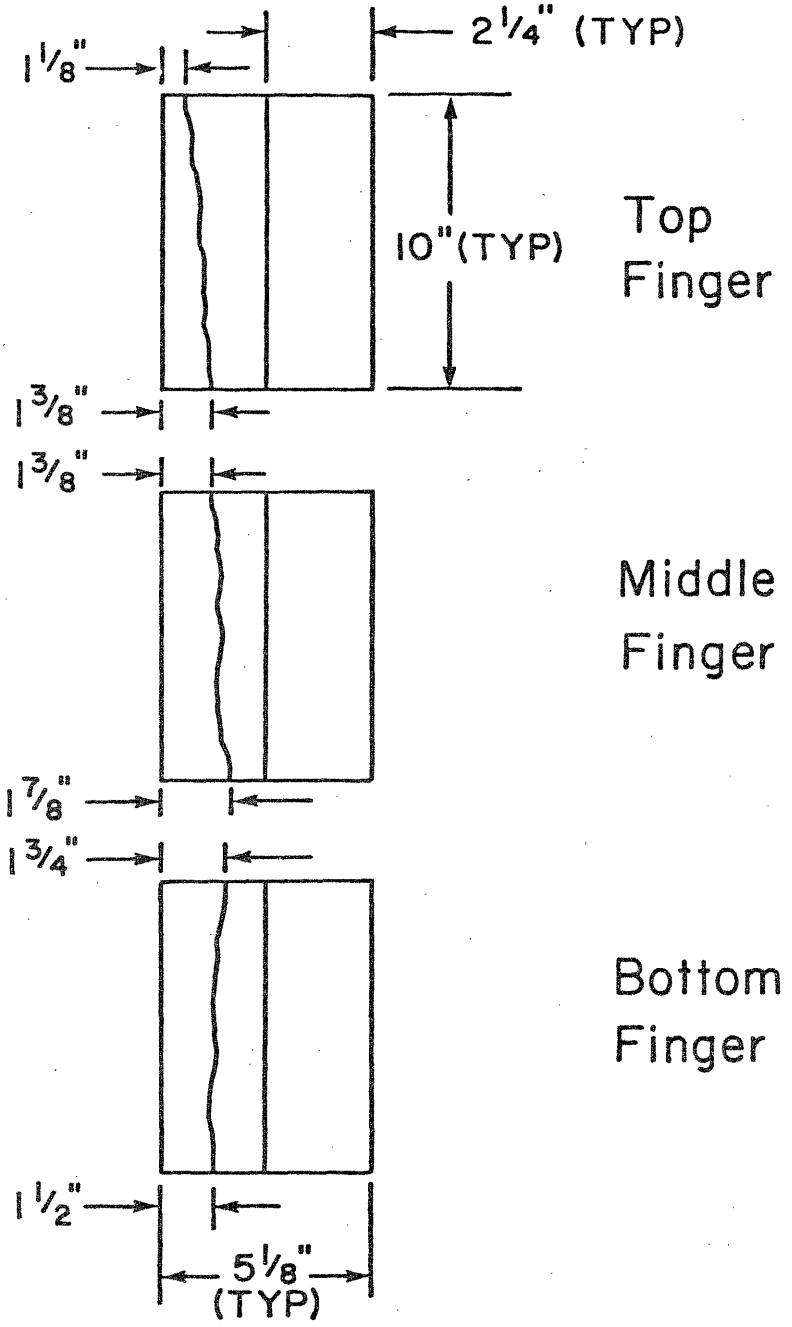

Figure 2.22 Approximate center of fracture "valley" to edge of LTM

subsystem. The local load distribution was found from assuming the VSBM/TTM combination to act as an elastic foundation for the LTM, taking the finite rigidity of the collar into account.

The calculations indicate that the large transverse force on each vertical collar causes the corner fingers to stretch far enough to prevent contact of the vertical faces of the horizontal and vertical collars (Fig. 2.18). Therefore, the local rotations could be resisted only by the fingers in vertical bending. The axial forces on the collars induced bending about a vertical axis thereby inducing a stress field similar to that in the LTM fingers (Figs. 2.19 and 2.20) and at a comparable level of combined stress.

The calculated numerical values of stress in the fingers of the LTMs and the collars differ somewhat but are of the same order of magnitude (twice the ultimate tensile strength of 2219). Precise comparisons would be of little value at present considering the indeterminate factors mentioned above. Most important, however, is the fact that the calculated stresses do not include concentration factors.

Fatigue Life Estimate

An estimate was made of the fatigue life to be expected for the HPDE FCS at a peak field of 4 T with most pulses at much lower values. For this purpose, the alternating stress was chosen arbitrarily at 86 ksi since most of the fatigue damage would occur at the higher stresses, and concentrations would tend to increase the stresses (or resultant strains) mentioned above. The curves of Fig. 2.23 were used for the prediction. They indicate 36 cycles using Reference 3 data and 10 times that for the assumed AEDC curve.

Figure 2.23 Comparison of life cycle curves used in magnet design and force containment structure calculations

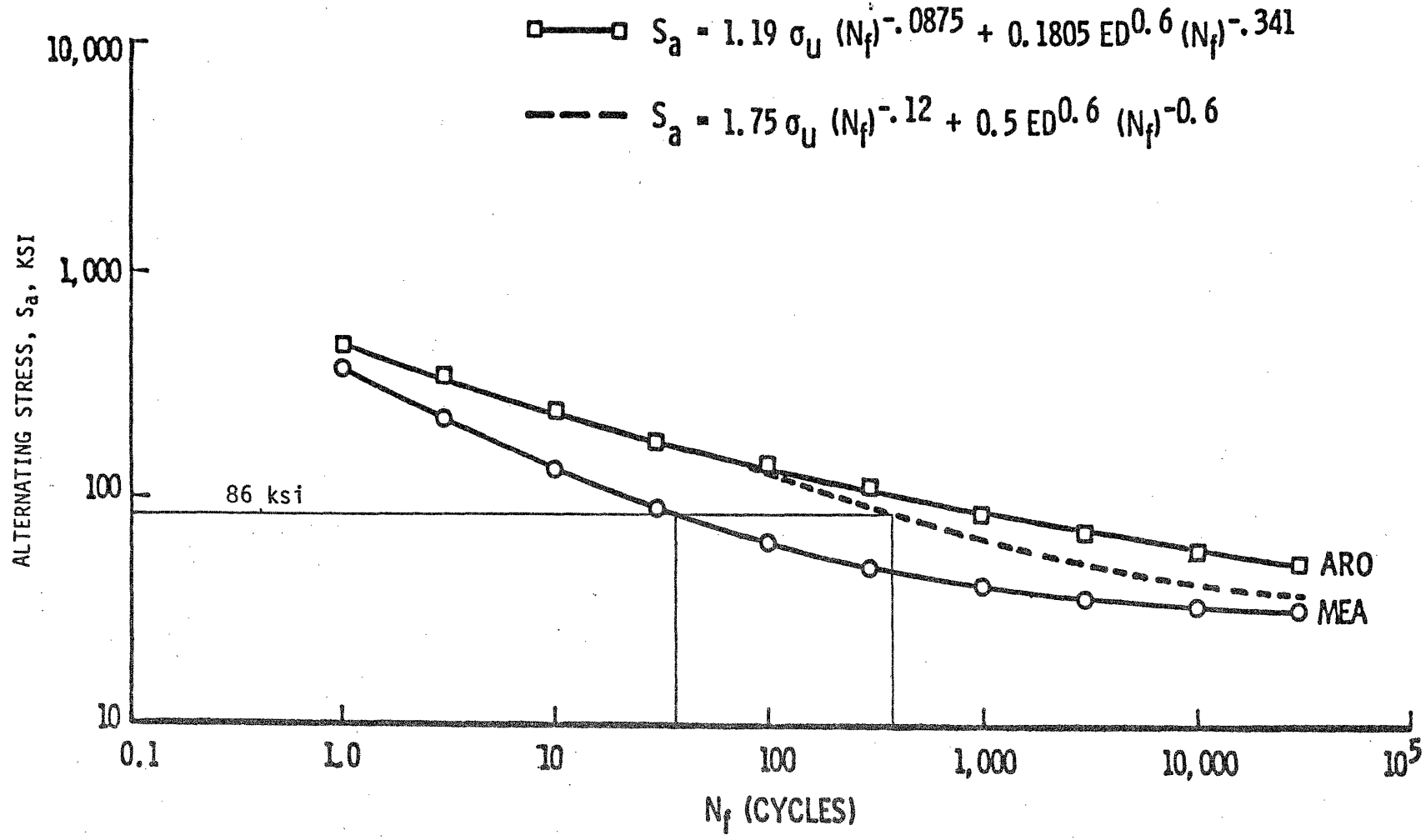

These results raise the question of possible cracking at the LTM and collar fingers at early stages in the life of the system. However, the small critical crack size (of the order of 1/32 inch at 83 ksi from a linear elastic fracture mechanics calculation) also indicates the potential difficulty of observing cracks during a casual inspection. A dye penetrant procedure, for example, would have been required.

2.2.4 Failure Scenarios

Sites and Modes

The calculated high stresses in the fingers of the LTMs and collars indicate that either could have been the site of initial failure (Figs. 2.17 and 2.18). Furthermore, if either set of fingers was to break suddenly, failure of the other set would be expected to follow within fractions of a millisecond.

After the LTM fingers broke, the axial stress wave resulting from the unloading traveled upstream. The mass of the LTM behind the front was moving upstream at 10 to 15 miles per hour. The wavefront reached the aluminum mass at the inlet in 2 milliseconds and the LTM applied an impact load to the components. During that time, and subsequent to it, the Lorentz side forces used the coil and LTM as a crowbar to provide enough additional overload to break the collar. The LTM then "unzippered" the VSBM/TTM subsystem.

In spite of the 0.13 m thickness, the sideplate is flexible and weak because of the vertical grooves cut into it. As a result, it might not affect the unloading process that would follow fracture of the LTM fingers. The sideplate also has a plane of weakness through the vertical groove at the

faceplate notch. The sudden upstream movement of the LTM would tend to break the plate along that groove. Also, the lateral pressure on the broken LTM would tend to throw it and the sideplate sideward. That could disengage the three vertical keys between the LTM and sideplate.

If the collar failed first then the sideplate would have been thrown free as the LTM fingers failed. The time differences involved are of the order of microseconds.

When the sideward VSBM/TTM stripping action reached the inlet region, the laternal force would tend to break the upstream collar. The LTM finger failure would occur shortly thereafter because of the sideways loading that would build up a large bending moment on the LTM with a peak at the observed fracture site. Furthermore, the compression load from the inlet end wave reflection would tend to maintain contact on the LTM at the upstream faceplate. As the LTM deflected sideward, the downstream compressive force would act on that deflection to increase the bending moment. The combination probably led to the observed upstream failure of the LTM.

The impact of the LTM on the faceplate could also account for the fracturing of the lips on the upper and lower tongues.

Lateral Lorentz forces on the bowed coil would be resisted by sideward components from tension forces in the conductors at the inlet and outlet saddles. The axial component would be resisted by the steel. The observed final position of the coil can be accounted for by that mechanism as the means of stopping the dynamic action. The copper stress would be 27,000 psi and the strain would be 0.015. The combination would be reasonably close to a representative

stress-strain curve for annealed copper at 100 K.

Using that type of stopping action, calculations were made that indicate the entire failure event occurred within 50 to 100 milliseconds.

Energy Budget

The stored magnetic energy at 4 T is approximately 160 MJ. The total fracture energy is estimated at 0.7 MJ. Plastic deformation of the copper coil could account for 7 MJ. Sliding friction of the steel masses could dissipate another 0.5 MJ. That total is approximately 8 MJ or 5 percent of the stored magnetic energy. On the other hand, the entire stored energy could be accounted for by an 8 K temperature rise in the copper coil (starting at 100 K) subsequent to the structural failure.

Future Work

The analysis leading to the above conclusions will be reviewed, refined and documented. These results will be presented as part of a workshop on the structural design basis for large superconducting magnets.

It is also interesting to consider the extent of the structural damage to a comparable superconducting magnet wherein the coils remained superconducting during the event and the total stored energy was available for mechanical deformation. This consideration will be incorporated into on-going safety and protection studies and will also be discussed at the aforementioned workshop.

REFERENCES

1. R.M. James, et al., "Investigation of an Incident During Run M1-007-018 MHD High Performance Demonstration Experiment (PWT) on December 9, 1982", ARVIN/CALSPAN Field Services, Inc. AEDC Division, Arnold Air Force Station, TN., April 1983.

2. H.J. Schmidt, et al., "Report on the MHD Performance Demonstration Experiment". For the Period October 1, 1976 to September 30, 1977. FE-1542-35. Sverdrup/Aro, Inc., March 1978.

3. Anon, "Dual Mode MHD Magnet, Vol. 2, Appedices". Magnetic Engineering Associates Report.

3.0 MAGNETIC TO KINETIC ENERGY CONVERSION FOLLOWING STRUCTURAL FAILURE

R.J. Thome and W.G. Langton

3.1 Summary

In this section, an idealized magnet structural failure problem will be analyzed to develop insight into the governing parameters, the sequence of events, and the time scale over which the events occur. The analysis is then applied to examples which show the dramatic difference in character if the coil is driven beyond its ultimate strength after the structure fails versus the case where the coil can absorb the total load without rupture even though some yielding is necessary.

The model and examples are based on an infinitely long solenoid configuration. This simple shape allows the important parameters to become apparent. The preliminary conclusions are:

(a) A protective circuit reaction involving dissipation in resistive elements following a major structural failure is unlikely to be effective on a fast enough time scale to limit the magnetic to kinetic energy conversion process in magnets using high current density windings.

(b) Windings with low enough current densities can absorb the total load following structural failure, thus limiting the kinetic energy conversion process, although this might involve substantial yielding and deformation of the winding. This is not usually a design requirement, but might form the basis for one criteria for large magnet design.

(c) Protective circuits involving inductive energy transfer can respond fast enough to limit the kinetic energy conversion process in high or low current density configurations. The range of coupling coefficients and time constants to allow this method to be effective are under study. This is the source of our interest in the use of multiple circuits for discharge of a TF coil system as begun this year and as discussed in Section 4.

The preliminary conclusions will be evaluated further as part of next years Large Magnet Safety and Protection Effort. Consideration will be given to model alteration to include non-solenoidal effects.

3.2 Model Description - Resistive Protection

Figure 3.1 shows a long thin solenoid consisting of a coil and an external structure. The coil produces a magnetic field B within the bore and has a radial build t_c and length ℓ_o. The magnetic field produces an outward radial pressure, $B^2/(2\ \mu_o)$ which is reacted by hoop tension F_c in the coil and F_s in the structure. The structure is assumed to be composed of a series of alternating strong and weak links where the latter are the conceptual equivalent of fasteners, welds or other stress concentrators in the structural material. In the model, the strong members have a radial build t_s and the weak members have a radial build, t_w. A force balance on the element shown requires:

$$F_s + F_c = \left(\frac{B^2}{2\ \mu_o}\right) r\ \ell_o \tag{3.1}$$

The stresses in the coil and structural components are related to the loads by:

$$F_s = \sigma_s\ t_s\ \ell_o = \sigma_w\ t_w\ \ell_o \tag{3.2}$$

$$F_c = \sigma_c\ t_c\ \ell_o \tag{3.3}$$

where

σ_j = hoop stress, $\quad j = s,w,c$

The coil and structure expand the same amount when the load is applied so geometric compatibility requires

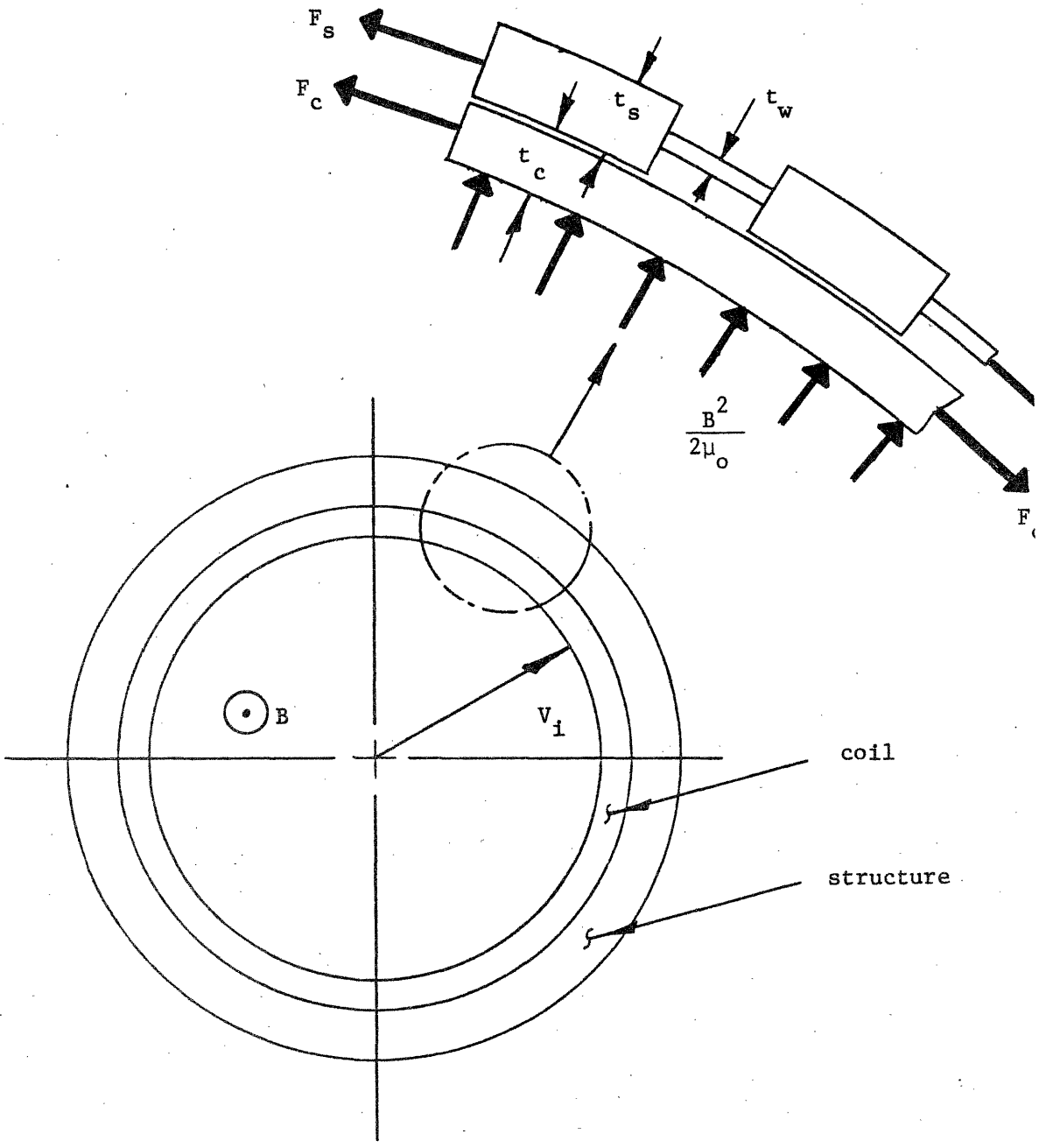

Fig. 3.1 Idealized Model of Solenoid with External Structure Having Weak Links

$$\varepsilon_c = f\,\varepsilon_w + (1-f)\;\varepsilon_s \qquad (3.4)$$

where:

ε_j = strain, $\quad j = s,w,c$

f = fraction of circumference occupied by weak links

The stress and strain in the materials are determined by the constituent relations. In this case, we will assume the ideal elastic stress-strain curves shown in Fig. 3.2a. The yield strengths for the structure and coil materials are σ_{wy} and σ_{cy}, respectively, and the ultimate strain capability of the coil corresponding to rupture is ε_u.

Figure 3.2b illustrates a typical design point without weak links where the coil and structure have the same strain and operate at some fraction of their respective yield strengths. Figure 3.2c, on the other hand, shows a possible condition for the first charge to the operating level when links are present which are weak enough (i.e., - t_w is small enough in the model) so that the links are loaded beyond yield and stretch plastically. The strain at each of the three points may be shown to be

$$\varepsilon_s = \frac{\sigma_{wy}}{E_s} \qquad \frac{t_w}{t_s} \qquad (3.5)$$

$$\varepsilon_c = \left(\frac{B^2}{2\,\mu_o}\;r - \sigma_{wy}\;t_w\right) / (E_c\,t_c) \qquad (3.6)$$

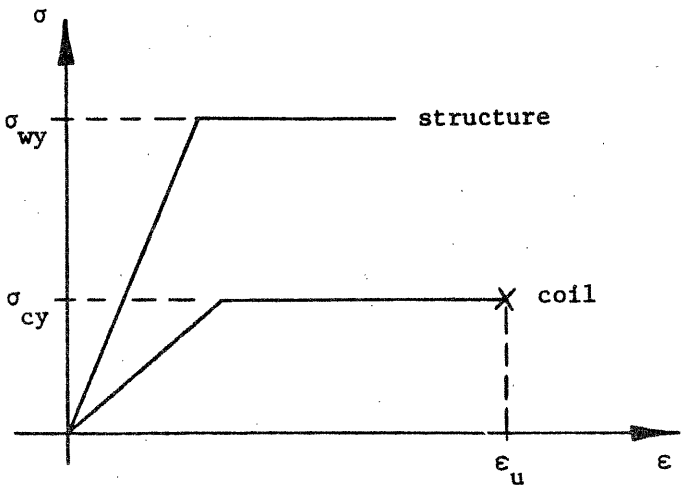

Fig. 3.2a Ideal elastic-plastic stress strain curves for the coil and structure

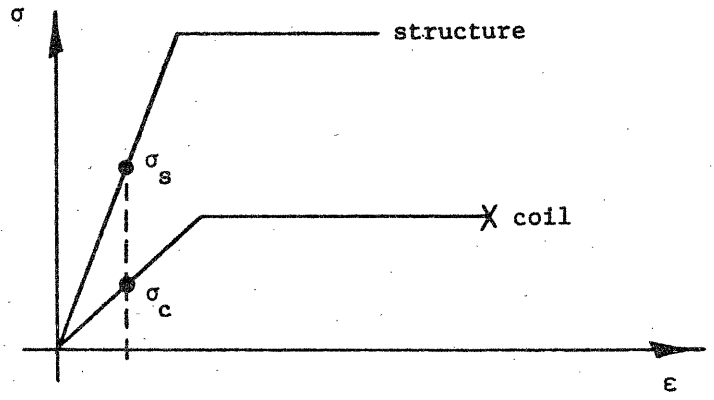

Fig.3.2b Typical design without "weak" links

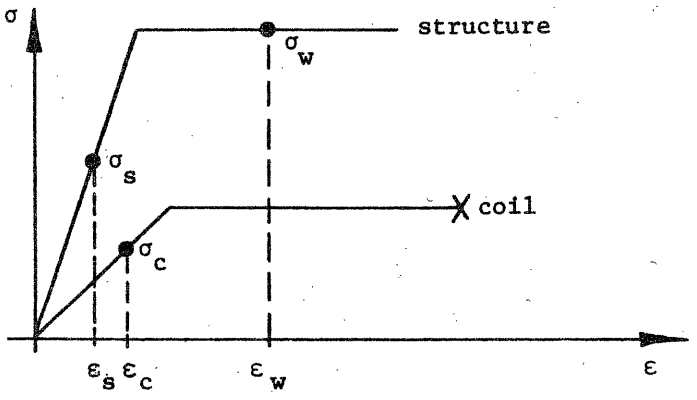

Fig. 3.2c Possible design with "weak" links

$$\varepsilon_w = f^{-1} \left[\varepsilon_c - (1-f) \ \varepsilon_s \right] \qquad (3.7)$$

where

E_j = modulus of elasticity, j = s,c

If the coil is discharged, the coil and strong components of the structure recover along the same curves, but, because of the yielding at w, the weak structure recovers along a different path. This is illustrated in Fig. 3.3 . The final state is represented by points c', s', and w' in the figure which assumes that the coil cannot pull away from the structure. The coil is left with a residual tension and the structure with a residual compression such that:

$$\sigma_{c'} = \frac{\left(\varepsilon_w - \frac{\sigma_{wy}}{E_s} \right) f}{\left[\frac{1}{E_c} + \frac{(1-f)\ t_c}{E_s\ t_s} + \frac{f t_c}{E_w\ t_w} \right]} \qquad (3.8)$$

$$\sigma_{s'} = - \ \sigma_{c'} \frac{t_c}{t_s} \qquad (3.9)$$

$$\sigma_{w'} = \sigma_{s'} \frac{t_s}{t_w} \qquad (3.10)$$

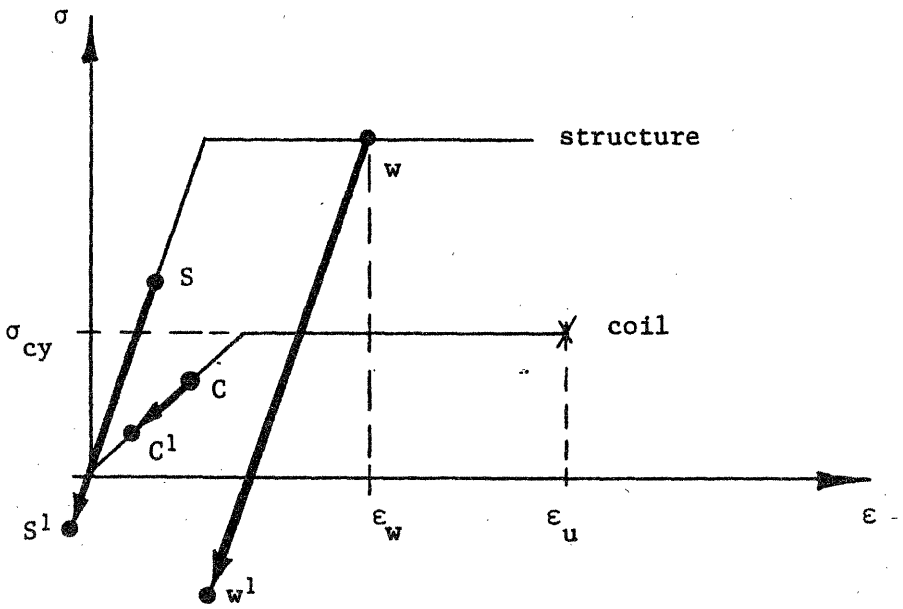

Fig. 3.3 On the first charge, the materials start at the origin and are loaded to c, s and w. On discharge s and c recover along the same curves, but because of the yielding at w, it recovers along a new curve.

If the coil is then repeatedly charged to the original point and discharged, the material will cycle between the primed and unprimed states in Fig. 3.3. Assume that, after a number of cycles, the weak links fail at t = 0 with the materials in the charged state, c, s and w, at $t = 0^-$. At t = 0 the entire electromagnetic load transfers to the coil and subsequent events depend strongly on whether the load is of sufficient magnitude and maintained for a long enough time interval to strain the coil material into the plastic range and up to its ultimate strain, ε_u, at which point the coil material also ruptures.

For simplicity, the weak links will be assumed to break simultaneously and uniformly around the periphery. Figure 3.4 then illustrates the force balance in which the electromagnetic load is accelerating the mass outward, but is restrained by the hoop tension in the coil. The force balance may be written as follows:

$$\frac{B^2}{2\mu_o} r \ell_o d\theta - 2F_{cr} \sin\left(\frac{d\theta}{2}\right) = \frac{M}{(2\pi r \ell_o)} r \ell_o d\theta \frac{d^2r}{dt^2} \qquad (3.11)$$

where:

M = total mass of coil and structure

As the coil expands radially, its cross section necks down such that

$$t_{cr} = t_c \left(\frac{r_i}{r}\right) \qquad (3.12)$$

where:

t_c = initial coil thickness when at radius, r_i

t_{cr} = coil thickness when expanded to a radius r

The restraining force, F_{cr}, provided by the coil depends on whether the coil material is in the elastic range, plastic range or beyond its

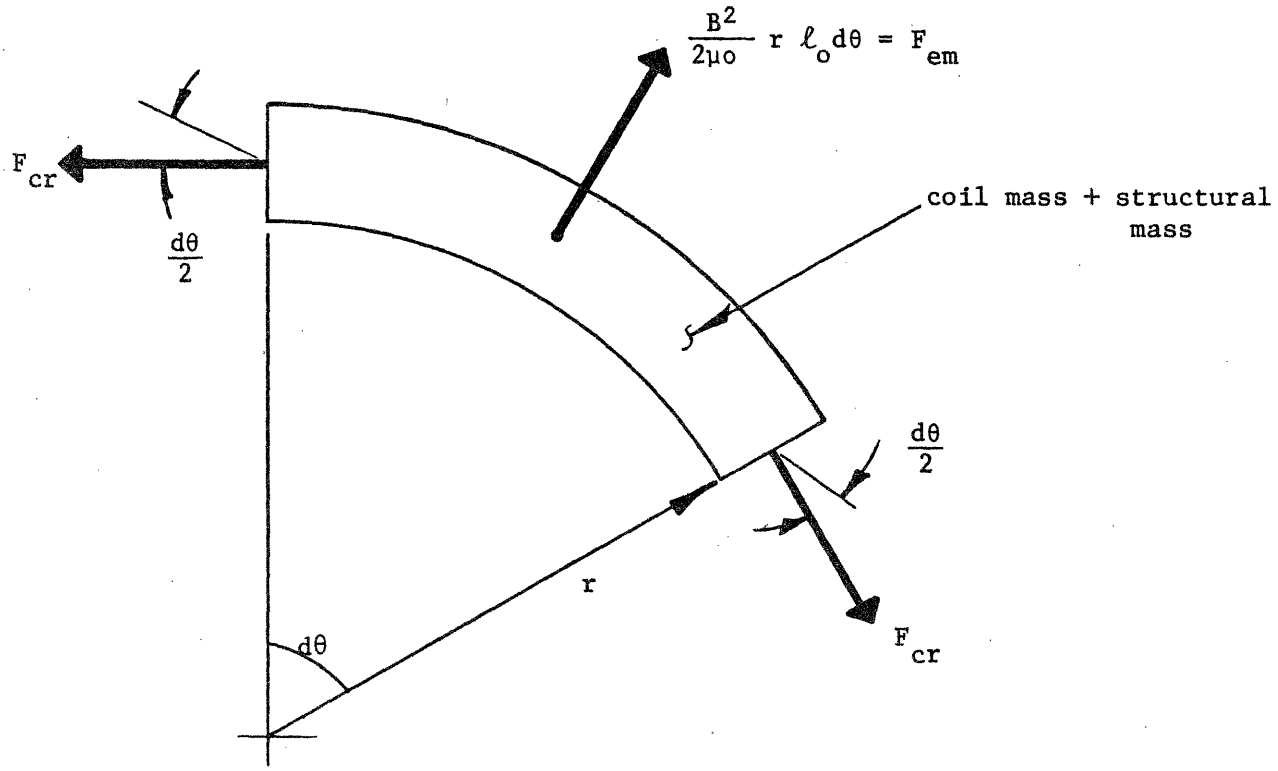

Fig. 3.4 Element of Coil and Structure Being Accelerated Radially by the Electromagnetic Force, F_{em} and Restrained by the Hoop Tension, F_{cr}, in the coil.

ultimate strain. Following the nomenclature in Fig. 3.3, this becomes

$$F_{cr} = \begin{cases} E_c\,(r/r_i - 1)\,t_c\,\ell_o & \text{, if } (r/r_i - 1) < \sigma_{cy}/E_c \\ \sigma_{cy}\,t_c\,\ell_o & \text{, if } (r/r_i - 1) > \sigma_{cy}/E_c \\ 0 & \text{, if } (r/r_i - 1) > \varepsilon_u \end{cases} \tag{3.13}$$

The electromagnetic force is determined by B which is dependent on the current in the coil and the circuit characteristics. Assume the circuit to be the coil with an initial inductance, L_o, in series with a resistor R(t) which can be later specified to characterize a superconducting coil with a discharge resistor or a conventional resistive coil. For an infinitely long coil, the inductance is proportional to the bore area, hence, as the coil expands its inductance changes such that

$$L = L_o \frac{r^2}{r_i^2} \tag{3.14}$$

where:

L_o = coil inductance when its radius is r_i

The circuit equation is given by

$$\frac{d}{dt}(LI) + IR(t) = 0 \tag{3.15}$$

Equations (3.11) to (3.15) may now be combined and normalized to produce the following governing equations.

$$\eta^2 \frac{dI_n}{d\tau} + 2I_n \eta \frac{d\eta}{d\tau} + I_n R_n = 0 \qquad (3.16)$$

$$\eta I_n^2 - F_o \gamma = \frac{d^2 \eta}{d\tau^2} \qquad (3.17)$$

where:

η = r/r_i

I_n = I/I_o

I_o = initial current

τ = t/τ_o

$$\tau_o = \sqrt{\frac{M r_i}{2 \pi r_i \ell_o B_o^2/(2 \mu_o)}} \qquad (3.18)$$

L_o = initial inductance

R_o = characteristic resistance = L_o/τ_o

R_n = $R(t)/R_o$

$R(t)$ = coil resistance as f(t)

$$\gamma = \begin{cases} \dfrac{E_c}{\sigma_{cy}} (\eta - 1) & \text{if } (\eta - 1) < \sigma_{cy}/E_c \\ 1 & \text{if } (\eta - 1) > \sigma_{cy}/E_c \\ 0 & \text{if } (\eta - 1) > \varepsilon_u \end{cases} \qquad (3.19)$$

$$F_o = \frac{\sigma_{cy} t_c \ell_o}{\left(\dfrac{B^2}{2 \mu_o}\right) r_i \ell_o} \qquad (3.20)$$

The independent variable in (3.16) and (3.17) is τ, the normalized time, the dependent variables are η, the normalized radius and I_n, the normalized current; R_n is a normalized resistance which can be a specified function to allow different discharge characteristics to be studied; γ is a function of η which determines if the restraining force supplied by the coil is in the elastic or plastic range or if the coil has been strained to rupture. F_o is a parameter determined by the characteristics of the coil structural system. It is a measure of the maxiumm load carrying capabilities of the coil relative to the initial magnetic load. The characteristic time, τ_o, is a measure of the time required to accelerate the entire mass of the system a distance r_i under the action of the total magnetic force initially available.

The resistance function R_n is normalized to $R_o = L_o/\tau_o$. If, for example, the coil were superconducting without a dump resistor and with its terminals essentially short circuited through its power supply then $R_n = 0$; if the coil were superconducting with a dump resistor, R_i in the circuit or if it were a conventional coil with a constant resistance then $R_n = R_i \tau_o/L_o$; if the coil were an expanding conventional solenoid with an initial resistance R_i and its cross-section necking down uniformly according to (3.12) then $R_n = (R_i \tau_o/L_o)(r/r_i)^2$. Since L_o/R_i would be the usual discharge time constant for these cases, we can define $\tau_d = L_o/R_i$ and rewrite these different cases as follows:

$$R_n = \begin{cases} 0 & \text{, if circuit resistance is zero throughout transient (eg - superconducting)} \\ \tau_o/\tau_d & \text{, if circuit has constant resistance } R_i \text{ throughout transient} \\ (\tau_o/\tau_d)\,\eta^2 & \text{, if coil has initial resistance } R_i \text{ and "necks down" during transient according to (3.12)} \end{cases} \tag{3.21}$$

Note that τ_o is determined by the mass and initial magnetic condition of the system and that the system circuit resistance cannot have much effect on the transient if $\tau_o \ll \tau_d$. This is illustrated in Section 3.3 together with the effect of the parameter F_o which determines whether the system strains beyond the ultimate strain and fractures or whether it is contained.

If $\tau_o \ll \tau_d$, then the resistance is ineffective and the coil current changes during the coil expansion so as to maintain constant flux linkage. Hence, for the solenoid in Fig. 3.1, the final field in the coil just before fracture is given by:

$$B_f = B/(1 + \varepsilon_u)^2 \tag{3.22}$$

and the stored magnetic energy per unit length just before fracture which is available for conversion to kinetic energy is:

$$E_f/\ell_o = (B_f^2/2\mu_o)\,\pi\, r_i^2\,(1 + \varepsilon_u)^2 \tag{3.23}$$

For the general case, the governing equations are non-linear but can be solved numerically by writing them in finite difference form and integrating forward in time. The approach assumes that the net force is constant during any interval $\Delta\tau$ and may be summarized as follows:

$$\left.\frac{d\eta}{d\tau}\right|_{m+1} = \left.\frac{d\eta}{d\tau}\right|_{m} + \Delta\tau \left[I_m^2 \eta_m - F_o \gamma_m\right] \tag{3.24}$$

$$\eta_{m+1} = \eta_m + \Delta\tau \left.\frac{d\eta}{d\tau}\right|_{m} \frac{(\Delta\tau)^2}{2} \left[I_m^2 \eta_m - F_o \gamma_m\right] \tag{3.25}$$

$$I_{m+1} = I_m \left\{ 1 - \Delta\tau \left[\frac{2}{\eta_{m+1}} \left.\frac{d\eta}{d\tau}\right|_{m+1} + R_{m+1} \left(\frac{1}{\eta_{m+1}}\right)^2 \right] \right\} \tag{3.26}$$

The initial conditions required to start the iteration are $I = 1$, $\eta = (1 + \varepsilon_c)$ and $\dfrac{d\eta}{d\tau} = 0$ at $\tau = 0$.

Equations (3.24) to (3.26) are in finite difference form and utilize simple forms for R_η (see 3.21) and γ (see 3.19). Since the procedure is numerical, more complex forms could be used if desired. For example, γ could be based on more realistic stress-strain relationships than the "ramps" shown in Fig. 3.3. The simplified model, however, is easier to visualize and illustrates the underlying physical interactions.

3.3 Model Description - Inductive Protection

The previous section considered the possibility of restraining the magnetic to kinetic energy conversion process by dissipating the magnetic energy in a resistor in the main coil circuit. This requires that the usual

discharge time constant, τ_d be of the same order as τ_o, the characteristic time for the magnetic force to accelerate the system mass. In many (perhaps most) cases this will be impractical because of the rapid response time and/or high voltages required to effect the discharge. In this section, therefore, we consider the possibility of restraining the energy conversion process by transferring some of the magnetic energy to another circuit which is inductively coupled to the first.

The presence of the secondary circuit alters (3.15) as follows:

$$\frac{d}{dt}(LI) + IR(t) + \frac{d}{dt}(MI_2) = 0 \tag{3.27}$$

where

M = mutual inductance between the original winding and the second circuit or electrically conducting body

I_2 = current in second circuit

A second electrical equation is required because of the second circuit.

$$L_2 \frac{dI_2}{dt} + \frac{d}{dt}(MI) + I_2R_2 = 0 \tag{3.28}$$

where

L_2 = self inductance of second circuit

R_2 = resistance of the second circuit

Equation (3.28) may be written in normalized form.

$$\frac{dI_{2n}}{d\tau} + \frac{d}{d\tau}\left(\frac{M}{L_2} I_n\right) + I_{2n}\left(\frac{\tau_o}{\tau_2}\right) = 0 \tag{3.29}$$

where

$I_{2n} = I_2/I_o$

$\tau_2 = L_2/R_2$

If we now assume $(\tau_o/\tau_2) \ll 1$, that is, that the time constant of the secondary is long compared to the characteristic time τ_o then (3.29) implies;

$$\frac{dI_{2n}}{d\tau} = -\frac{d}{d\tau}\left(\frac{M}{L_2} I_n\right) \tag{3.30}$$

In general, the force balance given by (3.11) would require a term added to the left side of the form

$$\frac{I}{\ell_o} B_2 \, r d\theta \ell_o \tag{3.31}$$

where

B_2 = field at solenoid segment in Fig. 3.1 due to current in second circuit

However, for the special case shown in Fig. 3.5, the second circuit is a passive infinitely long conducting shell inside the bore of the infinite solenoid. In this configuration, any current in the shell produces no field outside the shell and, specifically, $B_2 = 0$ at the winding so (3.31) is zero and the governing mechanical equation is (3.17) as it was in the previous section.

Furthermore, the mutual inductance between the shell and the winding may be shown to be a constant for this configuration even if the winding is expanding in time. Equation (3.29) and (3.30) may then be combined to yield the following electrical equation for this case.

$$(1 - k^2 \eta^{-2}) \eta^2 \frac{dI_n}{d\tau} + 2 I_n \eta \frac{d\eta}{d\tau} + I_n R_n = 0 \tag{3.31}$$

where

$k^2 = \frac{M}{L_2 L_o}$ = coupling coefficient

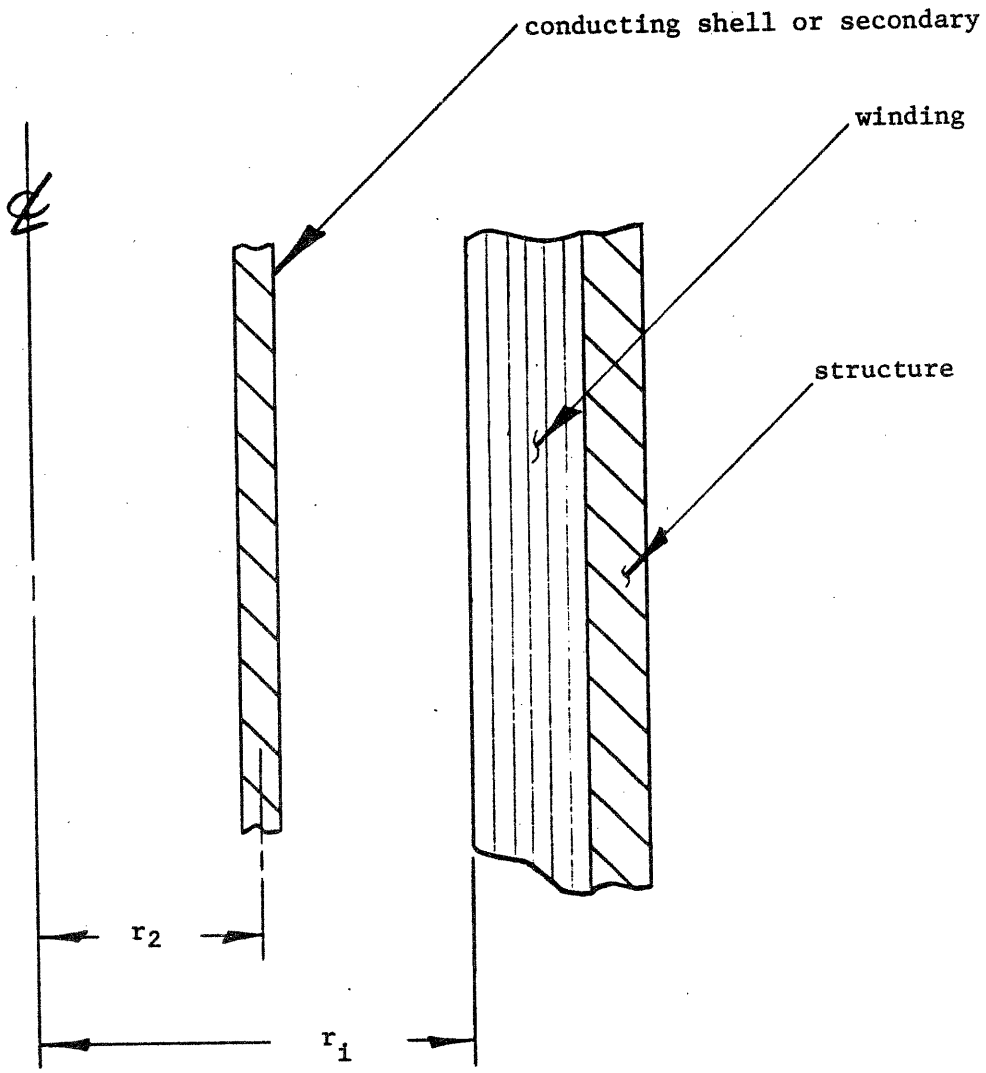

Fig. 3.5 Simple model of a conducting shell (or secondary) capable of trapping magnetic flux when the structure fails and winding expands radially.

Equation (3.31) is the same as (3.16) except for the multiplier on the leading term which causes a more rapid rate of change of I_n than if $k^2 = 0$ as it is in the previous section. Equation (3.30) then implies that this causes the current in the secondary to change at the same rate, hence, energy is transfered into the secondary.

The examples in Section 3.4 will show that the inductive energy transfer can be effective in restraining the conversion of the field energy to kinetic energy provided the coupling coefficient is sufficiently high. The model is simple but illustrates the basic concepts. Next year, consideration will be given to extending the analysis by relaxing some of the simplifying assumptions.

3.4 Solenoid Examples

3.4.1 Resistive Protection

As a hypothetical example, assume a long solenoid as in Figure 3.1 with a field B = 10 T and bore radius of 1 m. The winding build, t_c, and other characteristics are dependent on the overall current density, hence, consider two cases as outlined in Table 3.1.

Case 1 is for a relatively high current density and Case 2 is for a moderate to high level. They lead to substantially different values for t_c. The structural build, t_s, is based on a stress $\sigma_s = 4 \times 10^4$ psi. The total mass is that of the structure based on a steel density of 7.8×10^3 kg/m^3 and the winding based on 8.9×10^3 kg/m^3 with a packing factor of 0.7 applied to the latter. If a operating current level of 2×10^4 A is chosen then the inductance and stored energy per unit length can be shown to be 0.625 H/m and 125 MJ/m, respectively. The ratio of winding modulus to yield strength was

TABLE 3.1
SOLENOID CHARACTERISTICS

CASE	1	2
Magnetic Field, [T]	10	10
Bore Radius, [m]	1.0	1.0
Winding Current Density, [$10^7 A/m^2$]	3.3	1.86
Winding Radial Build, t_c	0.241	0.482
Structural Build, t_s [m]	0.168	0.182
Total Mass Per Unit Length, M/ℓ_o, [kg/m]	2.51×10^4	3.39×10^4
Operating Current, [kA]	20	20
Inductance Per Unit Length, L_o/ℓ_o, [H/m]	0.625	0.625
Stored Energy Per Unit Length, E/ℓ_o, [J/m]	1.25×10^8	1.25×10^8
Winding Modulus/Yield Stress, E_c/σ_{cy}	900	900
Winding Strain, ε_c	5×10^{-4}	5×10^{-4}
Characteristics Time, τ_o [s]	9.28×10^{-3}	1.17×10^{-2}
Load Characteristic, F_o	0.562	1.0
Winding Ultimate Strain, ε_u	0.2	0.2

assumed to be 900 and the ultimate winding strain at fracture was assumed to be 20%. In both cases the initial strain in the winding at operating current level was taken as 5×10^{-4}. The characteristic time may now be found using (3.18) and, as indicated in the table, is about 10 msec for each case. This is representative of the time required for the stored magnetic energy to accelerate the system mass and is quite rapid. The yield stress for the winding was assumed to be $\sigma_{cy} = 0.7\ (2 \times 10^4) = 1.4 \times 10^4$ psi. This value, together with some of the characrteristics found earlier, allow F_o to be found. Equation (3.20) indicates that F_o, the load characteristic, is a measure of the load carrying ability of the winding alone, at yield, relative to the magnetic load. Since it is substantially less than one for Case 1 and unity for Case 2, we expect the two cases to respond quite differently in the event of a structural failure.

Figures 3.6, 3.7 and 3.8 show the response for Case 1 following a structural failure at $t = 0$. The abscissa in each figure is time normalized to τ_o which is $\approx$ 10 ms as indicated in Table 3.1. Figure 3.6 shows the current in the coil normalized to the initial current and the transient which results for four different values of (τ_o/τ_d), the ratio of the characteristic time to the usual discharge time constant, $\tau_d = L_o/R_i$. The case of $(\tau_o/\tau_d) = 0$ corresponds to a zero resistance situation and increasing (τ_o/τ_d) implies circuitry with successively larger coil resistances. Note that the transient is well underway in only two times the characteristic time, τ_o. The normalized radial displacement is shown in Fig. 3.7 over the same time period and illustrates substantially different reactions depending on the value of (τ_o/τ_d). Higher values of (τ_o/τ_d) generate a condition where sufficient energy is dissipated rapidly enough in the resistance to limit the deformation. However, low values result in a deformation which is not limited. The critical condition

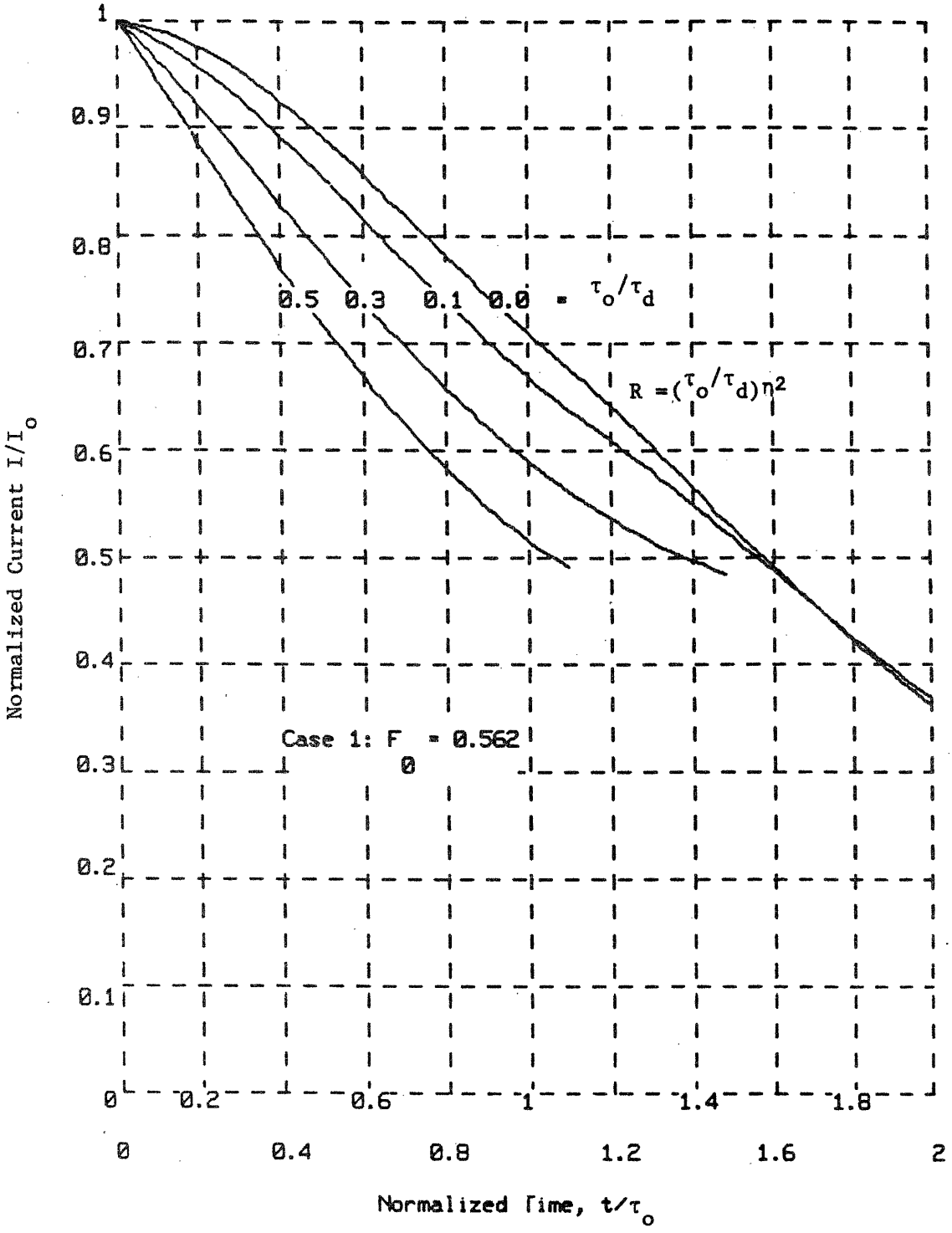

Figure 3.6 - Normalized Current vs Time for Case 1 and Selected Values of (τ_o/τ_d).

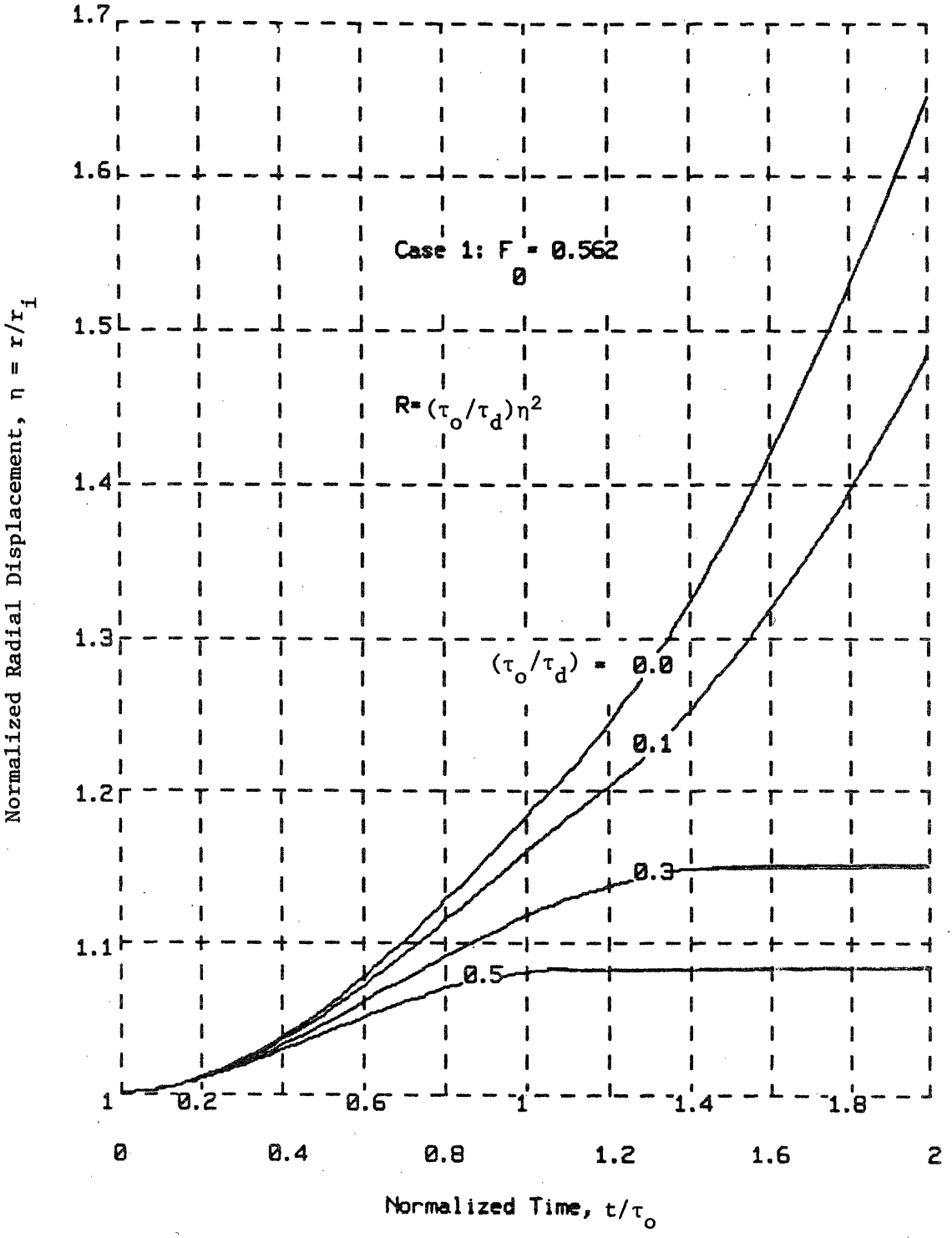

Figure 3.7 - Normalized Radial Displacement vs Time for Case 1 and Selected Values of τ_o/τ_d.

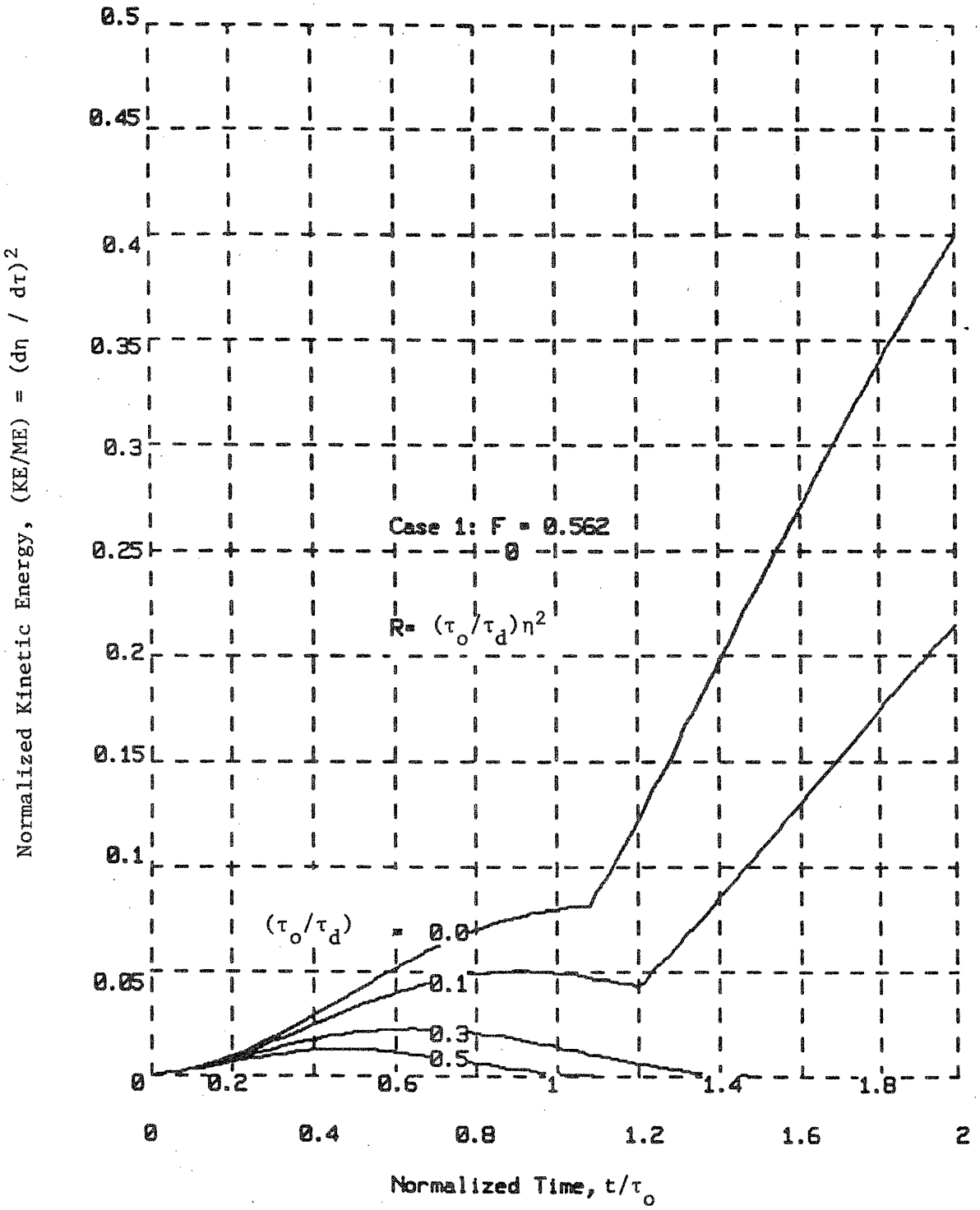

Figure 3.8 - Normalized Kinetic Energy vs Time for Case 1.

occurs when the ultimate winding strain, ε_u is exceeded. In these examples, $\varepsilon_u = 0.2$, therefore, if conditions are such that $\eta \approx 1 + \varepsilon_u \approx 1.2$ we would expect the winding to rupture and no restraint on conversion of the remaining magnetic energy to kinetic. This is shown in Fig. 3.8 which is a plot of the instantaneous kinetic energy per unit length normalized to the magnetic energy per unit length initially stored at $t = 0^-$. For high enough (τ_o/τ_d) the kinetic energy starts at zero, rises to a maximum and decreases to zero. However, if the energy is not dissipated fast enough, that is, if (τ_o/τ_d) is low enough, then the coil ruptures and the unrestrained magnetic to kinetic energy conversion occurs. Note that the sudden change in slope in Fig. 3.8 occurs at the time when the radial displacement in Fig. 3.7 passes through $\eta \approx 1.2$ where the ultimate winding strain is exceeded.

Case 1 illustrates that the unrestrained conversion of magnetic to kinetic energy can be averted even if $F_o < 1$ provided the usual discharge time constant is of the same order as τ_o. In many cases, however, this would require unrealistically high voltages and unrealisticially fast circuit response times since τ_o is likely to be small. As a result we will conclude preliminarily that a response involving resistive dissipation alone is not feasible. Next year this shall be investigated further to relate τ_o, τ_d and the required voltage to system characteristics.

It was noted earlier that a different response would be expected for Case 2 because $F_o = 1$. This is illustrated in Figs. 3.9, 3.10 and 3.11 which have axis labels corresponding to those discussed for Case 1. Figure 3.9 shows the normalized current transients for the same values of (τ_o/τ_d) as used in the previous case. Note from Table 3.1 that $\tau_o \approx 10$ msec for Case 2 also.

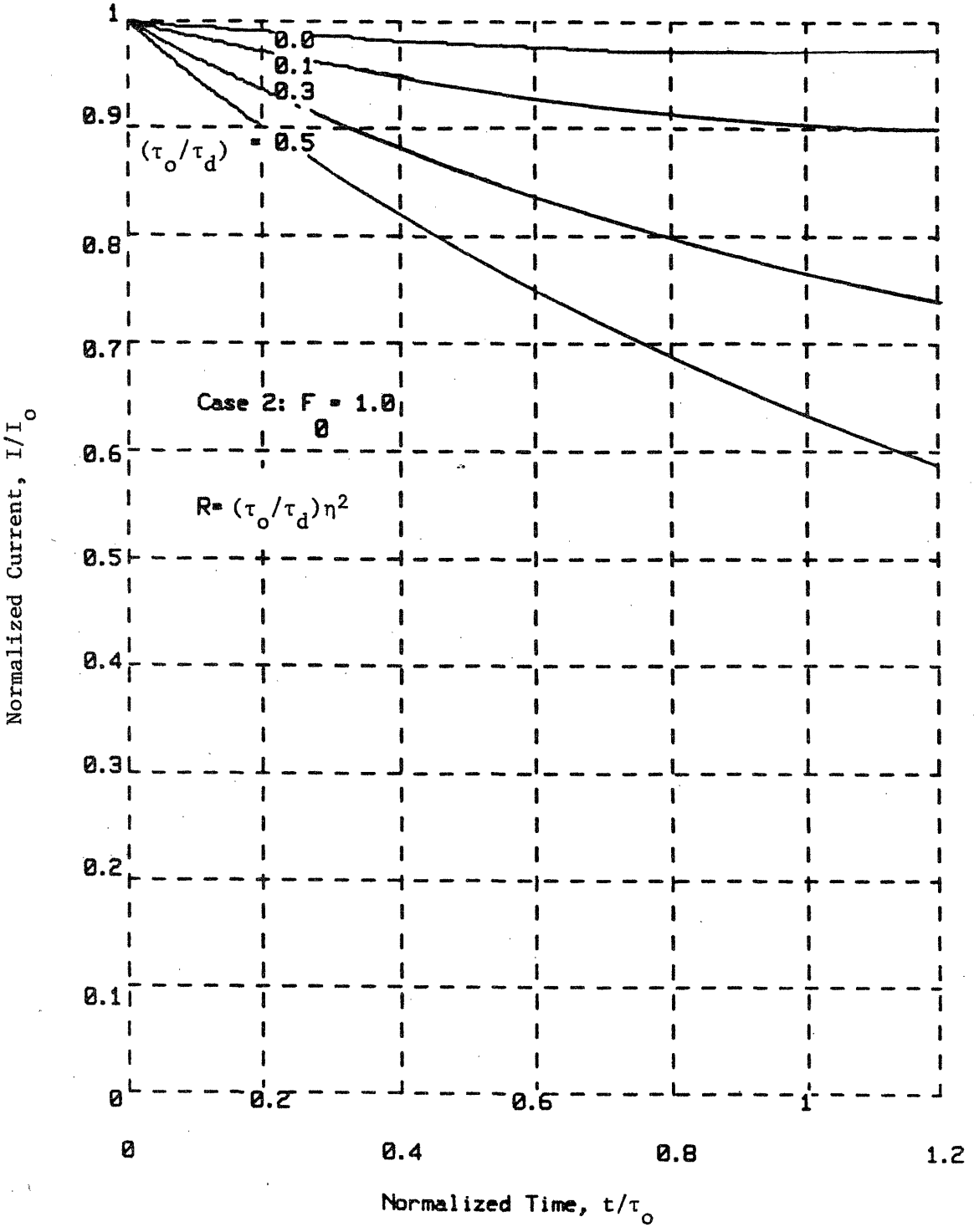

Figure 3.9 - Normalized Current vs Time for Case 2.

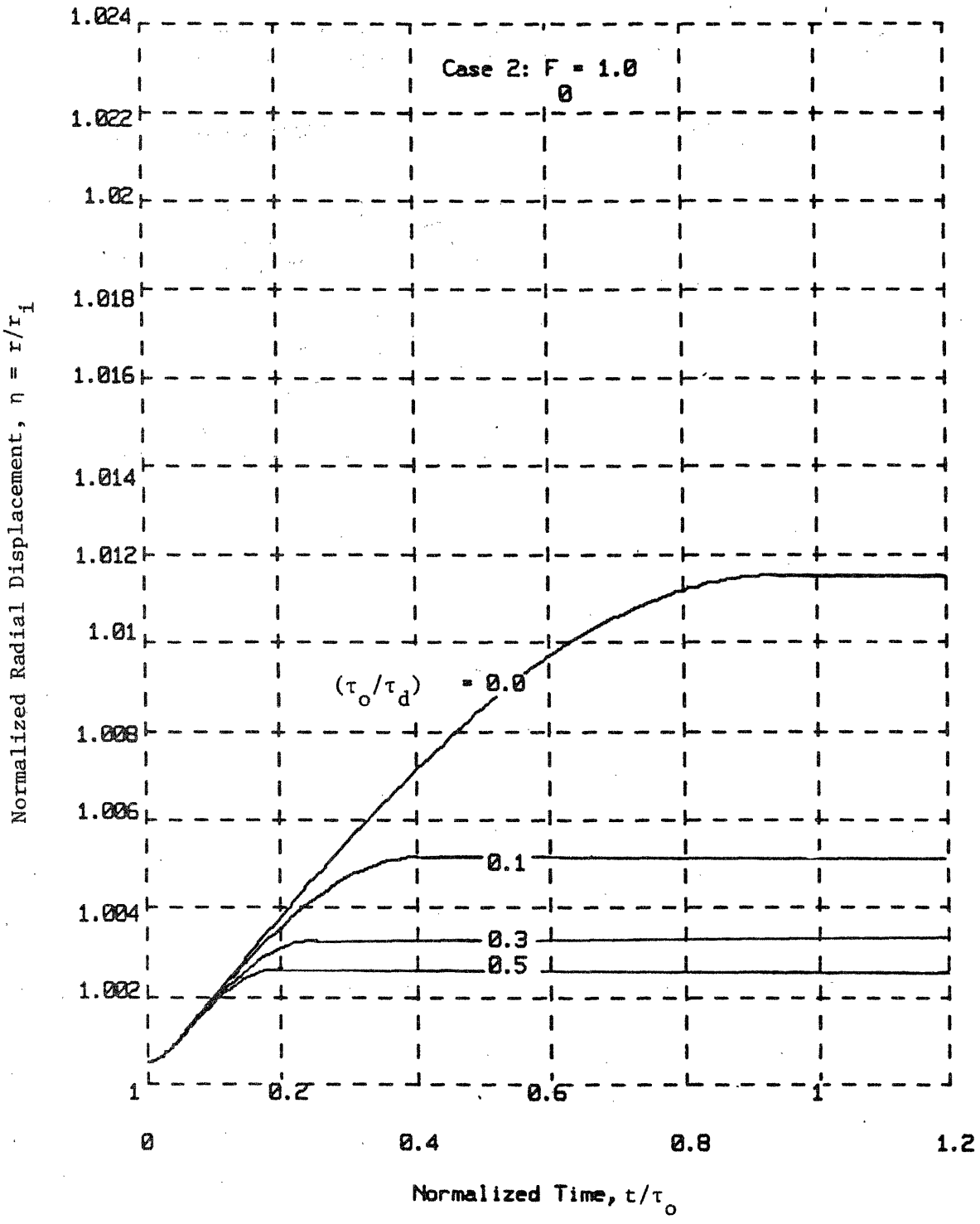

Figure 3.10 - Normalized Radial Displacement vs Time for Case 2.

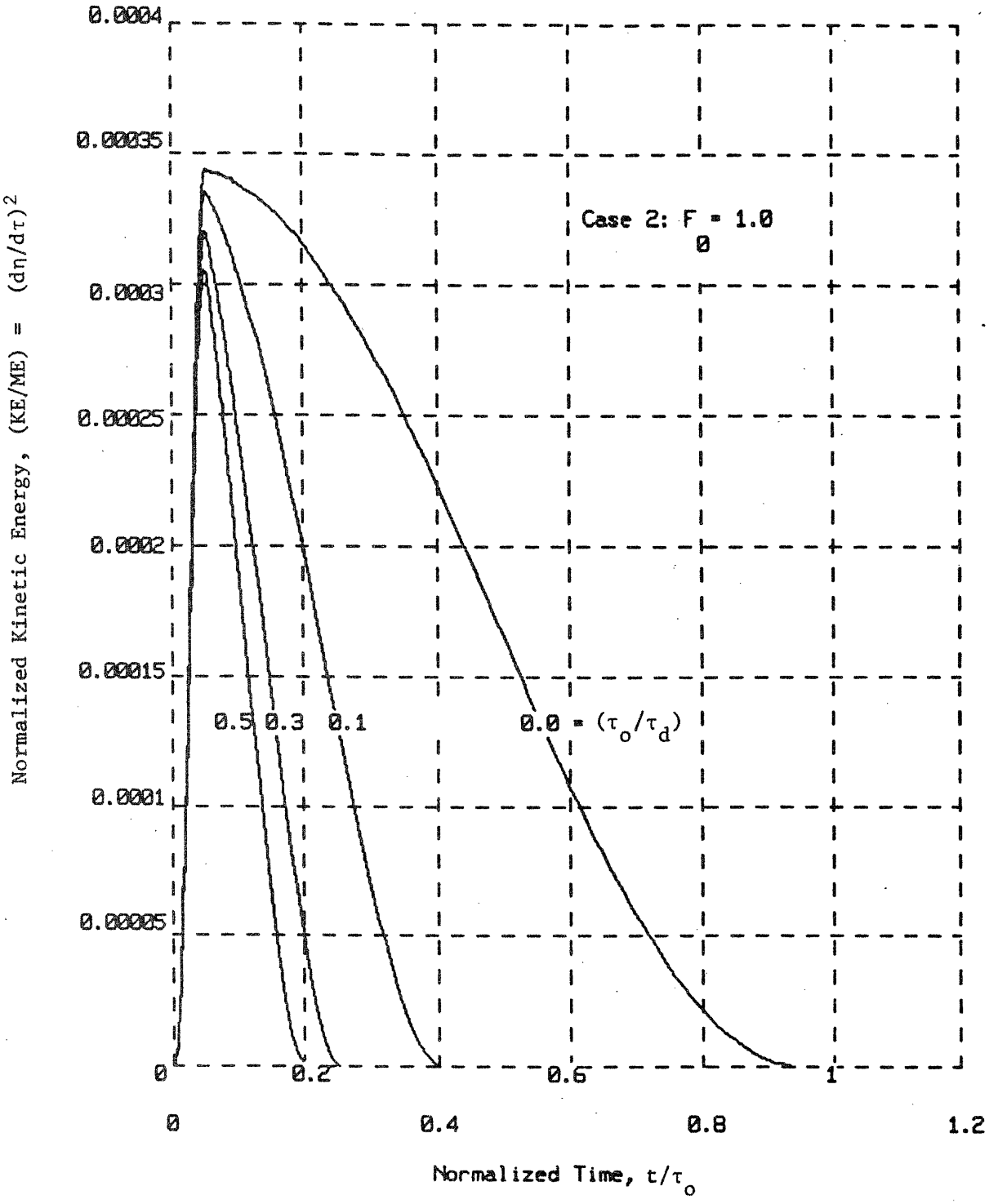

Figure 3.11 – Normalized Kinetic Energy vs Time for Case 2.

The normalized radial displacement is shown in Fig. 3.10 and is limited for all (τ_o/τ_d) because F_o is large enough for the winding to have sufficient strength to accept the load after the structure fails at t = 0. However, even though the winding strain does not reach the rupture condition (i.e. $\eta = 1 + \varepsilon_u \approx 1.2$), some yielding must occur at the levels indicated. Since $E_c/\sigma_{cy} = 900$, yielding would be expected at about $\eta = 1 + (900)^{-1} \approx 1.001$, hence all of the cases shown cause the winding to yield plastically. Figure 3.11 gives the normalized kinetic energy which returns to zero for all cases, including $(\tau_o/\tau_d) = 0$. The break in the kinetic energy curves occurs at the yield point where the functional form of the restraining force by the winding changes form (see (3.19)).

Case 2 shows that a coil with a high enough F_o can restrain the magnetic to kinetic energy conversion process even if the resistive dissipation is zero (i.e. $(\tau_o/\tau_d) = 0$) although yielding and winding deformation may take place. It may be possible to translate this into a safety oriented design criteria for coils of a more complex geomerty than the ideal solenoid, hence, this will be investigated next year.

Case 1 will now be reconsidered with successively larger values of F_o and with $(\tau_o/\tau_d) = 0$ to show the change in results as the load characteristic, F_o, is varied. Figures 3.12 and 3.13 show the normalized current and radial displacement vs time, respectively. Figure 3.13 indicates that the displacement corresponding to ultimate winding strain (i.e., $\eta \approx 1.2$) is exceeded for $F_o < 0.82$. This is confirmed in Fig. 3.14 which shows that the conversion to kinetic energy is unrestrained for $F_o < 0.82$. The case of $F_o = 0.8$ is particularly interesting since it represents a case where sufficient energy can be absorbed by the coil deformation to cause the kinetic energy to pass through a

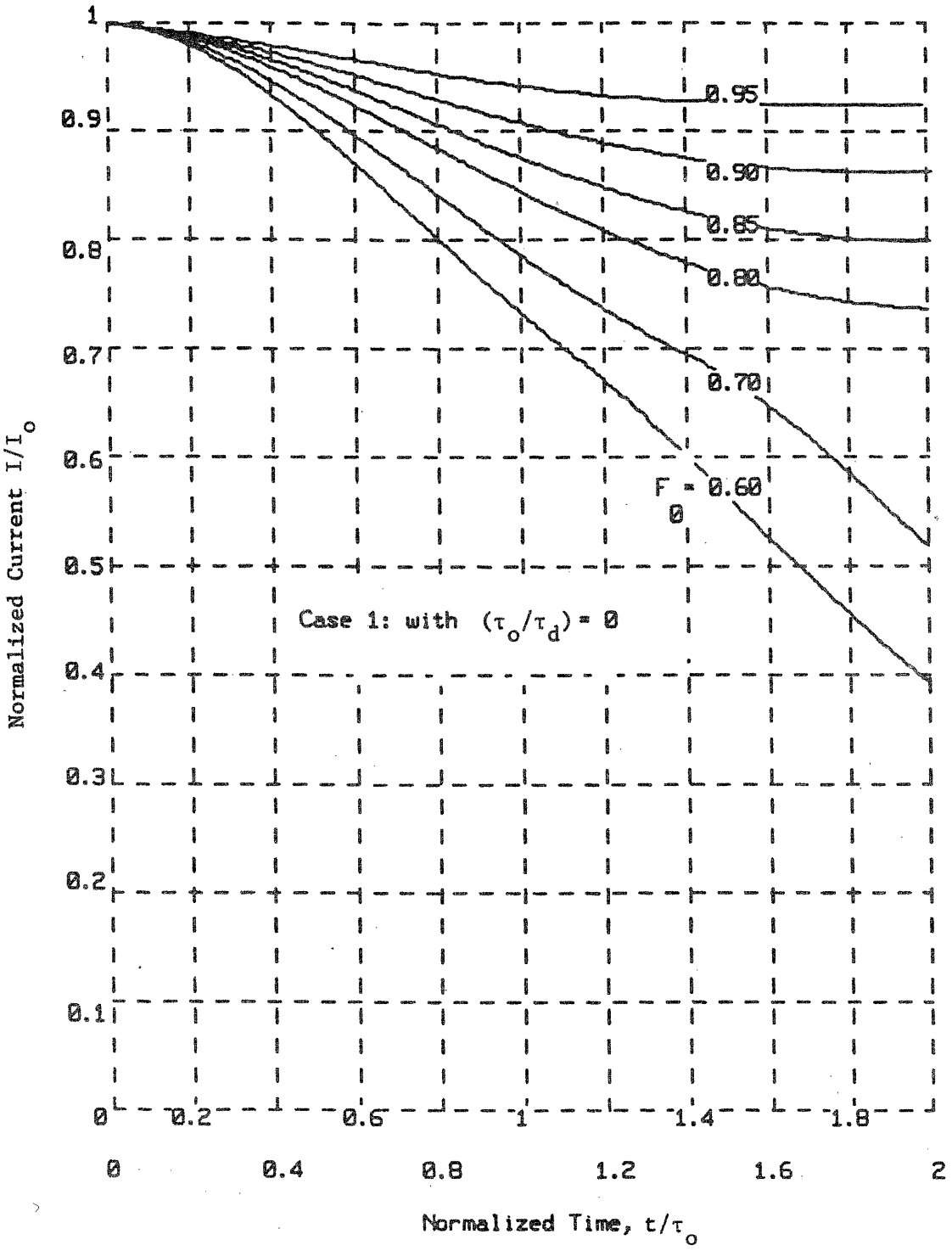

Figure 3.12 - Normalized Current vs Time for Case 1 with various Values of F_0 and $(\tau_o/\tau_d) = 0$

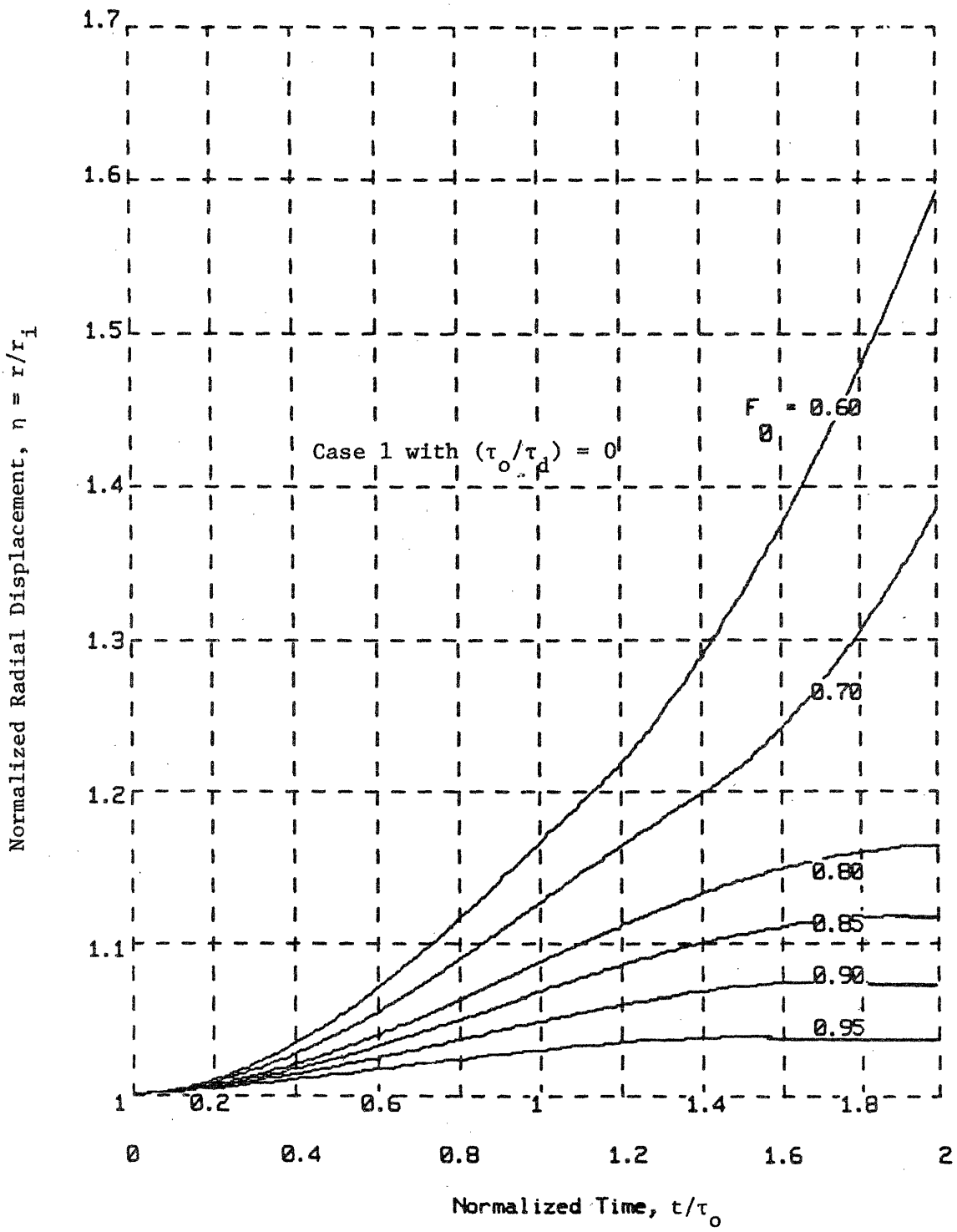

Figure 3.13 – Normalized Radial Displacement vs Time for Case 1 with Various Values of F_0 and $(\tau_o/\tau_d) = 0$.

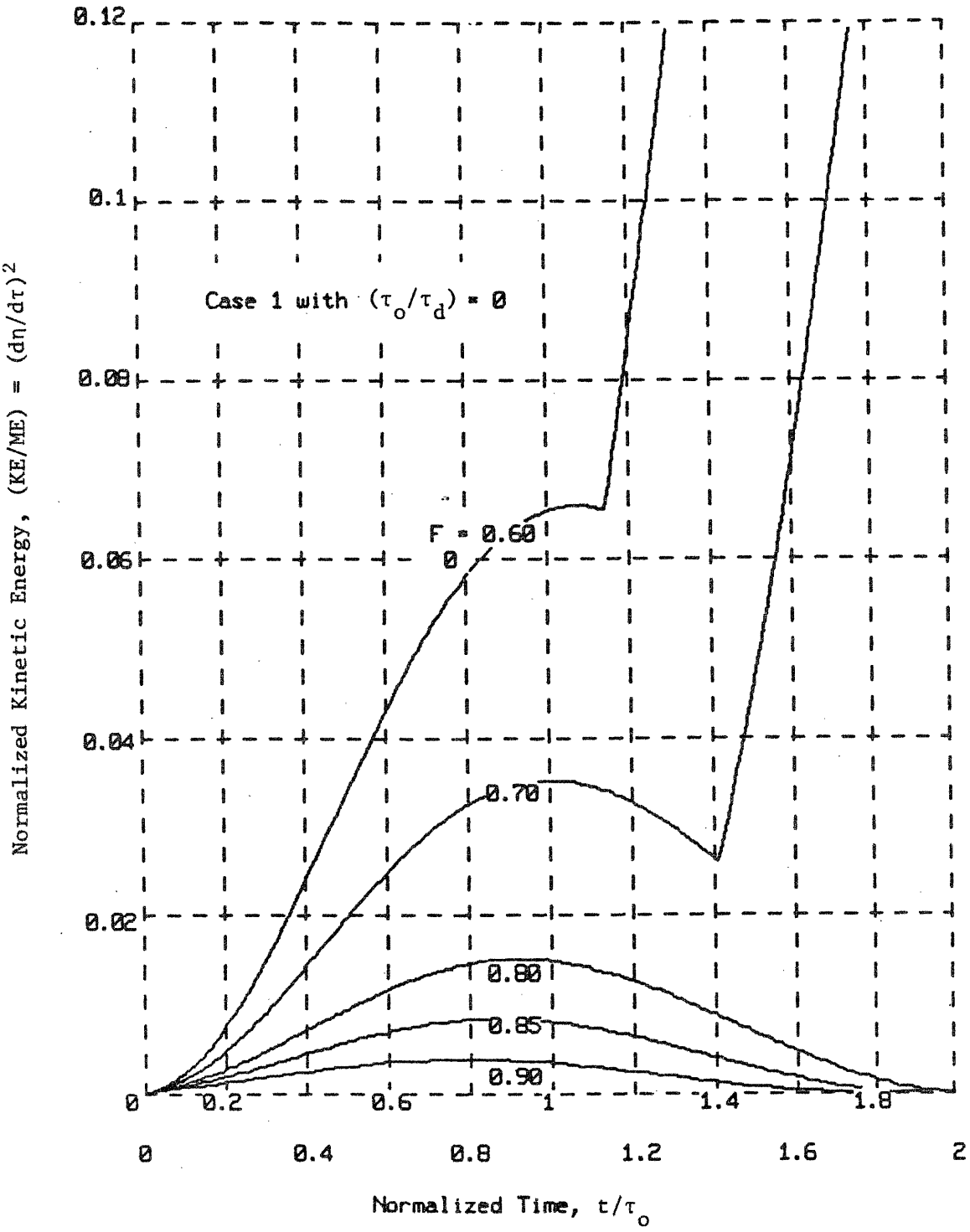

Figure 3.14 - Normalized Kinetic Energy vs Time for Case 1 with Various Values of F_0 and $(\tau_o/\tau_d) = 0$

local maximum and start to decrease, however, the ultimate strain is eventually achieved at the sudden change in slope on this curve and the winding ruptures.

3.4.2 Inductive Protection

This section will illustrate the ability of a secondary circuit to prevent unrestrained expansion even if $F_o < 1$ provided the coupling coefficient between the primary and secondary circuits is sufficiently high. The winding and structural characteristics in this example correspond to $F_o = 0.7$ and $R = 0$ for the primary circuit which leads to unrestrained conversion of magnetic to kinetic energy as shown in Fig. 3.14, which corresponds to a coupling coefficient of zero.

For the simple case shown in Fig. 3.5, the coupling coefficient may be shown to be

$$k^2 = \frac{M^2}{L_o L_2} \tag{3.32}$$

$$k^2 = \left(\frac{r_2}{r_1}\right)^2 \tag{3.33}$$

Equation (3.33) has a particularly simple form for this geometry and is limited to the range $0 \leq k^2 \leq 1.0$.

The results for this case are plotted in Figs. 3.15 to 3.17 for selected values of coupling coefficient, k^2. Figure 3.15 shows that the presence of the secondary ($k^2 \neq 0$) allows the current in the winding to fall faster initially and that this effect can occur on the fast time scale which is of the order of τ_o. Figure 3.16 shows that if k^2 is high enough (i.e., $k^2 > 0.4$ for this case) then the radial displacement is limited because the ultimate winding strain, corresponding to $\eta = 1.2$ in this figure, is not attained. This is also indicated in Fig. 3.17 which shows that the magnetic to kinetic energy conversion

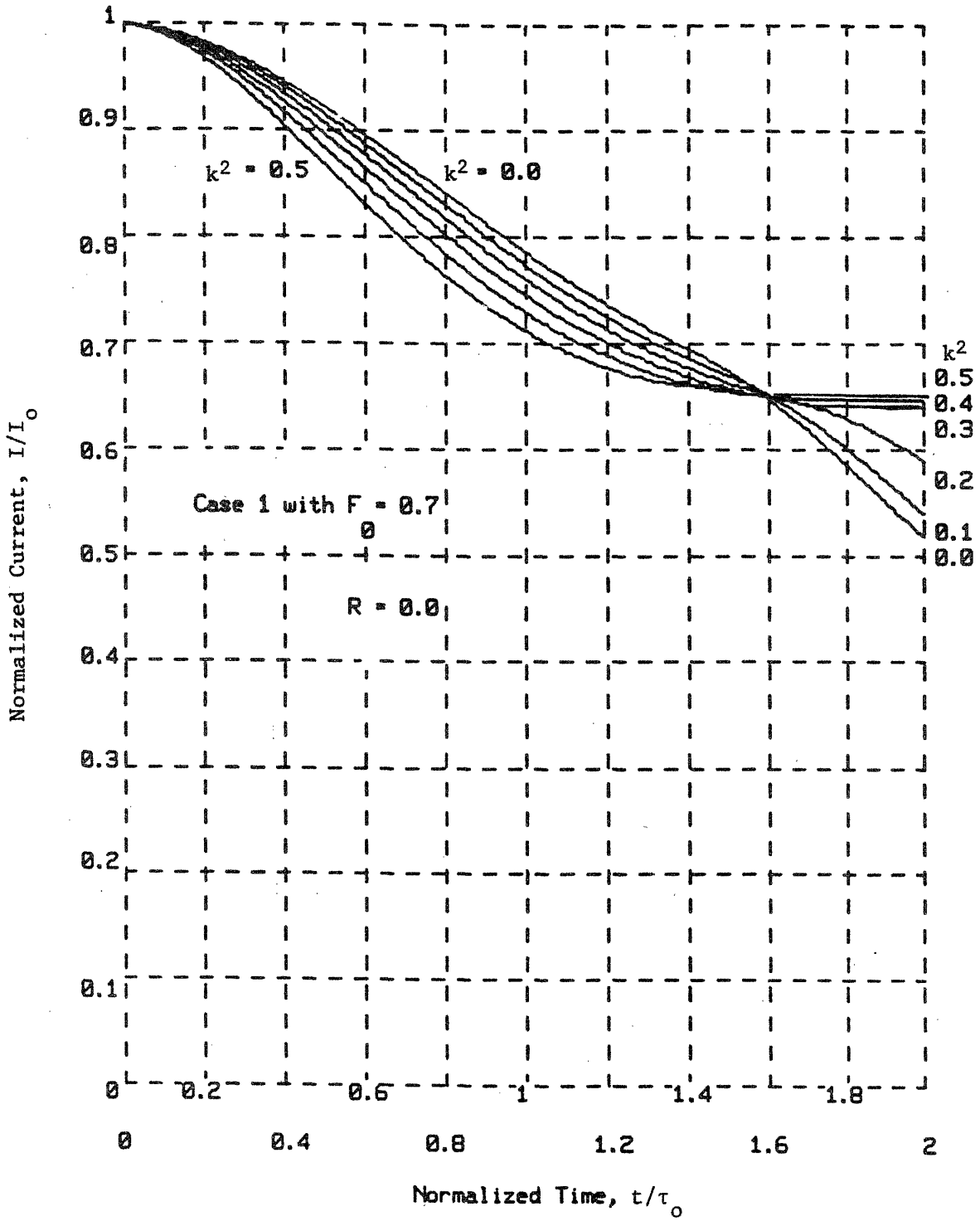

Figure 3.15 - Normalized Current vs Time for $F_0 = 0.7$, R = 0 and Selected Coupling Coefficients, k^2.

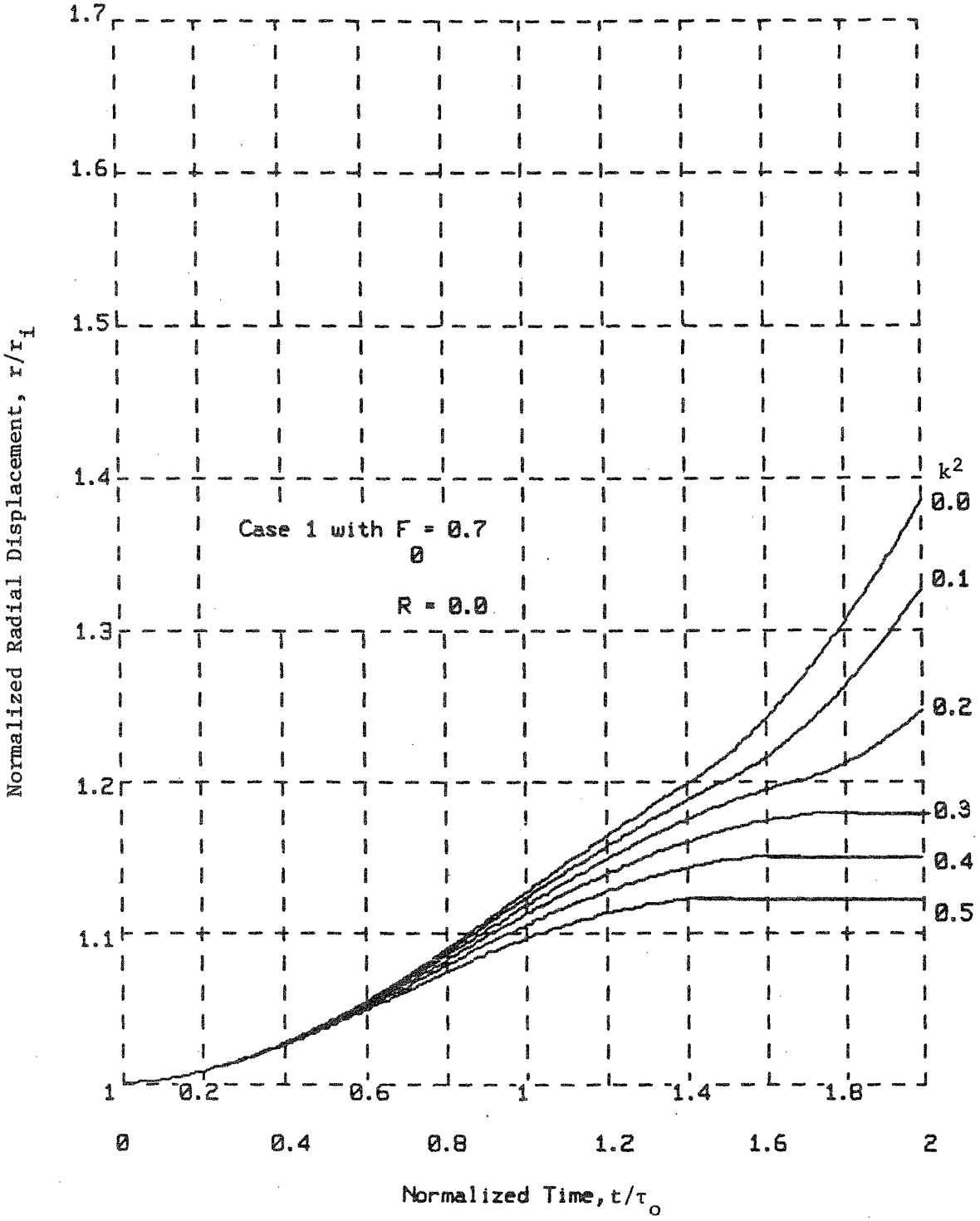

Figure 3.16 – Normalized Radial Displacement vs Time for F_0 = 0.7, R = 0 and Selected Values of Coupling Coefficient, k^2.

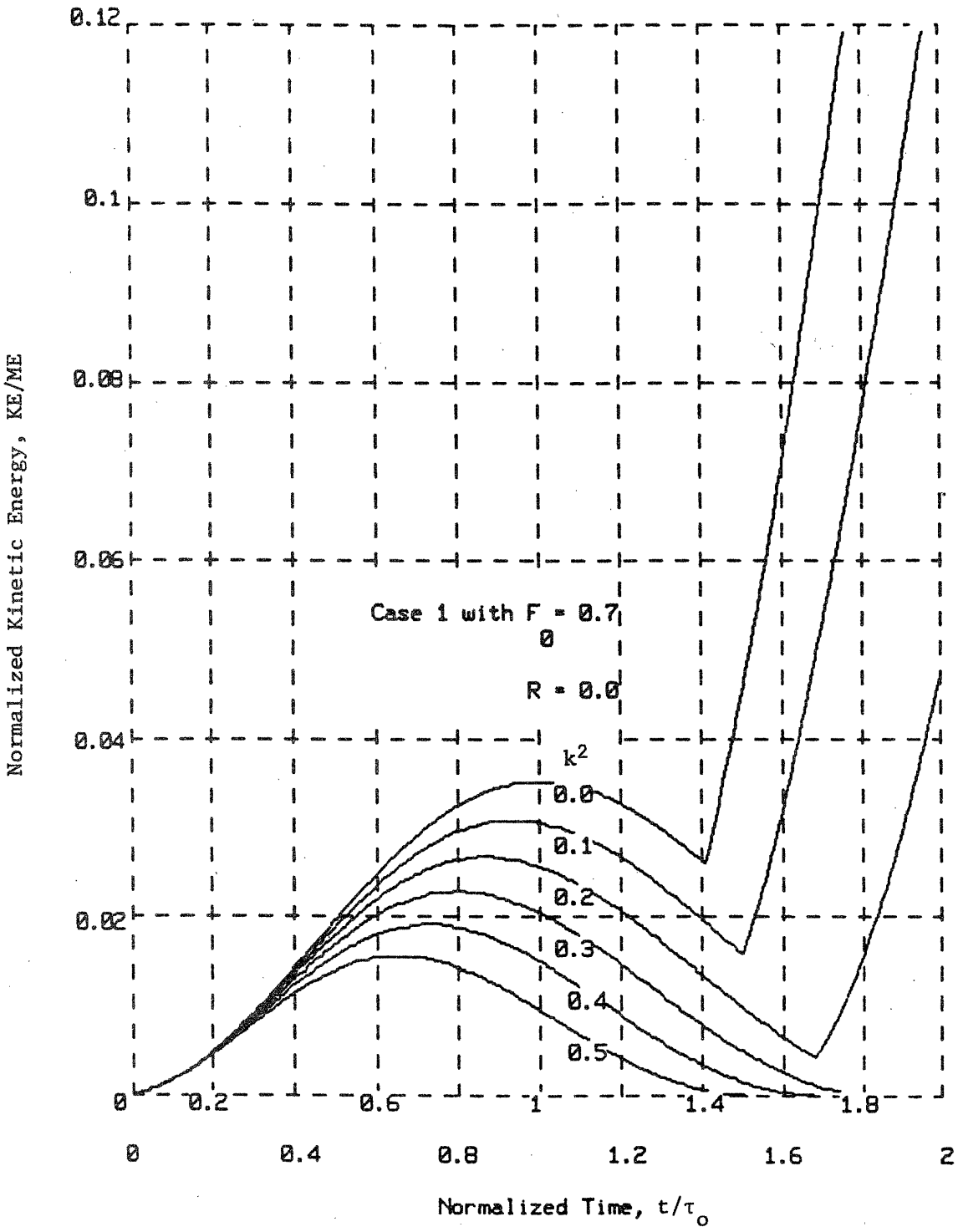

Figure 3.17 – Normalized Kinetic Energy vs Time for $F_0 = 0.7$, $R_0 = 0$ and Selected Values of Coupling Coefficient, k^2.

process returns to zero kinetic energy for $k^2 > 0.3$. Lower values of k^2 represent a condition where the secondary is unable to absorb sufficient energy for this level of F_o before the ultimate strain is reached and the winding ruptures.

This example, though simple, illustrates the potential advantage of using inductive coupling to restrain magnetic to kinetic energy conversion because it can be effective on a fast enough time scale with reasonable levels for coupling coefficients. Next year this will be developed further, in conjunction with the multiple circuit TF coil system characteristics described in Section 4.0.

Appendix C

Marston, P.G., et al.,

Magnet Failure Workshop

Journal de Physique, Coll. C1, Supp. 1, Tome 45, pp. C1-637 - C1-641, January 1984

JOURNAL DE PHYSIQUE
Colloque C1, supplément au n° 1, Tome 45, janvier 1984 page C1-637

MAGNET FAILURE WORKSHOP

P.G. Marston°, H. Desportes*, M. Morpurgo**, P. Komarek***, K. Van Hulst+, D. Hackley++, J.L. Young+++ and K. Kibbe*

Massachusetts Institute of Technology, Plasma Fusion Center, Cambridge, MA 02139, U.S.A.
**C.E.N.-Saclay, DPh-STIPE, 91191 Gif-sur-Yvette, France*
***C.E.R.N., 1211 Geneva 23, Switzerland*
****Kernforschungszentrum, Postfach 3640, D-7500 Karlsruhe, F.R.G.*
+University of Nijmegen, High Field Magnet Laboratory, NL-6525 ED Nijmegen, The Netherlands
++General Dynamics Convair, P.O. Box 551147, San Diego, CA 92138, U.S.A.
+++Westinghouse Electric Corporation, 700 Braddock Avenue, East Pittsburgh, PE 15112, U.S.A.
**Oak Ridge National Laboratory, Oak Ridge, Tennessee 37830, U.S.A.*

1.0 Introduction

The dictionary defines failure as nonperformance or an unacceptable want of success. (The definition implies that the results should have been avoided). In an emerging technology such as ours, the boundaries of expectations and "unacceptable success" are often ill defined. Failures are often touted as hugh successes (occasionally rightfully so) and exceptional technological achievement can become dismal failure (if expectations are too high).

We all, however, have experienced problems of one sort or another and the basic purpose of the workshop was simply to communicate these so that new or future workers don't make the same mistakes.

2.0 Summary of Discussions

2.1 Marston began the discussion with a brief description of a number of specific failures, many of which occurred during the technology's infancy when we didn't understand stability, transposition, frictional heating etc.* He emphasized that the technology is now adequately mature that future problems will result primarily from the failure to use readily available information rather than from some hitherto unknown physical phenomena.

2.2 Desportes discussed two aspects of system design which are of continued concern. The first being the differences in technology and design approach for large and for small systems and the second, the problems of manufacturing technology. He described a problem with the large, thin solenoid for the CELLO experiment wherein despite a careful and conservative design and verification test program, the magnet failed because of a tiny inclusion in the monolithic conductor causing it to break. Fortunately the break was near the end of the solenoid and was able to be repaired. He commented that multi strand cable with adequate capacity to allow a few breaks might have avoided the problem.

2.3 Dave Hackley then introduced a new potential problem which is related to the recent rapid expansion of activity in large magnet systems. This is the need

---

°Chairman.

*those things which, with the wisdom of hindsight, are so obvious that we should recognize our capability for stupidity (a reflection which may serve us well if we are to avoid future failures).

for definition and delivery of clear instructions for minimum risk operation. The General Dynamics LCT coil is one of six different designs from six different manufacturers. Documentation delivered with the coil is so voluminous that there is a real danger that certain safety considerations will be overlooked. GD has recognized the potential hazard and is now writing concise operating and safety procedures. Hackley also noted that his conference paper discussed many of the design and manufacturing problems encountered with their "Large Coil".

2.4 Morpurgo identified some problems due to mistakes during design, construction and operation and emphasized that the latter is most common. The most worrisome problems during design of new and different systems are "the things you don't think of". He described a problem with the early Big European Bubble Chamber due to an unanticipated torque on the untransposed conductor (Ref. Para. 3.4). Problems during construction and particularly during operation of both superconducting and conventional magnets result from inadequate attention to inspection and safety procedures (taking short cuts, ceasing to worry about well behaved systems, etc.). It is not unusual to see protective circuits bypassed or protective devices eliminated (or not replaced when they fail).

2.5 Lynn Young discussed some of the detailed problems during the design and construction of the Westinghouse "Large Coil" arising from the requirement to develop an advanced conductor (Nb_3Sn, ICCS) simultaneously with the development of a severely constrained (by the original specification) coil design. Their experience is a good example of the problems to be expected when working with unproven manufacturing technology. He emphasized the need for early, formalized Fault and Risk Analysis which should include the manufacturing technology and equipment when new processes have to be developed to satisfy design requirements.

2.6 These comments led naturally to a discussion by Peter Komarek of safety analysis about which he is the author (with Friedrich Arendt) of an excellent paper. /1/ Peter described the "painful" questioning by reactor safety people as fusion enters the engineering phase and concluded that we don't have the information that we should to predict probability of failure availability, lifetime, etc. He described a few of the more important faults and abnormal operating conditions which a magnet should survive (see Ref. 1) and also pointed out the dangers of accepting performance demands (from the physicists) which result in machine designs having inadequate conservatism for reliable operation.

2.7 Van Hulst's presentation underscored two elements of failure. The first being that all system components have a finite lifetime and designs should accommodate their routine inspection, replacement and the consequences of premature failure. In a high field facility such as Nijmegen, one such component is winding itself for which burnout is not uncommon. In the failure reported, however, an arc occurred which caused current to flow radially in certain elements of a dewar structure. The Lorentz interaction of this current with the large axial field component twisted the dewar apart. The accident is a good example of the very strong (and unanticipated) force distributions which can occur during abnormal conditions in a magnetic system.

2.8 The final panelist, Keith Kibbe, is involved with the technical contract management for LCP and was therefore asked to comment on the findings and recommendations of the 1979 U. S. DOE "Electrical Problems Committee Report" which concluded that many of the problems had their roots in management. (The salient comments of the report are reproduced below). Although it was the general feeling of both the panel and the audience that management was not a serious problem, the chairman emphasized that the management of large, first-of-a-kind, high technology projects is tricky business, particularly if a large (and new) team must be put in place to complete the project.

3.0 Specific Problems Discussed

3.1 HPDE (High Performance Demonstration Experiment) Cryogenic MHD Magnet/2/

This very large 6 T magnet (1 m square x 7 m long bore) suffered catastrophic structural failure in December, 1982.

The force containment structure for the winding was fabricated from a large number of high strength aluminum elements which were keyed and bolted together. The design was complex, there were multiple load paths and the material was brittle at low temperature. Although these factors contributed, the principal cause of failure was a design error wherein the stress analysis did not identify a very high local stress associated with deformation from a relatively small transverse load.

Although the design flaw was apparent (after considerable inspection and analysis), to suggest that (in this case) the designers were not competent or that the project did not proceed in a careful and cautious manner would not only be unfair to the project staff, but would obviate the impact of the lesson to be learned which is that mistakes can (and will) be made, even in well managed, competently staffed projects.

3.2 An early NASA split coil pair failed as a result of radial deformation of the winding at its inside diameter thus allowing one of the I.D. turns to slip axially. Designers still often underestimate the stiffness of winding composites and thus underestimate deformations, winding stresses and the percentage of winding load taken by outer support structure.

3.3 On the first cooldown of the Argonne 12' Bubble Chamber it was impossible to fill the helium vessel adequately to cover the top coil. The circumferential dimension of the annular vessel was so large that the pressure drop of the boil off gas flowing around the half circumference to the (single) vent pipe depressed the liquid level (180° from the vent pipe). Modification to allow venting at two locations solved the problem.

3.4 There have been a number of problems associated with unanticipated force distributions. Morpurgo's experience with the Big European Bubble Chamber was the result of the Lorentz interaction of parasitic current loops induced in the untransposed conductor by the radial field component (near the end of the solenoidal winding). A change in field thus created a torque on the conductor until the induced parasitic currents decayed. The twisting conductor created an intermittent short to the cryostat. After considerable discussion it was decided to open up the magnet and find the cause of the problem (good decision - good lesson).

On the first test of the two region high field superconducting magnet at McGill, the outer (NbTi) region was energized first with zero current in the inner Nb_3Sn tape region. Induced, diamagnetic currents and resulting Lorentz forces crushed the inner region.

3.5 Several of the early magnets suffered from flux jumps (large filament, untwisted conductors). One was the 1969 MIT Hybrid's superconducting region wherein, although the conductor was fully stable, the energy in the flux jumps was adequate to blow the helium completely out of the cooling channels.

Many of the early magnets also suffered from poor thermal insulation, poor electrical insulation and "hard to find and repair" vacuum leaks. Continued problems such as these relate to a large degree to a simple lack of proven manufacturing technology. New devices and processes, however simple they may be, are invariably fraught with nasty little surprises of the type referenced earlier by Lynn Young. One of the Westinghouse LCP conductor problems was associated with small metallic "slivers" which were "rolled" out of the ICCS sheath by the tube mill. The LBL TPC magnet failed for the same reason. A piece of metal which was "rolled" off the surface of the winding tube punctured the insulation causing a short which for the (necessarily) high current density winding of a "radiation thin" magnet such as TPC proved to be catastrophic.

Magnet problems are often initiated by other elements of the system. ESCAR, for instance, failed as a result of a power supply which wouldn't shut off when told to (by the protection circuits). PLUTO suffered an arc during an unnecessary "dump" caused by a false signal. A number of such problems have been reported. Many are the result of inattention to detail during the final stages of

construction and early test (when money is low, time is short, and technicians are weary).

4.0 Conclusion

The technology has suffered the usual growing pains and problems and a few failures of serious proportion and consequence. It has also produced some magnificent achievements. It is too soon for conclusions more profound than that.

5.0 References

1. F. Arendt and P. Komarek, "Potential Failures and Hazards in Superconducting Magnet Systems for Fusion Reactors," Nuclear Technology/Fusion, Vol. 1, October, 1981.

2. H. Becker, J. M. Tarrh, and P. G. Marston, "Failure of a Large Cryogenic MHD Magnet," presented at MT-8 Conference, Grenoble, September, 1983.

ELECTRICAL PROBLEMS COMMITTEE INTRODUCTION

- Laboratories and companies responded openly and candidly to this review.
- In many cases, they were anxious to recommend changes that can be made to improve the electrical equipment situation.
- Laboratory management did not appear to be very interested in this review (PPPL was an exception to this comment)

ELECTRICAL PROBLEMS COMMITTEE FINDINGS

- Lack of Project Approach
  - Hampers obtaining trouble free, tested equipment.
  - (TFTR and MFTF have made good progress in this area)
  - Results in lack of clear definition of responsibility
- Resource limitations have resulted in
  - Lack of interest on the part of large industrial firms
  - Limited small company participation
  - Compromises in technical performance
- Resource limitations along with schedule pressures have resulted in "short cuts" being taken that have resulted in cost and schedule problems later on.
- The program has evolved to the point where the hardware requirements and electrical equipment must be managed as fully engineered systems
  - Engineering must be a full partner with physics
- Early systems definition, configuration and interface definition and analysis of technical and schedule risks have been inadequate to minimize problems with hardware components and systems performance.
- The fusion program can benefit from a commonality of electrical equipment including
  - MFE standards
  - Spare policy
  - Pooling of equipment and spare parts
- Problems in electrical equipment have resulted from:
  - Incomplete specification and procurement documents by the buyer
  - Less than thorough administration of these documents
  - Insufficient technical involvement by the users technical expertise in the suppliers and sub-tier suppliers plants during design, fabrication, and testing activities
  - Inadequate communications between buyer and seller
  - Inadequate equipment documentation from supplier
  - Inadequate testing both by supplier and user
  - Insufficient care in using "standard" equipment in "non-standard" applications
- The program has reached the phase where quality assurance and reliability consideration must be consistently applied
- Insufficient open discussion of hard engineering problems within the MFE program.

ELECTRICAL PROBLEMS COMMITTEE RECOMMENDATIONS

- Additional steps should be taken by the MFE laboratories to projectize and to incorporate project methodology into electrical equipment development and purchase activities. Clear definition of responsibility is a must.
- DOE should take the necessary steps to further interest the large electrical equipment suppliers and to assure the small companies of their continued participation to supply reliable, proven electrical equipment needed to support the MFE program. This should also provide additional technical capability in the design, manufacturing, testing and operation of electrical equipment.
- Funding and schedular allocations should be revised to support obtaining reliable working equipment and facilities.
- Engineering should be made an equal partner with physics.
- Action should be taken to require early system definition, configuration and interface definition and formal analysis of technical and schedule risks to minimize problems with hardware components and systems performance.
- DOE should work with IEEE to establish a fusion power engineering committee to generate standards for the MFE program.
- DOE should establish a spares policy including delivery of initial spare parts with equipment. This should include mechanisms for sharing between laboratories and projects.
- DOE should take action to bring together the laboratories to establish a more uniform procedures and practices for acquiring, testing, acceptance, installing, and documenting electrical equipment.
- Reliability and QA programs should be implemented and utilized more extensively. Furthermore, a quality assurance audit should be conducted to establish the level of QA now being applied and to make recommendations.
- The program should promote and encourage more open professional discussion of engineering problems within the MFE program.

Appendix D
MIT Memorandum (Marston, P.G.) to PETC (Arrigoni, T.W.)
January 25, 1984

Plasma Fusion Center
Massachusetts Institute of Technology
Cambridge, Massachusetts 02139
Telephone: 617/253-8100

MEMORANDUM

DATE: January 25, 1984

TO: T.W. Arrigoni/PETC

FROM: P.G. Marston

RE: Magnet/Flow Train Integration Effort in support of APT

Background

There has never been a detailed study addressing and optimizing the packaging of the channel in the bore of the magnet. We did a little work several years ago in collaboration with NASA, AVCO, and MEPPSCO (references attached). That effort resulted in a factor of two improvement over prior studies (twice the power out of the same magnet bore) but did not adequately deal with the details of channel electrical connections and plumbing or with the impact (reduction in bore size) of having access to the magnet bore at the median plane of the magnet (i.e. the ability to bring power and plumbing connections directly through the sides of the magnet rather than having to bring everything out the ends of the magnet bore).

Proposed Work

The effort proposed herein would be in collaboration with both AVCO and Westinghouse (individually) and working with them would address the detailed design problems associated with the channel electrical and hydraulic connections and the cost impact of magnet configurations wherein electrical leads could be brought out along the median plane either through room temperature penetrations (through the cryostat) or via a roll-apart superconducting magnet design.

The effort will not only answer some hard questions about the detailed system design and reliability of the electrical and hydraulic connections, but is also expected to further reduce the magnet bore (and cost) beyond that already achieved with the referenced earlier work.

The anticipated additional cost for the magnet (only) related effort is $25,000. If we can get approval to begin this work during February, the effort would be complete by the end of this fiscal year.

P.G. Marston

PGM/psl

Appendix E
Method of Calculating Magnet Size Parameter VB^2
MIT Plasma Fusion Center
April 1984

Method of Calculating Magnet Size Parameter, VB^2

MIT Plasma Fusion Center

April 1984

In investigating costs of MHD magnets, it is important to determine how magnet system cost varies with magnet size. For example, a curve of magnet cost vs. size based on cost data available for smaller magnets can be extrapolated to indicate the expected costs for larger magnets.

The magnet size parameter, VB^2, is a convenient measure of magnet size for use in examining cost vs. size effects. The V is a nominal warm bore volume and the B is peak on-axis magnetic field. These terms are defined in Figure E1. (It should be noted that the volume, V, as defined in Figure E1 is not the actual volume of the warm bore, but is only a "characteristic" volume, which is the product of the bore cross-sectional area at the inlet and the active length.)

This parameter is appropriate because the power generated in an MHD duct is theoretically proportional to the duct volume and to the square of the magnetic field. It is an easy value to calculate because peak on-axis field, active length and bore area at plane of channel inlet are generally readily available, even for preliminary magnet designs.

A more rigorous size parameter would be that given below:

$$\text{Size Parameter} = \int_{\ell=0}^{\ell=L_a} b^2 a d\ell$$

where ℓ is the distance along axis from channel inlet, a and b are the warm bore area and on-axis field, respectively, at distance ℓ and L_a is the active length. However, experience has shown that the two methods of determining the parameter give results that are in reasonably close agreement and the method shown in Figure E1 is more convenient, particularly for preliminary studies where exact field profiles are not determined.

In actual cases, the power generated in particular MHD channel/magnet combinations may not always be proportional to the magnet size parameters. Power will vary with the effectiveness of packaging of the channel in the bore (how much of the available bore volume is actually used for plasma) and with the specific design of the channel itself.

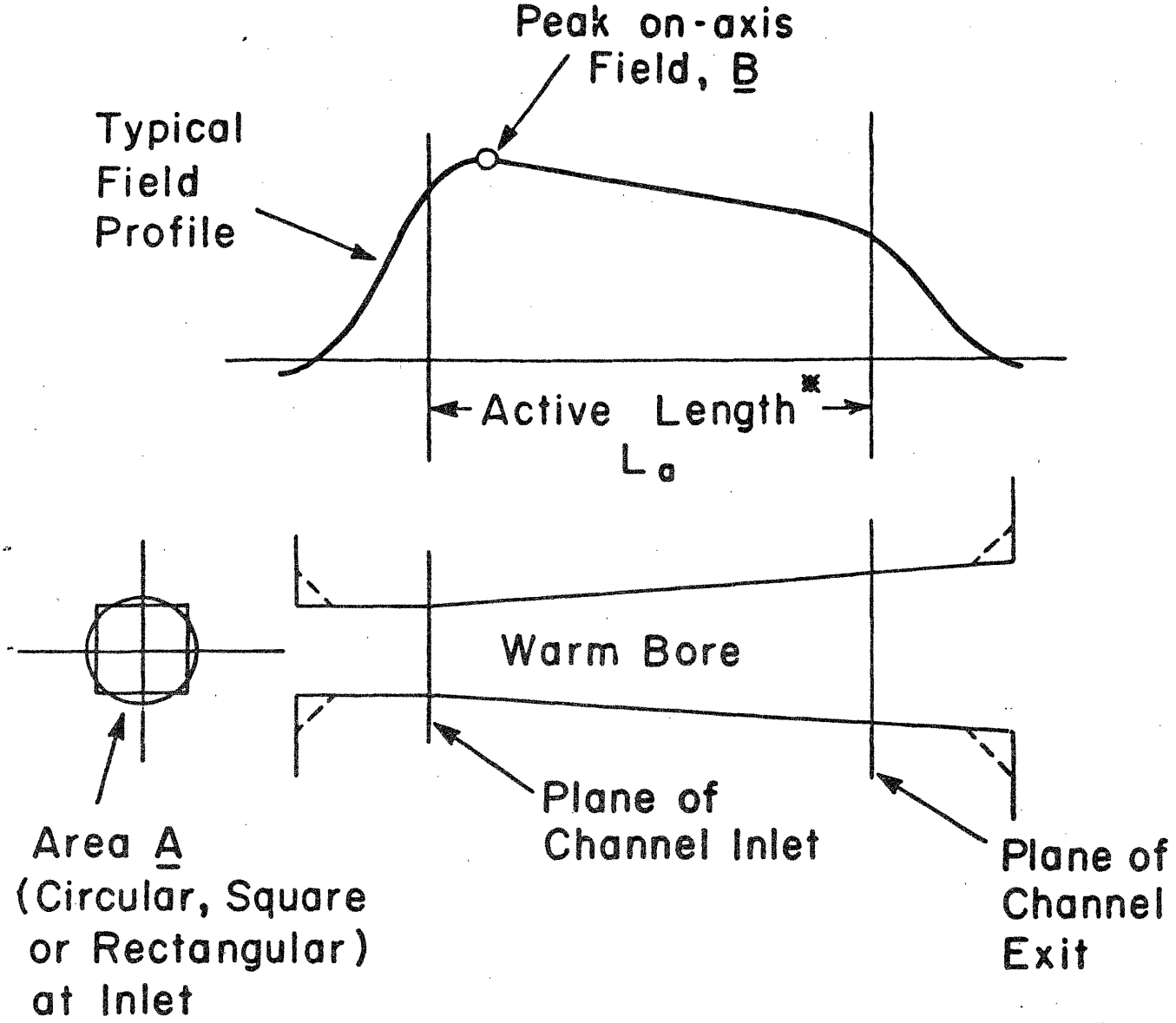

Characteristic Volume, $V = A \times L_a\ (m^3)$

Magnetic Size Parameter $= VB^2\ (m^3\ T^2)$

* For purposes of magnet comparison, active length is taken as the distance along the channel axis from the point where inlet field is 0.8 B to where exit field is 0.6 B.

Figure E1 Method of calculating magnet size parameter, VB^2

Appendix F

MIT Letter (Hatch, A.M.) to Multi-Tech Corp. (Greene, M.) March 10, 1983, with Attachment

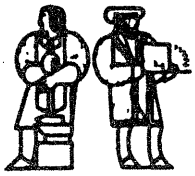

Plasma Fusion Center
Massachusetts Institute of Technology
Cambridge, Massachusetts 02139
Telephone: 617/253-8100

March 10, 1983

Dr. Munroe Greene
Multi-Tech Corporation
Box 4078
Butte, MT 59702

Dear Dr. Greene:

In response to your request in our telephone conversation of March 3, 1983, we have prepared a brief description of a 4.5 T superconducting magnet system for use with the 29 MWe supersonic channel MHD generator which you described in your earlier conversation with Peter Marston.

The description, together with a curve of on-axis magnetic field vs. distance along channel and an outline sketch of the magnet are enclosed with this letter.

The description and data are, of course, preliminary in nature and intended only to give a general picture of what would constitute a typical 4.5 T superconducting MHD magnet system. The budgetary price of 30×10^6 for the installed system, mentioned in our conversations, is also only a preliminary estimate.

If you have any questions about these data, please contact me.

Sincerely,

A. M. Hatch

AMH/bak
Enclosures

xc: P. G. Marston
J. M. Tarrh
A. M. Dawson

Description

4.5 T Superconducting MHD Magnet System

This description applies to the conceptual design of a magnet system to provide the magnetic field required for a supersonic MHD channel intended to produce approximately 29 MWe.

System Description

The system consists of the magnet and accessory equipment, comprising subsystems as listed below:

Magnet assembly, including warm bore liner
Cryogenic support equipment
Power supply and discharge equipment
Vacuum pumping equipment
Protection/control equipment and instrumentation

The magnet assembly consists of liquid helium cooled superconducting coils in a cryogenically-insulated enclosure (vacuum vessel) with a cavity (warm bore) extending through the center horizontally, open at both ends. A water-cooled warm bore liner is provided inside the cavity. The outline dimensions of the magnet assembly and the dimensions of the cavity (inside liner), which diverges from plasma upstream (inlet) to plasma downstream (exit) end, are shown on Figure 1. The cavity is designed to house the MHD channel, which is inserted and withdrawn from the large (exit) end opening. The magnetic field in the cavity is oriented in a primarily horizontal direction perpendicular to the long axis of the cavity. The magnet does not incorporate a ferromagnetic flux-return-path or other means to reduce fringe magnetic fields. The magnet is designed to be stationary, permanently mounted on a foundation provided as a part of the power plant facility.

The cryogenic support equipment consists of a helium refrigerator/liquefier, a helium compressor package, storage tanks, heat exchangers, transfer lines and controls as required for cooling down the superconducting magnet windings, maintaining them continuously at liquid helium temperature during facility operating and standby periods, and warming up the windings when an extended dead plant condition is anticipated.

The power supply and discharge equipment consists of a rectifier-type dc power supply, discharge resistors, circuit-breakers and controls as required for charging the magnet, maintaining it at the desired field strength during MHD generator operation and discharging it under both normal and emergency (fast) shut-down conditions.

FIG 1

OUTLINE - 4.5 T MHD MAGNET

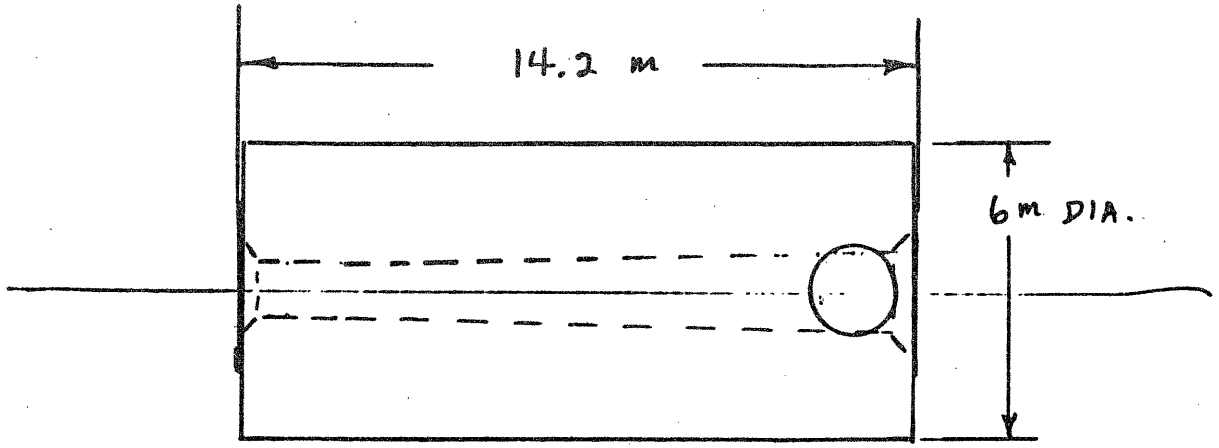

TOP

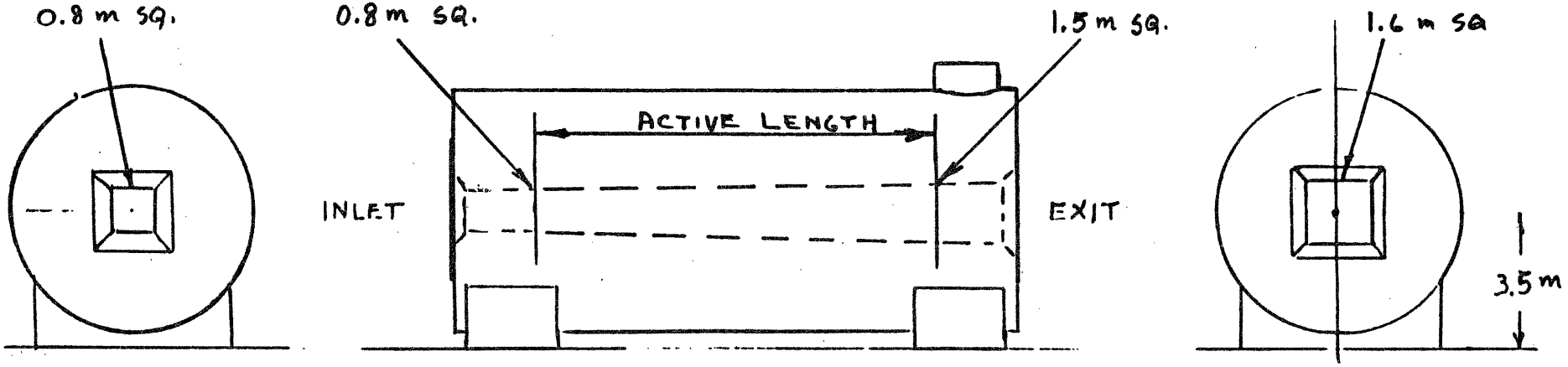

ELEV.

3/8/83

Vacuum pumping equipment consists of diffusion pumps and mechanical pumps for evacuating the magnet vacuum vessel prior to and during initial magnet cooldown and for removing from the vacuum vessel any helium leakage that may occur from the coil container during magnet operation. A utility vacuum pumping system for servicing the cryogenic support equipment is also provided.

Protection and control equipment consists of instrumentation to detect abnormal conditions in the magnet system and controls to automatically activate protective measures. Also included are instruments and controls to permit remote monitoring and manual control of major functions of the magnet and associated equipment at the power plant control room.

The magnet system includes, in addition to the above subsystems, piping and wiring necessary to interconnect subsystem equipment items and to connect these items to local utility outlets provided as part of the facility. Utility requirements are summarized in Table I.

Magnet Assembly

The design characteristics of the magnet assembly are given in Table II.

The major components comprising the magnet assembly are as listed below:

- Superconducting windings (coils) including winding substructure
- Winding containment vessels
- Main force containment structure
- Thermal radiation shield
- Low-heat-leak support struts
- Vacuum vessel (magnet enclosure) including warm bore
- Water-cooled warm bore liner
- Vapor-cooled electrical leads
- Internal instrumentation wiring and piping

Windings and Substructure

The magnet windings consist of a pair of saddle-shaped coils of copper-stabilized niobium titanium cable-type conductor. The turns are insulated from each other and are individually supported by a substructure consisting of stacks of fiber glass-plastic bars or plates notched to fit the conductors. The windings are bath-cooled by liquid helium and are designed for cryostatic stability.

The windings are designed to produce the on-axis field profile shown on Figure 2.

TABLE I

MAGNET SYSTEM

UTILITY REQUIREMENTS

Electric Power (60 Hz.)			
Power supply - Maximum charging	4160 V	750 KW	3ϕ
- Steady state of operation	4160 V	250 KW	3ϕ
Refrigerator/liquefier	220 V	8 KW	1ϕ
Refrigerator compressors	440 V	350 KW*	3ϕ
Utility vacuum pump	220 V	15 KW	3ϕ
Diffusion pumps, main vacuum (2)	440 V	24 KW	3ϕ
Fore pumps, main vacuum (2)	440 V	20 KW	3ϕ

Cooling Water (80°F max., 50 psig except 100 psig for warm bore liner)		
Power supply (rectifiers; diodes)		25 GPM
Discharge resistors		30 GPM
Refrigerator compressors		110 GPM
Refrigerator/liquefier		3 GPM
Diffusion pumps, main vacuum (2)		5 GPM
Fore pumps, main vacuum (2)		5 GPM
Warm bore liner	Steady-state	30 GPM
	Emergency	150 GPM
Water-cooled power bus		25 GPM

Liquid Nitrogen (30 psig)	
Refrigerator pre-cooling (steady-state)	110 ℓ/hr.
Magnet radiation shield, transfer lines, etc. (steady-state)	40 ℓ/hr.

*Nominal running power with power factor = 0.9. Starting requires 3 x running power.

TABLE II

MAGNET DESIGN CHARACTERISTICS

Magnetic Field:	
Peak on-axis field	4.5 T
Active field length	10 m
Field at start of active length	3.6 T
Field at end of active length	2.7 T
Dimensions:	
Aperture, warm bore inlet*	0.8 m x 0.8 m
Aperture, start of active length*	0.8 m x 0.8 m
Aperture, end of active length*	1.5 m x 1.5 m
Aperture, warm bore exit*	1.6 m x 1.6 m
Vacuum vessel overall length, including water-cooled warm bore liner	14.2 m
Vacuum vessel outside diameter	6 m
Winding Characteristics	
Design current	20,000 A
Winding current density (J)	1.4×10^7 A/m^2
Ampere turns	15.2×10^6
Inductance	3.5 henries
Stored energy	700 MJ
Weights:	Tonnes
Conductor	75
Substructure	60
Superstructure and coil containment vessels	125
Thermal radiation shield, cold mass supports, etc.	20
Vacuum vessel	80
Miscellaneous	10
Total Magnet Weight	370

*Inside water-cooled warm bore liner

FIG. 2

CURVE OF ON-AXIS FIELD
VS
DISTANCE ALONG AXIS

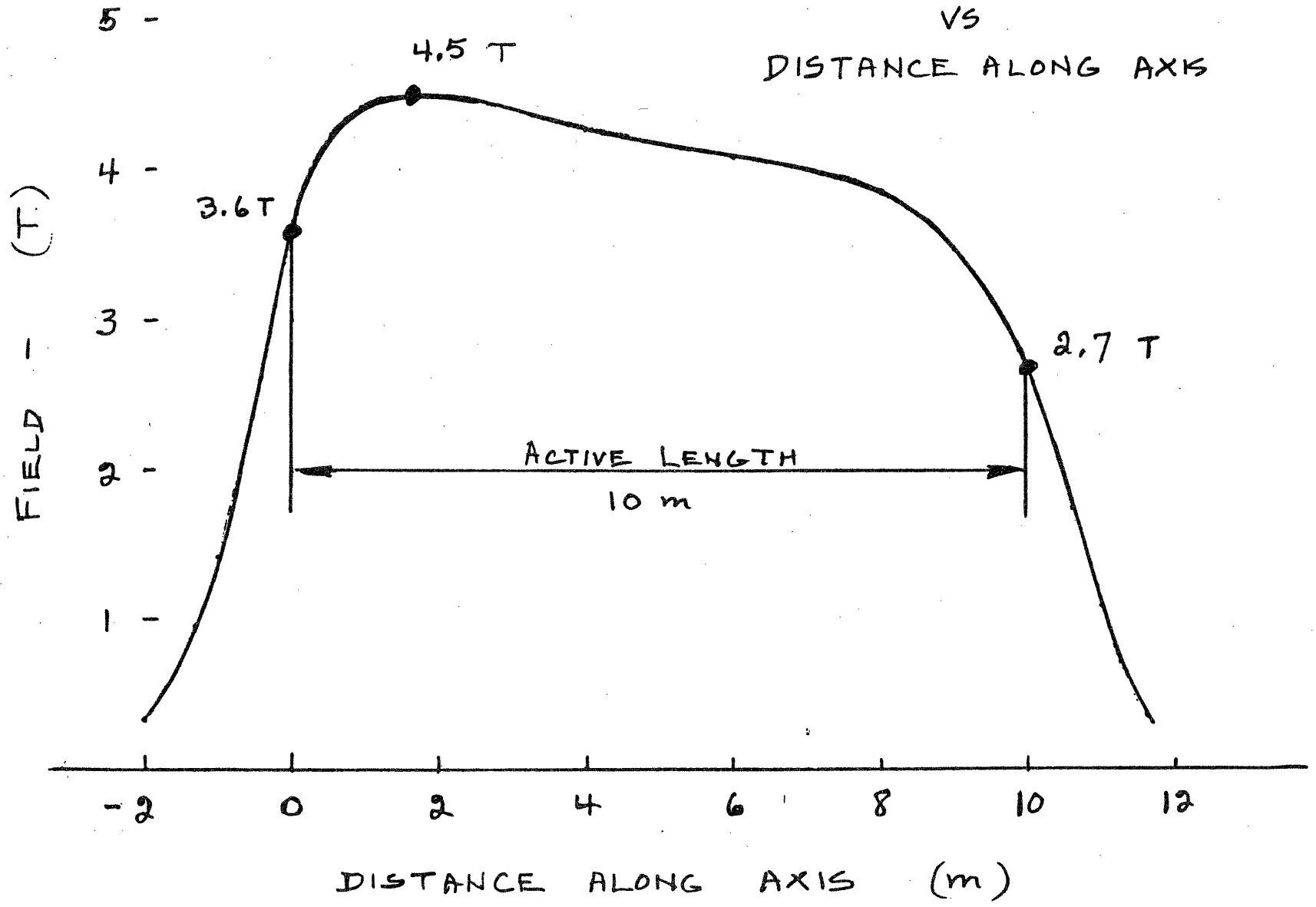

Winding Containment Vessels

The two winding containment vessels enclose the two saddle coils and follow closely the contours of the coils. The vessels are mounted on either side of the centerline of the magnet and seat against each other on the vertical plane through the centerline. They are separate units, identical in design except that one is right-handed and the other left-handed. Cross-connections are provided to distribute liquid helium between the vessels and to maintain equal pressures within them.

The main functions of the vessels are to maintain the windings in a bath of liquid helium and to serve, in combination with the main structure, as structural support for the coils. The coil containment vessels are located inside a vacuum vessel and are designed for a maximum internal pressure of 3 atmospheres with an external vacuum. The containers are designed to carry the entire longitudinal magnetic force produced by the coil-ends and to share radially outward (vertical and transverse) magnetic loading with the main force containment structure.

The coil containment vessels, plenum chambers and covers are made of Type 316 low-cabron nitrogen stabilized stainless steel (316 LN).

Main Force Containment Structure

The major function of the force containment structure (superstructure) is to hold the magnet windings in place against magnetic forces. This structure surrounds the coil containment vessels and is exposed to the vacuum existing in the vacuum vessel. Magnetic forces on the windings are carried via substructure into the walls of the coil containment vessels and through them to the superstructure, which is clamped or welded to them. In the end-turn regions of the magnet the superstructure is integral with the coil containment vessels and consists mainly of stiffeners and/or gussets welded to the coil containers. In the middle region, the superstructure consists of built-up I-beams and tie-bolts clamped around the coil containers but not welded to them.

The entire force containment structure is designed in a manner so as to provide maximum access to structural welds and to winding containment vessel welded joints for inspection purposes.

The force containment structure is made of Type 316 low carbon, nitrogen stabilized (316 LN) stainless steel.

Thermal Radiation Shield

The thermal radiation shield consists of an aluminum alloy shell covered with multi-layer insulation, located within the vacuum jacket and forming a thermal radiation barrier between the cold mass (winding and main structure) and the warm surfaces of the vacuum jacket including the warm bore tube. The purpose of the shield is to minimize thermal (radiative) heat transfer from the warm walls of the vacuum jacket to the cold mass. The aluminum alloy shell of the shield is maintained at liquid nitrogen temperature by a system of tracer tubes attached to the shell and supplied with liquid nitrogen from bulk storage. Blankets of multi-layer insulation are attached to both sides of the aluminum alloy shell.

Vacuum Jacket and Warm Bore

The vacuum jacket is a cylindrical vessel, mounted horizontally, with a square warm bore extending from one end to the other along the horizontal centerline. The purpose of the vacuum jacket is to enclose the magnet cold mass assembly and thermal radiation shield and to provide vacuum insulation around these items. The warm bore of the vacuum jacket serves to support the warm bore liner which in turn supports the MHD channel. Stacks are provided at the top of the vacuum jacket at the exit end and inlet end for cryogenic piping, electrical connections and instrument wiring communicating with the magnet winding and cold mass. Connections are provided in the lower portion of the vacuum jacket for vacuum (diffusion) pumps and also for safety blowout disks. Manhole covers are provided on the vacuum jacket so that with the internal pressure returned to atmospheric, personnel will have access to the inside of the jacket for inspection purposes. Large sections of the vacuum jacket shell on both sides are so designed that they may be completely removed to provide full access to the middle portion of the cold assembly in the event that major overhaul is required.

The vacuum jacket and bore tube are constructed of 304 stainless steel.

Water-Cooled Warm Bore Liner

The magnet is provided with a warm bore liner to protect the magnet against accidental discharge of energetic plasma from the MHD train or intense electrical arcing in the power takeoff.

The warm bore liner covers the entire inside of the magnet bore including the end flares and a portion of the end-faces of the magnet vacuum vessel. The interior of the magnet warm bore is lined with an insulating material, such as NEMA G-7 glass reinforced silicone, to provide insulation between the warm bore liner and the magnet.

Appendix G
Outline of 6 Year Engineering and Manufacturing Program for Superconducting Magnet for 35 MWe MHD Power Train

MIT Plasma Fusion Center

April 1984

Superconducting Magnet for a 35 MW_e MHD Power Train

1.0 Summary

The science and industrial base for Superconducting Magnet manufacture are in place. The engineering details and manufacturing technology require considerable effort before a magnet of this size can be installed with acceptable risk. The problems and required technologies, and a program to meet their needs, are defined herein.

The estimated characteristics of the magnet are shown in Figure 1. The total cost of a six year program of development, design, manufacture, installation and test is estimated at $50 million. The distribution and profile of these funds are approximately as follows:

Distribution	Millions of '84 dollars
Installed component cost (contract to industry)	30
Contingency	10
Supporting Development (contract to industry)	6
Supporting Analysis & Review, Program Management, Technical Monitoring, (provided by MIT)	4
TOTAL	50

Profile

Year 1	3
2	5
3	6
4	14
5	16
6	6
TOTAL	50

2.0 Problems

2.1 Risk

It is important to understand that the cost/risk assessment for the superconducting magnet is quite different from that for other flow train components. Of the basic MHD generator components, the magnet is not only by far the most costly, but is similarly the most costly and time consuming to repair should it fail. As was recently demonstrated in Tennessee by the HPDE, a magnet failure can easily kill an entire program.

Confidence in the reliability of this component has its roots in detailed solutions to the detailed engineering problems and in the development and demonstration of manufacturing technology at the required scale. Therefore, although the basic understanding of this component is excellent and there is absolutely no question about the fact that such a unit can be built, it is necessary to put considerable effort into the following basic elements to reduce these risks to acceptable levels.

2.2 Conductor

A superconductor capable of operating at a minimum current of 25 kA and satisfying the needs of the design loads and fabrication logistics does not exist. The steps to develop such a conductor and the manufacturing capability to produce it are straightforward but must be implemented prior to construction. Conductor design details will obviously drive the magnet design details. The conductor is the most critical element of the program and development must start immediately.

2.3 Structural Design Basis

The behavior of structural materials at 4.2 K is not well understood. Considerable experimental study and materials qualification and verification must be performed to satisfy design credibility. Code considerations relevant to operation in a commercial power plant environment must be satisfied.

2.4 Design Selection

Several satisfactory design alternates have been identified in previous studies (ref. 1). Additional effort is required to select that design which is most suitable to this application. This selection will be influenced by the site location and comparative considerations of fabrication on site versus transportation problems. It will also be influenced by considerations of quality control and inspection depending on the importance of these elements as derived from the studies of 2.3 above.

The most important element of this effort is, however, a detailed study of the magnet/flow train integration and interfacing including an overall systems analysis with a strong focus on protection.

3.0 Technology Development

The focus of this effort is obviously to answer the above questions. The principal elements of conductor design and qualifications, structural design and materials qualification, and system design assessment must be carried out in parallel with suitable interaction and iteration to generate a satisfactory system design. As demonstrated in the above referenced report, the elements of this activity and the process by which a rational selection will be made are well understood.

The total cost of this development effort is estimated at $6 million, with most of that being spent during the first three-year period.

The elements of the total development and construction program and their schedule are outlined in Figure 2.

Ref. 1, MHD Magnet Technology Development Summary (PFC RR83-6), Massachusetts Institute of Technology, Plasma Fusion Center, November, 1983.

Superconducting Magnet for a 35 MW_e MHD Power Train

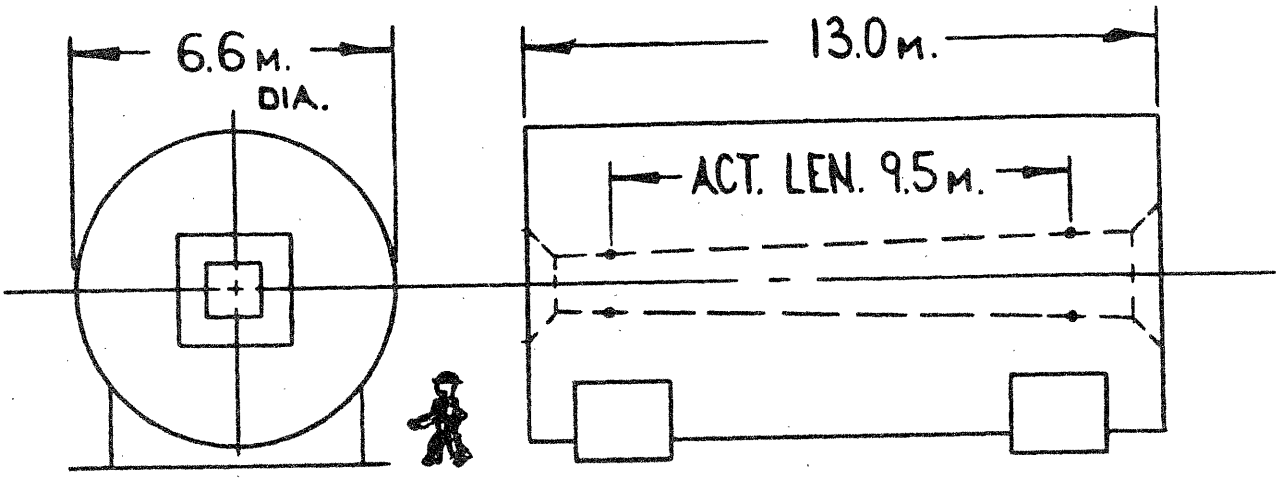

Figure 1

Characteristics

Peak Field on Axis	4.5 T
Length of active field	9.5 m
Field at start of active length	3.4 T
Field at end of active length	2.6 T
Inlet Aperture	0.9 x 0.9 m
Aperture at end of active length	1.6 x 1.6 m
Ampere Turns	15.6×10^6
Stored Energy	7×10^8 J
Total Weight	370 Tonnes

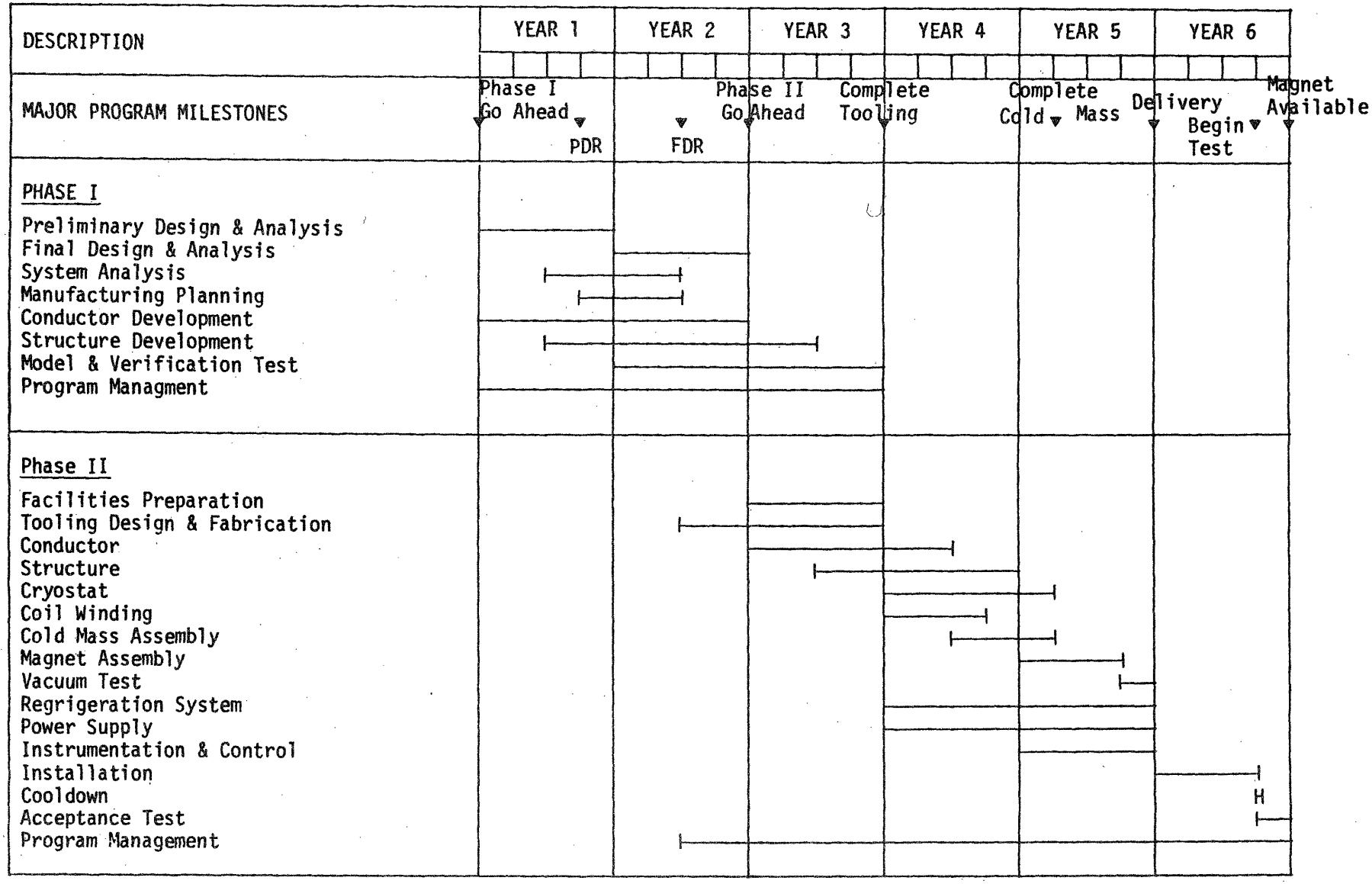

FIGURE 2: TOTAL PROGRAM SCHEDULE